ウマの組織由来間葉系幹細胞を用いた
骨軟骨再生に関する研究

山口大学大学院連合獣医学研究科

村田　大紀

2015 年 9 月

Table of contents

General introduction

Locomotor apparatus is one of the composite apparatus that consist of many organ systems. The major feature in this apparatus is the performance of mechanical motion. Skeletons and muscles are key components of locomotor apparatus which make it possible to form individual body shape, to maintain them, and to move any parts of the body or to translate the whole body. Skeletons are composed of bone, cartilage, ligaments, and joints, and these elements form a skeletal system. Skeletal system and muscular system take roles as the active and the passive parts of locomotor apparatus, and these two parts are integrated and work as a functional unit.

All component cells of the skeletal system developed from the mesoderm. Mesoderm is differentiated into three types of connective tissue which are fetal tissues, reticular tissues, and fibrous tissue during the early stages of the fetal period. The amount of these tissues increase as they develop, and then they begin to differentiate into fetal trunk and limbs during the early stages of fetal development with distinctive features and function for each part of them. Progenitor cells in areolar connective tissue differentiated into bone and cartilage which are important part of supporting tissues organization. Cartilage and bone generate from each of mesenchymal progenitor cells, which are chondroblast or osteoblast. These cells produce extracellular matrices such as collagen fibers, proteogrycans, and so on.

In particular, cartilage generates from mesenchymal connective tissues at the late stage of fetal period. The connective tissues contain the star-shaped primitive mesenchymal cells. Thereafter the connective tissues develop into perichondrium in which fibroblast-like spindle-shaped cells differentiated from the the primitive

mesenchymal cells. The spindle-shaped cells differentiated into round-shaped chondroblast which produce cartilaginous matrix. Cartilage development is due to the proliferation of chondroblasts in the perichondrium and due to the production of cartilaginous matrix by the chondroblasts. A chondroblast is surrounded by the extracellular matrix secreted by itself, and so the cells are isolated from each other. Subsequently, the chondroblasts are clastic, and form small groups of mature chondroblasts isolated from each other with small amounts of extracellular matrix. Mature chondroblasts called chondrocytes, which become able to produce the entire cartilaginous matrix. The mature cartilage is covered with the perichondrium which consists of collagen fibers and fibroblast-like spindle-shaped cells. The cells can differentiate into chondroblasts and produce new cartilage by accrementation. However, hyaline cartilage on the articular surface doesn't have the perichondrium. Therefore, articular cartilage doesn't have the ability of self-recovery. And also, the lack of blood supply is another reason of poor self-recovery and regeneration of articular cartilage. Cartilage is a hypovascular or avascular tissue, and so the exchange of metabolites between chondrocytes and surrounding tissues is carried out through the water diffusion from the blood vessels into the surrounding connective tissues, including synovial membrane, and bone tissue under the cartilage. Because of that, there is a limitation in the cartilage thickness in order to survive the innermost layer of the cells.

In the middle of maturity of skeletal system, long bone develops in the longitudinal direction through the process of endochondral ossification, which occurs in the growth plate at the boundary between basis and epiphysis. The tissues of skeletal system consist of collagen fibers, extracellular matrix, and the cells to produce them, and form supporting tissues which are highly specialized. Bone forms a strong protective and supportive framework, and its robust nature is owing to calcium deposit

between collagen fibers and extracellular matrix. Cartilage takes many different forms, and to form a smooth joint surface at the both ends of bone and to play an important role in neonatal bone formation by supporting structures in certain areas. Joint is a complex structure, which consists of two bones and gives various degrees of mobility by various structures and function of individual joints. In addition, other tissues of skeletal system include ligament which consists of strong and flexible bundles of collagen fibers and gives the stability of joint, and tendons which attaches muscle to bone. Functional and/or morphorogical differences among the various tissues of the skeletal system are mainly dependent on the variation on the nature and the proportion of the stromal and fibrous components in the extracellular matrix.

Cartilage has the most distinctive structures among connective tissues consisting of skeletal system. The structural property of cartilage is an extracellular matrix consisting of collagen fibers, elastic fibers, proteoglycans (PGs), and a lot of water (approximatly 70% of gross wet weight). This special composition gives cartilage tough and flexible properties. Cartilage is generally divided into three types, which are hyaline cartilage, fibrocartilage and elastic cartilage, in accordance with the differences on the proportion of the collagen fibers and elastic fibers in extracellular matrix. Hyaline cartilage is mostly found at the joints of long bones (articular cartilage) in adult mammals. Fibrocartilage forms intervertebral discs, meniscus, and articular disks of temporomandibular joint, and is ossificated as age advances. Elastic cartilage is found at epiglottis and pinna, and supports these structures from inside these tissues. The collagen and elastic fibers provide stiffness to cartilage. And also, assembly and regular array of more than one hundread PGs provide flexibility to cartilage, as explained the structure of PG composing core protains and a lot of GAGs. GAGs are divided into two types, that is, sulfated GAGs (chondroitin sulfate and keratan sulfate) and non-sulfated

GAGs (hyaluronic acid). They are combined to form the central prop of complex molecules. GAGs provide cartilage the excellent property on holding water, and make cartilage increase flexibility and elasticity.

Bone consists of the cells and extracellular matrix called osteoid (osseous tissue) which is mainly composed of type I collagen fiber and calcified by deposition of hydroxyapatite. Thus, bone becomes to have strength and hardness. Bone has three types of the cells, which are osteoblasts, osteocytes and osteoclasts. Osteoblasts lining up on the bone surface synthesize osteoid and calcifie it. Osteocytes are almost inactivated osteoblasts trapped within the bone matrix and considered to have a function as a mechanosensor to bone. Osteoblasts and osteocytes are derived from primitive mesenchymal cells called as osteogenic cells. Osteoclasts which are polynuclear phagocytes derived from macrophages-monocytes have the capacity to erode the bone and play an importan role in relentless bone turnover.

The surface of the bone is composed of lamellar bone which forms compact bone and surrounds cancellous bone consisting of thin tubecular bones and bony plates. Compact bone forms wall of diaphysis, on the other hand cancellous bone occupy in some portion of medullary cavity at the center of diaphysis. Cancellous bones consist of trabecular bones forming irregular meshes and containing spaces between trabecular bones. Hematopoietic bone marrow generally exists in medullary cavities and also in trabecular bone spaces (Clancy et al. 2006). Both ends of the long bone, that is, articular surface of epiphysis, are protected with hyaline cartilage called as articular cartilage.

Periosteum covers the outer surface of the bone without covering the articular surface and the surface region of the bone attached with tendons and ligaments, on the other hand endosteum covers the inner surface of the bone. The periosteum binds to joint capsule away from the surface of the bone near the joint. It is required for blood

supply to the bone, bony growth, bone regeneration, and repairing a bone fracture. The periosteum is composed of inner bone formation layer consisting of cells and outer protection layer consisting fibers. The bone formation layer is located just on the surface of bone and capable of forming neoplastic bone. This layer contains the numerous sensory nerve fibers, vascular and lymphatic network distributed into bone. And also, preosteoblasts, the progenitor cells which differentiate into osteoblasts, exist in the layers. The layer holds osteogenic capacity for life, and this function is important in physiological bone regeneration and repair. The inner surface of the bone is covered with endosteum facing to medullary cavities and covering with cancellous bone, so it forms the boundary between the cancellous bone and bone marrow. Endosteum is composed of single-layerd and squamous cells which are premature progenitor cells. These progenitor cells can differentiate into either osteoblast or osteoclasts (Bragulla H et al. 2007). The endosteum is in contact with capillaries of the bone marrow and capable of forming neoplastic bone as well as periosteum.

Although progenitor cells in periosteum and endosteum have the ability of regenerating bone tissue, bone regenration could be caused only under the following two conditions.

1) The distribution of mesenchymal progenitor cells.

2) The proliferative ability of the progenitor cells.

On the healing process of bone fractures, granulation tissues appear in the gaps between the fractured bones. Primary healing process of bone fracture generally occurs in the cases that the fractured bones are fixed completely and the gaps between the fractured bones are tiny. Neoplastic bones are formed in the gaps of fractured bones and the stumps of two fractured bones are combined with each other to form one piece of bone again. In the case that the gaps of two fractured bones are too wide, secondary healing

process of bone fracture probably occurs. In this case, fibrous connective tissues bridge the gaps of two fractured bones at the beginning, and then callus is formed on the tissues. On the long healing process after that, compact bones are formed by mineral deposits on callus. Bone is one of the tissues which particularly have rich distribution of vascular tissue, and that shows the importance of bone metabolism. Dense vascular networks are observed only in bone but also in periosteum, endosteum, and bone marrow.

In the middle of fetal period, bones begin to replace cartilages at the primary endochondral ossification center. On the growing process of fetal period, skeletal precursor structures consisting of cartilage (primary bone) are formed to support the fetal growth and change the fetal feature. In this primary bone composed of cartilage, rapid mitosis is repeated until the beginning of the ossification and the actual growth and feature of a whole body are determined. In many cases, primary bones work as a framework structure on the process of the replacement of cartilage by bone. Factors affecting bone formation are inductive mediators such as bone morphogenetic proteins and cell division-inducing factors. Cartilage in primary bone is gradually reformd in its shape on a certain stage of development, and absorbed slowly and replaced by bone tissues.

On the early stage in embryonic development, supporting tissues consisting of connective tissues are replaced by bone tissues. This process is called as endochondral ossification or indirectly ossification and the bones formed through the process are called as endochondral bone. Most of mature bones including long bone such as femur formed through the process of endochondral ossification.

Proximal hindlimb from the trunk is composed of femoral bone as skeleton of the femur. Femur is the most powerful bone in long bones. Femur is basically divided into

three part such as proximal extremity, shaft of femur, and distal extremity with specific difference. Distal extremity of the femur is provided with trochlea groove on the dorsal side and medial and lateral condyle on the palmar side. Both condyles and proximal extremity of tibia are contiguous with meniscus between them to form femorotibial joint. Femoral trochlea is composed by two ridges. Both ridges are separated by groove and form the femoropatellar joint with patella. Emergence period of ossification center and closing period of growth plate are different between horses and pigs. In equine femure, primary ossification center appear in the two months of pregnancy, secondary ossification center appear in the six months of pregnancy, and growth plate close at the age of three years and a half (Bragulla H et al. 2007). And also, in swine femure, primary ossification center appear in the six months of pregnancy, secondary ossification center appear just before giving birth, growth plate close at the age of three years and a half (Bragulla H et al. 2007).

Femoropatellar joint and femorotibial joint are synovial joints, which are called true joint or diarthrodial joint and composed of three common structures such as extensive joint capsule, joint cavity, and articular cartilage. The joint allows the two bones to move largely on each articular surface, which is lubricated by synovial fluid and maintained by joint capsule.

The joint capsule consists of two layers such as the outer fibrous layer and inner synovial layer. Fibrous layer includes articular ligament and this ligament strengthen the outside of the joint capsule. Fibers of this layer are contiguous to periosteum or perichondrium and the layer has only limited blood supply. Therefore, once damaged, the layer needs a long time to repair. On the other hand, synovial membrane layer which backs joint capsule is composed of many kinds of tissues such as cells, blood vessels, lymphatic vessels, and nerves. This layer forms both synovial villi and synovial folds

and consists of endosynovial layer and subsynovial layer. The endosynovial layer is composed of two types of cells derived from mesenchyma. One is called type A synovial cell which is a large macrophage-like cell with developed goldi apparatus and many lysosome. The other is called type B synovial cell which is a fibroblast-like cell with many rough endoplasmic reticulum and produces some joint-specific molecules.

The joint cavity is filled with synovial fluid which is viscous pale yellow liquids, and the fluid improves the sliding of each articular surface and reduce the friction between the articular surfaces. Synovial fluid is secreted into the joint cavity from synovial membrane. The membrane isn't devided from joint cavity by epithelium, so the fluid isn't so much as simple secretions as highly-specialized liquid extracellular matrix derived from synovial membrane. The major component of synovial fluid is hyaluronan secreted from type B synovial cells, and liquid component of the fluid is transudate leaked from the synovial membrane capillaries. These components make easy the constant exchange of oxide, carbon dioxide, and metabolic product between the synovial fluid and blood. Theses substances are the main source of nutrients for articular cartilage.

Articular cartilage is firmly attached to the thin bone layer under the cartilage in epiphysis and not covered with perichondrium so that articular surface is very smooth. In the extracellular matrix of articular cartilage, fiber bundles are arranged according to the mechanical force loaded by tensil and compressive force. And the extracellular matrix has strong elastic force to absorb shocks. Articular cartilage generally has no distribution of blood vessels and nerves, and is composed of four layers such as superficial zone, intermediate zone, radial zone, and calcified zone. Superficial zone is a superficial layer and consists of tightly woven collagen fibers. These collagen fibers curve in arche shape toward the surface, running alongside each other near the surface.

These running patterns of collagen fibers increase the strength of superficial zone of articular cartilage. Intermediate zone consists of a uniform structure without cells. Radial zone is composed of collagen fiber bundles running radially and connecting partially each other. Calcified zone is the calcified part in which collagen fibers connect articular cartilage to subchondral bone. Subchondral bone is composed of lamellar bone and calcified cartilage under the articular cartilage. The lamellar bone is cortical bone which supports violent movement of the joint, protects articular cartilage from bone axially load, and accelerates the metabolism in deep layer of articular cartilage. Articular cartilage is a hypoxic tissue and given nourishment through SF diffusion. On the other hand, in the small part of the cartilage, nutrients reach articular cartilage via the blood vessels of bone marrow. PGs highly contained in articular cartilage have the high hydratability and make it easy to transport the metabolites to the cartilage.

Osteoarthritis (OA) is a degenerative disease of synovial joint caused by abuse and causes degenerative changes in cartilage on both epiphyses of two bones in the joint at first. Articular cartilage is eventually gouged, and one epiphyses of cortical bone is rubbed with the other. Both cortical bone surfaces are deformed to get hard and shick. Further abuse of joint makes small spicule peel and float in the synovial fluid. Equine OA is similar to human OA except for the points of the ages and causes. However, OA progresses with not only the degeneration of articular cartilage but also screlosis of subchondral bone, so bone and cartilage are required to be treated simultaneously in horses as same as humans (Lane et al. 2004; Smith et al. 2005).

Horses, in particular Thoroughbred race horses, have many kinds of joint diseases such as intra-articular fracture (IAF), osteochondritis dissecans (OCD), and subchondral bone cysts (BC). These diseases are serious for horses, because OA can secondarily progress rapidly. For the treatment of those diseases, arthroscopic surgeries have been

accepted worldwide in recent years. For IAF and OCD in particular, excision of bone or cartilage fractures and curettage of degenerated bone and cartilage under the arthroscopy have been accepted. However, aim of this treatment is only to remove fractures and degenerative tissues, not to reconstruct the lost osteocartilage. And also, to treat BC, not only steroid injection into the joint cavity, curettage of degenerated osteocatilage, and drilling into bone marrow cavity under the arthroscopy, but also cancellous bone graft implantation under joint open have been recommended for bone cysts. However in any treatment, hyaline cartilage contiguous to surrounding normal cartilage is not reformed, and rather fibrocartilage irregularly covered over the defect. Equine OA progresses with the repeated loads to the joint surface during racing, so the lesions are limited to the load-bearing site (Bodo et al. 2000). Therefore, mosaic plasty method has been considered for the application to not only humans but also horses (Bodo et al. 2004). Although mosaic plasty method has been known to improve the OA symptom improvement, the method has been accompanied by some problems including the loss of healty cartilage at unload-bearing site and the restriction of transplantable osteocartilage in equine medicine as well as human medicine (Bentley et al. J Bone Joint Surg (Br). 2003). In the femoral condyle which is redilection site of bone cyst, joint function with low frictional resistance is required. Therefore, hyaline cartilage, not fibrocartilage, are also needed to be regenerated contiguously to normal cartilage. Osteochondral regeneration is important to establish the most effective treatment for the defect both of articular cartilage and subchondral bone. In particular, it is suitable for hyaline cartilage regeneration to implant only cells without articficial substance.

Chapter 1

Osteochondral regeneration on femoral trochlear groove (non-load-bearing surface) using scaffold-free three-dimensional structure of porcine adipose tissue-derived mesenchymal stem cells

1.1 Introduction

Osteoarthritis (OA) is a major joint disease contributing to midlife and geriatric locomotor dysfunction, and the associated disability can decrease quality of life (expectancy) in humans (Muraki et al., 2009). Medical countermeasures for OA should thus be diligently investigated. OA slowly progresses not only as a result of traumatic injuries to joint structures (Gelber et al. 2000), but also through many exacerbating factors such as age, sex, body mass index, occupation, bone shape, and genetic factors regulating proteolytic enzymes (Femandes et al., 2002; Ding et al., 2006; Muraki et al., 2009). In advanced OA, cartilage degeneration and subchondral bone sclerosis may be worsened by the usual mechanical load of daily activities (Mankin et al., 1982), and therefore, surgical strategies to reconstruct both the bone and cartilage have been investigated to restore joint structure and function (Lane et al., 2004). A particular issue of interest in recent studies has been the complete regeneration of hyaline cartilage covering the subchondral bone.

Although a clinical study of osteochondral autografts from non-load-bearing sites into the deteriorated sites showed favorable outcomes following surgery (clinical improvement in 79-94% of OA patients) (Szerb et al., 2005), but also demonstrated the loss of clinically sound cartilage (Bentley et al., 2003) and the chondrocyte death associated with autologous osteochondral transfer (Huntley et al., 2005). Studies on surgical procedures using a combination of artificial bone and autologous chondrocytes seeded into a collagen scaffold have also shown favorable restoration of cartilage (Fujisato et al., 1996; Funayama et al., 2008). However, some studies have suggested accociated problems such as isolation of few chondrocytes from a small piece of normal cartilage (Fujisato et al. 1996), and the small number of obtainable chondrocytes after in

vitro culture (Fujisato et al. 1996), and dedifferentiation of chondrocytes during passaging in culture (Diaz-Romero et al., 2005). To solve these problems, stem cells have been recently received attention in a study (Tatebe et al., 2005).

Stem cells are defined as immature cells that have the ability for self-renewal and the potential for multilineage differentiation into specific cells. Mesenchymal stem cells (MSCs) derived from bone marrow (BM) and adipose tissue (AT) have been mostly used to demonstrate differentiation into bone and cartilage in vitro (Pittenger et al., 1999; Zuk et al., 2002). BM-derived MSCs (BM-MSCs) have been investigated in experimental implantation studies (Im et al., 2001; Nam et al., 2013), but unfortunately, a successful outcome of regeneration of hyaline cartilage and bone has been difficult in large animals (Zhou et al., 2006). BM-MSCs appear to have some disadvantages including decreased numbers and deterioration of the cells depending on senescence and natural transformation caused by genomic instability (Gurevitch et al., 2009). With age, the number of BM-MSCs may decrease due to transformation of red BM to yellow BM (Gurevitch et al., 2009). Previous experiments have shown age-related decreases in the yield rate, growth rate, and differentiation potential of BM-MSCs in rats and humans (Stolzing et al., 2008; Asumda et al., 2011). On the other hand, the advantages of AT-derived MSCs (AT-MSCs) are that abundant cells can be isolated from AT and their cellular proliferation rate may be higher in mature animals (Zuk et al., 2001). Furthermore, given that obesity is undesirable in OA patients, the regenerative strategy for bone and cartilage using unwanted AT could be reasonable and acceptable by many OA patients. It has been reported that AT-MSCs hardly differentiate into chondrocytes (Nakamura et al., 2012). However, a recent study using rabbits demonstrated the regeneration of bone and cartilage after implantation of scaffold-free three-dimensional (3D) constructs of AT-MSCs into osteochondral defects (Ishihara et al., 2014). This

report also contains a novel strategy for scaffold-free cell implantation. Preclinical studies using experimental animals are crucial for evaluating not only the effects of new drugs but also the usefulness of diagnostic and therapeutic procedures.

Previous studies indicated that scaffolds composed of materials such as collagen and hyaluronic acid could be useful for promoting cell adhesion, proliferation, and chondrogenic differentiation (Lu et al., 2010; Yoon et al., 2011), and may be also useful for seeding stem cells for implantation into osteochondral defects (Chen et al., 2011; Unterman et al., 2012). Bone regeneration using AT-MSCs seeded into hydroxyapatite has also been investigated (Arrigoni et al., 2013). However, artificial materials may induce a xenobiotic reactions through an immune reactions in the tissue (Park et al., 2010), and in addition, subchondral bone regeneration may not be completed (Robinson et al., 1993; Nakayama et al., 2013).

In many previous studies, bone and cartilage regeneration through various cell therapies has been evaluated in the knee joint of rabbits (Koga et al., 2008; Dashtdar et al., 2011; Lee et al., 2011; Yoshioka et al., 2011; Suzuki et al., 2012). However, to obtain meaningful results that are appropriate for extrapolating bone and cartilage regeneration to human OA, we expect that pigs will provide more appropriate animal models than rabbits. Microminipigs (MMPigs) have similar behavior patterns to human daily life, as they spend time standing and walking in the daytime and sleeping at night (Kawaguchi et al., 2011; Takeishi et al., 2012). In contrast, rabbits usually sit in cages. This study was designed to evaluate the regeneration of articular cartilage and subchondral bone using 3D constructs of autologous AT-MSCs in MMPigs.

1.2 Materials & Methods

1.2.1 Animals

Three MMPigs (Fuji Micra, Shizuoka, Japan), designated Animal No. 1 (male), Animal No. 2 (female), and Animal No.3 (male) were used in this study. Their body weights and ages were 13.8 kg and 25 months, 14.6 kg and 23 months, and 24.0 kg and 24 months, respectively. All procedures in this study were approved by the Animal Care and Use Committee of Kagoshima University (Approval No. A11037).

1.2.2 Isolation and expantion of AT-MSCs

Ten to fifteen grams of cervical AT per animal was aseptically obtained under general anesthesia. The AT samples were minced and digested for 90 min in phosphate-buffered saline (PBS) containing 0.1% collagenase (Collagenase Type I; Worthington Biochemical, Lake Wood, NJ). The digested cell suspensions were filtered through a 70-μm pore diameter membrane (Cell Strainer; BD, Franklin Lakes, NJ) and centrifuged at 160 × *g* for 5 min at room temperature. After decanting the supernatant, the pellet was rinsed with PBS and centrifuged. The supernatant was removed, and the pellet was resuspended and plated in a 150-cm^2 culture dish (Tissue Culture Dish ϕ 150; TPP, Trasadingen, Switzerland) in complete culture medium (CCM): Dulbecco's Modified Eagle's Medium (DMEM; Life Technologies, Carlsbad, CA) containing 10% fetal bovine serum (FBS; Thermo Fisher Scientific, Waltham, MA) and 1% antibiotic-antifungal preparation (100 U/mL Penicillin G, 100 μg/mL streptomycin, 0.25 μg/mL amphotericin B; Antibiotic-Antimycotic; Life Technologies). Following incubation at 37 °C under 5% CO_2 for 7 days, the cells adhering to the bottom of the dish were washed with PBS and cultured in CCM. The medium was changed on day 7

at Passage 0. At day 10, the cells were harvested with 0.25% trypsin and 1 mM EDTA (Trypsin-EDTA; Life Technologies) diluted by adding five volumes of PBS, and centrifuged. After decanting the supernatant, the pellet was rinsed with CCM, and the cells were replated at 5×10^5 cells per 150-cm^2 dishes and cultured for 6 days. The medium was changed every 3 days for 6 days during Passage 1. This serial process of passaging was repeated until the cells were required for analysis and construct creation. The cells were used for creating the constructs at Passage 4. Immunological surface markers and multipotency of the cells were analyzed at Passage 5.

1.2.3 Genetic specificity of AT-MSCs

Ten thousand cells were used to analyze the specific gene expressions in MSCs. Total RNA from the cells was prepared with an RNA isolation kit (MirVana miRNA Isolation Kit; Life Technologies), according to the manufacturer's instructions. The isolated RNA was then converted to cDNA and amplified with the TAKARA RT-PCR system (PCR Thermal Cycler MP; Takara Bio, Otu, Japan) and RT-PCR kit ((ReverTra Dash; Toyobo, Osaka, Japan). Specific PCR primers were used to amplify octamer-binding transcription factor 4 (OCT-4), sex-determining region Y box 2 (SOX-2), kruppel-like factor 4 (KLF-4), cellular myelocytomatosis oncogene (C-MYC), and homeobox protein NANOG (NANOG) as premature marker genes. The conditions and expected sizes of the products are summarized in Table 1.1.

1.2.4 Molecular specificity of AT-MSCs

Ten thousand cells were resuspended in 500 µl of staining buffer (SB; PBS containing 1 % FBS) and incubated for 30 min at 4 °C with 20 µg/ml FITC-conjugated

antibodies against CD34 (BD), CD45 (BD), CD90 (BD), or CD105 (Abcam, Cambridge, UK). Non-specific FITC-conjugated mouse immunoglobulin G1κ (BD) was used as a negative control. The characteristics of the antibodies are listed in Table 2. The FITC-labeled cells were washed with SB and resuspended in 500 μl of SB for fluorescence-activated cell sorting (FACS) analysis. Cell fluorescence was evaluated as a strong shift in the mean fluorescence intensity (MFI) on flow cytometry using a FACS Aria II instrument (BD). The data were analyzed using FACS Diva software (BD).

1.2.5 Tri-lineage analysis

1.2.5.1 Osteogenic differentiation assay

To investigate osteogenic differentiation, the AT-MSCs were placed in 6-well plates (6 Well Plate-N, Nest Biotech, Wuxi, China) in CCM at an initial density of 5×10^3 cells/cm^2. After 24 h of incubation, the medium was replaced with osteogenic induction medium (Differentiation Basal Medium-Osteogenic; Lonza, Walkersville, MD), supplemented with 100 μM ascorbic acid, 10 mM β-glycerophosphate, and 1 μM dexamethasone, for 2 weeks. Production of calcium apatite crystals in the osteogenic extracellular matrix was evaluated with alizarin red staining in the wells of a culture plates. The osteogenic marker genes were osteocalcin (OC), osteonectin (ON), and alkaline phosphatase (ALP). The reaction products were electrophoresed in a 2% agarose gel (Agarose WP; Wako Pure Chemical Industries, Osaka, Japan), and the expression of specific genes was determined based on the expected size of the bands that were labeled with SYBR Green (Takara Bio). The PCR primers and conditions, and the expected sizes of the products are summarized in Table 1.1.

1.2.5.2 Chondrogenic differentiation assay

To investigate chondrogenic differentiation, AT-MSCs (5×10^5) were resuspended in a 15-ml culture tube (SuperClear Centrifuge Tubes; Labcon, Petaluma, CA) in 500 µl chondrogenic induction medium (Differentiation Basal Medium-Chondrogenic; Lonza) supplemented with 4.5 g/l $_D$-glucose, 350 µM L-proline, 100 nM dexamethasone, and 0.02 g/l transforming growth factor beta 3. Chondrogenic differentiation was induced in pellet cultures for 2 weeks. The chondrogenic cell pellets were fixed with 10% neutral-buffered formalin (NBF), embedded in paraffin, and cut into 5-µm sections using a micro-section instrument. The sections were stained with alcian blue to detect cartilage-specific proteoglycans. The chondrogenic marker genes were sex-determining region Y-box 9 (SOX-9) and aggrecan (AGG). The reaction products were electrophoresed in a 2% agarose gel (Agarose WP; Wako Pure Chemical Industries), and the expression of specific genes was determined based on the expected size of the bands that were labeled with SYBR Green (Takara Bio).

1.2.5.3 Adipogenic differentiation assay

Adipogenic differentiation began when AT-MSCs reached a density of 5×10^3 cells/cm^2 in 6-well plates in CCM. Following a 24-h pre-incubation, the medium was replaced with Adipogenic Induction Medium (Lonza), supplemented with 4.5 g/l $_D$-glucose, 100 µM indomethacin, 10 µg/ml insulin, 0.5 mM 3-isobutyl-1-methylxanthine, and 1 µM dexamethasone, for 3 days for induction of specific genes and molecules. Adipocyte-specific intracellular lipids were stained with oil red O. The adipogenic marker genes were adipocyte fatty acid binding protein 2 (AP2) and peroxisome proliferator-activated receptor γ2 (PPAR-γ2). The reaction products were electrophoresed in a 2% agarose gel (Agarose WP; Wako Pure Chemical

Industries), and the expression of specific genes was determined based on the expected size of the bands that were labeled with SYBR Green (Takara Bio).

1.2.6 Preparation of 3D constructs of AT-MSCs

At least 4×10^7 AT-MSCs were used to produce each autologous construct for Animal No. 1 and Animal No. 2. The cells were inoculated into eight 96-well plates (Sumitomo Bakelite, Tokyo, Japan) with 5×10^4 cells/well. After undisrupted incubation for 48 h, the cells formed aspheroids with a diameter of about 700 μm in the bottom of the wells. About 760 spheroids were placed in a cylindrical mold and incubated in CCM until implantation (7 days). When the mold was carefully removed, a columnar construct of 4 mm in diameter and 6 mm in height appeared and was used for the following autologous implantation (Figure 1.1A). The general outline of this method of construction has already been reported (Nakayama et al., 2013; Ishihara et al., 2014).

For animal No. 3, at least 1.2×10^8 AT-MSCs were used to produce each autologous construct. The cells were inoculated into twenty-four 96-well plates (Sumitomo Bakelite) with 5×10^4 cells per well. After undisrupted incubation fro 48 h, the cells formed spheroids with a diameter of about 700 μm in the bottom of the wells. About 2300 spheroids were placed in a cylindrical mold and incubated in CCM until implantation (7 days). When the mold was carefully removed, a columnar construct of 6 mm in diameter and 8 mm in height appeared (Figure 1.8A). They were used for the following autologous implantation (Figure 1.8C). This process was repeated to make this columnar construct. The general outline of this method of construction has already been reported (Nakayama et al., 2013, Ishihara et al., 2014).

1.2.7 Implantation of the three-dimensional construct of AT-MSCs

The implant surgery was performed under general anesthesia using oxygen and isoflurane inhalation following pre-medication with sedatives and analgesics. Both femoropatellar joints were incised from the outside, and the femoral trochlear groove was exposed. Using a surgical trephine with an outer diameter of 4 mm, the articular cartilage and the subchondral bone were drilled to a depth of 6 mm at the center of the groove for Animal No. 1 and Animal No. 2. After removing a column of cartilage and bone, a cylindrical osteochondral defect was created in each groove (Figure 1.1B). A columnar construct (4 mm in diameter and 6 mm in height) composed of spheroids of AT-MSCs was autografted into the osteochondral defect in the right hind limb (Figure 1.1C), while no graft was implanted into the defect in the left limb (control defects, Figure 1.1B).

Using a surgical trephine with an outer diameter of 6 mm for Animal No. 3, the articular cartilage and the subchondral bone were drilled two coupled holes to a depth of 8 mm at the center of the groove. Taking out two column of osteocartilage and trimming the edge between two columnar defects, an elliptic cylindrical osteochondral defect was created in each groove (Figure 1.8B). Two columnar construct (6 mm in diameter and 8 mm in height) composed of spheroids of AT-MSCs was autografted into the osteochondral defect in the right hind limb (Figure 1.8C), and nothing was implanted into the defect in the left limb (control defects, Figure 1.8B).

1.2.8 CT assessment of the osteochondral defects

Postoperatively, the implants and the osteochondral defects were followed up

every month for 6 months after surgery in Animal No. 1 and for 12 months in Animal No. 2 using computed tomography (CT) scans of both stifles. For assessment, longitudinal section images were obtained at the maximum diameter in the lateral views of the cylindrical defect and the maximum diameters of the radiolucent area in the images were evaluated at 0.5-mm intervals between 0 and 4 mm.

In Animal No. 3, the implants and the osteochondral defects were followed up every month for 12 months after surgery using computed tomography (CT) scans of both stifles. As shown in the figures, longitudinal section images were obtained at the maximum diameter in the lateral views of the elliptic cylindrical defect.

1.2.9 MR assessment of the osteochondral defect

The implants and the osteochondral defects were examined at 12 months after surgery using magnetic resonance (MR) imaging of both stifles. For assessment, longitudinal section images were obtained at the maximum diameter in the lateral views of the elliptic cylindrical defect. The maximum diameters of the defect in the images were evaluated at 2-mm intervals.

1.2.10 Pathological assessment of the ostechondral defects

Animal No. 1 was euthanized at 6 months after the surgery, and Animal No. 2 was euthanized at 12 months after surgery. The macroscopic findings were scored with the ICRS gross grading scale (Table 1.3). Both distal femurs were fixed in 10% NBF for 1 week and then longitudinally sectioned parallel to the trochlear groove. The tissue was paraffin embedded following decalcification with formic acid for 1 week, and embedded in paraffin. Serial sections (3-μm thickness) were placed on glass slides and

evaluated by Masson trichrome saining, and alcian blue staining, and immunohistochemistry using specific antibodies against collagen type II (Col-II; 1:100 dilution; Daiichi Fin Chemicals, Takaoka, Japan) and an Avidin-Biotin Enzyme Complex system (VECTASTAIN ABC Standard Kit; Vector Laboratories, Southfield, MI). The histopathologic findings were also scored with the ICRS histological grading scale (Table 1.4).

Animal No. 3 was euthanized at 12 months after surgery. The macroscopic findings were scored with the ICRS gross grading scale (Table 1.6). The histopathologic findings were also scored with the ICRS histological grading scale (Table 1.7).

1.3 Results

1.3.1 Genetic characteristics of AT-MSCs

Porcine AT-MSCs adhering to the bottom of the culture dish were spindle shaped and proliferated well (Figure 1.2A), reaching over 1×10^6 and 1×10^7 cells at Passage 3 and Passage 4, respectively. The genetic markers of OCT-4, SOX-2, KLF-4, C-MYC, and NANOG were all positive (Figure 1.4A).

1.3.2 Molecular characteristics of AT-MSCs

A strong shift in MFI on flow cytometry was detected with antibodies against CD90 and CD105 (Figure 1.3A,B), while no signals were detected with antibodies against CD34 and CD45 (Figure 1.3C,D).

1.3.3 Multipotency of AT-MSCs

1.3.3.1 Osteogenic differentiation

Following osteogenic induction, AT-MSCs aggregated and contracted to form a colony (Figure 1.2B), and expressions of specific marker genes including ALP, OC, and ON were detected (Figure 1.4B). These cells also showed appropriate characteristics of the stroma, including staining with alizarin red, indicating the presence of calcium apatite crystals (Figure 1.2B).

1.3.3.2 Chondrogenic differentiation

RT-PCR of AT-MSCs placed in chondrogenic induction medium revealed the expressions of marker genes, including SOX-9 and AGG (Figure 1.4B). Histological

observation of the cell pellets showed a hyaline cartilage-like structure that was positively stained with alcian blue (Figure 1.2C).

1.3.3.3 Adipogenic differentiation

Adipogenic induction of the AT-MSCs resulted in adipocyte-like flattened cells with small lipid vesicles that were positively stained with oil red O (Figure 1.2D). RT-PCR revealed a significant increase in adipogenic marker genes expressions such as AP2 and PPAR-γ2 (Figure 1.4B).

1.3.4 CT images and grades of the defects

The reduction in the subchondral radiolucent area of the implanted site became more dramatic at 2 or 3 months after surgery compared with the control site in the both animals (Figure 1.5). CT images at 6 months after surgery for Animal No. 1 are shown in Figure 1-5A. A radiopaque area emerged from the boundary between the bone and the implant and increased more steadily upward and inward for the implanted defect (the right femur) as time passed after the surgery, compared with the control site in Animal No. 1. The radiolucent area of the implant diminished in a stepwise and then degraded to a diameter of 1 mm by 5th month after surgery. CT images at 12 months after surgery for Animal No. 2 are shown in Figure 1.5B. A radiopaque area of the implant emerged in the same manner as in Animal No. 1, gradually progressed, and then filled the entire osteochondral defect at 12 months after surgery. On the other hand, in the control site, a radiopaque area emerged in the shallow layer, but subchondral bone formation was not completed at all in the deep layer. The maximum diameter of the radiolucent area in the implanted site diminished stepwise manner and became 0 mm at

12 months after surgery. The control site remained at a diameter of 2.5 mm.

CT images at 12 months after surgery for Animal No. 3 are shown in Figure 1.9. A radiopaque area emerged from the boundary between the bone and the implant and increased more steadily upward and inward for the implanted defect (the right femur) as time passed until 6 months after the surgery, compared with the control site. And then, radiopaque areas of the implant gradually progressed, and then entirely filled the entire osteochondral defect at 12 months after surgery. On the other hand, in the control site, radiolucency was remained in the shallow layer and subchondral bone formation was also not completed at all in the deep layer.

1.3.5 MR images of the defect

MR images in the implanted site showed that the signal pattern at the surface of articular cartilage was restored near to the normal pattern of surrounding sound cartilage, and the new bone formations under the cartilaginous tissue was almost complete (Figure 1.9). On the other hand, images in the control site showed that low intencity on the surface layer of the defect seemed to be fiblous tissue and high intencity on the deep layer seemed to be adipose tissue (Figure 1.9).

1.3.5 Macroscopic appearance, histopathology, and grades of the defects

Macroscopic examination of Animal No. 1 revealed that the surface of the implanted defect was covered with the abundant cartilaginous white tissues (Figure 1.6A), while cartilaginous tissue was scarce and the surface was depressed in the control site (Figure 1.6B). Similarly, in Animal No. 2, the surface was quite uniformly covered

with abundant cartilaginous white tissues and the boundary to the surrounding normal cartilage was unclear in the implanted site (Figure 1.6C), compared with the finings at the control site (Figure 1.6D). The average macroscopic scores for the implanted site were higher than those for the control site in Animal No.1, while the differences between the scores for the implanted site and the control site were decreased in Animal No. 2 (Table 1.3).

Histopathological sections of Animal No. 1 at 6 months after surgery showed that thickened fibrocartilage had developed over the subchondral bone that was regenerating in the implanted site (Figure 1.7A,B). The surface of the cartilage was smooth, and the boundary with the surrounding normal cartilage was obscure at the implanted site (Figure 1.7A). Meanwhile, the surface was collapsed and irregular at the control site (Figure 1.7C,D). The fibrocartilage showed more intense alcian blue staining and Col-II immunostaining at the implanted site (Figure 1.7E,F) compared with the control site (Figure 1.7G,H). In Animal No. 2 at 12 months after surgery, partially thickened fibrocartilage was mounted on the developed subchondral bone at the implanted site (Figure 1.7I,J). The surface of the cartilage was smooth, and the boundary with the surrounding normal cartilage was obscure, although small areas of endochondral ossification persisted at the center, and small amounts of adipose tissue had differentiated at the bottom part of the site (Figure 1.7I). Subchondral bone was symmetrically reconstructed in the defect and was covered by a mixed matrix of hyaline cartilage and fibrocartilage, in which clusters and columnar clusters of cells were observed (Figure 1.7J). In the control site, fibrocartilage had immediately covered the defect, but the subchondral ossification was poor (Figure 1.7K,L). The hyaline cartilage showed more intense and uniform alcian blue staining and Col-II immunostaining at the implanted site (Figure 1.7M,N) compared with the control site (Figure 1.7O,P). The

average of histologic scores for the implanted sites were distinctly higher than those of the controls in both animals (Table 1.4).

Macroscopic examination of Animal No. 3 showed that the surface was uniformly covered with abundant cartilageous white tissues, but the boundary to the surrounding normal cartilage was clear in the implanted site (Figure 1.10A), as same as the control site (Figure 1.10B). Averages of macroscopic scores of the implanted sites were higher than those of the controls in both animals (Table 1.6).

The histopathological sections of Animal No. 3 showed that partially thickened fibrocartilage was mounted on the developed subchondral bone in the implanted site (Figure 1.10C,D). The surface of the cartilage was smooth, and the boundary with the surrounding normal cartilage was obscure, although small areas of endochondral ossification persisted at the center, and small amounts of adipose tissue had differentiated at the bottom part of the site (Figure 1.10C). On the control site, the fibrocartilage immediately covered the defect, but the subchondral ossification was poor (Figure 1.10G,H). The hyaline cartilage was stained more intensely and uniformly with alcian blue and Col-II immunostaining in the implanted site (Figure 1.10E,F) compared to the control site (Figure 1.10I,J). Averages of histologic scores of the implanted sites were distinctly higher than those of the controls in both animals (Table 1.7).

1.4 Discussion

Human AT-MSCs have been shown to be positive for CD90, which suppresses the cancerization of stem cells (Zola et al., 2007), and CD105, which is associated with the cellular response to blood vessel formation and TGF-β1 (Zola et al., 2007). The porcine AT-derived and spindle-shaped cells adhering to the bottom of the culture dish in the present study were strongly positive for CD90 and CD105. CD34, which is involved in cell adhesion and is expressed in hematopoietic stem cells (Zola et al., 2007), and CD45, which activates T and B lymphocyte receptors in hematopoietic cells (Zola et al., 2007), were both negative in the porcine AT-derived cells. Because human hematopoietic cells but not human MSCs were positive for these molecules (Chen et al., 2011; Guo et al., 2006), the porcine AT-derived cells may not be contaminated with hematopoietic cells (Casado et al., 2012). Genetic markers specific for human MSCs, such as SOX-2, OCT-4, and NANOG (Riekstina et al., 2009), KLF-4, and C-MYC (Windmolders et al., 2014), were detected in the porcine cells by RT-PCR (Tang et al., 2012). Moreover, the osteogenic, chondrogenic, and adipogenic potential of the cells was confirmed, and we therefore defined them as porcine AT-MSCs.

In accordance with a previously described original procedure, we constructed scaffold-free 3D implants (diameter: 4 mm; height: 6 mm) composed of 760 spheroids each containing 5×10^4 autologous AT-MSCs. The 3D multicellular constructs were implanted into osteochondral defects in pigs and followed up using CT to observe bone regeneration in the defect. In Animals No. 1 and 2, radiopaque ossification emerged and increased from the boundary between the bone and the construct. The reduction in the subchondral radiolucent area of the implanted sites became more dramatic 2 or 3 months after surgery compared to the control sites (Figure 1.5). Thus, the difference in

bone regeneration compared to the control site can be observed using CT at least 3 months after implantation. Subsequently, the radiolucent areas diminished upward and inward and became grade 1 at 6 or 7 months and grade 0 at the 12th month after implantation. The cross-sectional CT images obtained 6 and 12 months after implantation in Animals No. 1 and Animal No. 2, respectively, may mirror the histology because the localization, size, and shape of the radiolucent and radiopaque areas entirely corresponded with those of the fibrocartilage and regenerated bone. To further discriminate between cartilaginous and fibrous tissues in the radiolucent area, magnetic resonance imaging should be used.

The higher average macroscopic scores may suggest better improvement in superficial features at the implanted sites, compared with the control site (Table 1.3). However, the differences in the average scores between the control and implanted sites were lower in Animal No. 2 (euthanized at 12 months after surgery) than in Animal No. 1 (euthanized at 6 months after surgery). All four features in the ICRS gross grading scale system, including coverage, neocartilage color, defect margins, and surface, were improved at the implanted site compared with the control site in Animal No. 1, whereas a difference in neocartilage color only was seen between the two sites in Animal No. 2. The results in Animal No. 2 were not consistent with a previous study using rabbits, in which a more degraded macroscopic appearance of the control defect (diameter: 4.8 mm; depth: 5 mm) was observed at 12 months after implantation (Ishihara et al., 2014). Based on the results, we speculate that the superficial features may improve spontaneously from 6 to 12 months after surgery for this size of osteochondral defect (diameter: 4 mm; depth: 6 mm) in MMPigs. To discriminate the superficial features caused by spontaneous repair from those caused by MSC-based regeneration in this size of defect, further evaluation of the pathology at 6 months after surgery will be

appropriate in MMPigs. Other studies are needed to determine methods for repairing osteochondal defects with larger diameters and depths, which could never repair by themselves (Figure 1.9 and 1.10).

We also obtained higher average histologic scores at the implanted sites in both animals, which may indicate desirable osteochondral recovery compared with the controls in both animals (Table 1.4). As summarized in Table 1.5, regarding the histological features in Animal No. 1, distinct differences were observed in the surface, matrix, subchondral bone, and cartilage mineralization between the implanted and control sites. At the implanted sites, a smooth and continuous surface was restored by thickened fibrocartilage. Underneath that, endochondral ossification progressed upward and inward from the boundary between the construct and bone. The results distinctly suggest fibrocartilage formation and endochondral ossification during the process of MSC-based regeneration were present at the implanted site, compared with features such as an irregular surface, fibrous granulation matrix, and inappropriate cartilage mineralization in the control defect. On the other hand, in Animal No. 2, a smooth and continuous articular surface was restored through cartilage formation at both sites, but subchondral bone was distinctly more satisfactory at the implanted site than at the control site, in which the trabecular pattern was completely absent (bone was detached) in the bottom half of the defect. Subchondral bone was symmetrically reconstructed in the defect and was covered by a mixed matrix of hyaline cartilage and fibrocartilagein which clusters and columnar clusters of cells were observed at the implanted site. These findings were similar to data reported previously reported in rabbits (Ishihara et al., 2014), and may suggest transformation of fibrocartilage into hyaline cartilage during the process of MSC-based osteocartilage regeneration. Because neither hyaline cartilage nor cell clusters were seen in the implanted defect site in Animal No. 1, transformation of

fibrocartilage into hyaline cartilage may begin between 6 and 12 months after implantation. However, more time may be required to regenerate pure, high-quality hyaline cartilage as well as complete subchondral regeneration in the implanted defect.

Similarly, partially thickened fibrocartilage at the center of the defect also suggests that a longer time may be needed to complete subchondral regeneration. In addition to previous studies investigating bone and cartilage regeneration using scaffold-free MSC implantation (Koga et al., 2008; Dashtdar et al., 2011; Lee et al., 2011; Yoshioka et al., 2011; Suzuki et al., 2012; Toghraie et al., 2012). Consistent with a previous study on rabbits (Ishihara et al., 2014), we report here the successful outcome of osteochondral regeneration with scaffold-free AT-MSC constructs in MMPigs. Although further studies will be required, we conclude that implantation of a scaffold-free 3D construct of AT-MSCs into an osteochondral defect will regenerate the original structure of the cartilage and subchondral bone over the course of 1 year.

Table 1.1 List of PCR primers

Marker	Gene	Sequence (Forward / Reverse)	Ann. Temp. (℃)	Fragment (bp)
Premature	Oct4	5'-GTCGCCAGAAGGGCAAAC-3' 5'-CAGGGTGGTGAAGTGAGGG-3'	57.0	157
	Sox2	5'-CCCTGCAGTACAACTCCATGAC-3' 5'-GGTGCCCTGCTGCGAGTA-3'	59.0	85
	Klf4	5'-CGGCAAAACCTACACGAAGAGT-3' 5'-AGTTCATCTGAGCGGGCAAAT-3'	59.0	119
	Nanog	5'-CTTATTCAGGACAGCCCTGATTCTTC-3' 5'-AAGACGGCCTCCAAATCACTG-3'	59.0	613
	c-Myc	5'-GGATTCCGCCTCGTT-3' 5'-TCTCCAAGCATCACTCG-3'	55.1	184
Osteogenic	ALP	5'-ATGAGCTCAACCGGAACAA-3' 5'-GTGCCCATGGTCAATCCT-3'	56.0	131
	OC	5'-TCAACCCCGACTGCGACGAG-3' 5'-TTGGAGCAGCTGGGATGATGG-3'	68.0	204
	ON	5'-TCCGGATCTTTCCTTTGCTTTCTA-3' 5'-CCTTCACATCGTGGCAAGAGTTTG-3'	57.5	187
Chondrogenic	Sox9	5'-CCGGTGCGCGTCAAC-3' 5'-TGCAGGTGCGGGTACTGAT-3'	57.5	119
	AGG	5'-TTCCCTGAGGCCGAGAAC-3' 5'-GGGCGGTAATGGAACACAAC-3'	65.5	194
Adipogenic	PPARγ2	5'-GCGCCCTGGCAAAGCACT -3' 5'-TCCACGGAGCGAAACTGACAC-3'	59.8	238
	aP2	5'-GGCCAAACCCAACCTGA-3' 5'-GGGCGCCTCCATCTAAG-3'	59.8	167
Housekeeping	GAPDH	5'-ACCACAGTCCATGCCATCAC-3' 5'-TCCACCACCCTGTTGCTGTA-3'	60.0	450

Oct4, octamer-binding transcription factor 4; Sox2, sex determining region Y box 2; Klf4, kruppel-like factor 4; Nanog, homeobox protein NANOG; C-Myc, cellular myelocytomatosis oncogene; ALP, alkaline phosphatase; OC, osteocalcin; ON, osteonectin; Sox9, sex determining region Y-box 9; AGG, aggrecan; PPARγ2, peroxisome proliferator-activated receptor γ2; aP2, adipocyte fatty acid binding protein 2; GAPDH, glyceraldehyde-3-phosphate dehydrogenase.

Table 1.2 List of antibodies

Antibody	Company	Clone	Epitope	Dilution
CD34	BD	581	O-glycosylated transmembrane glycoprotein	1:5
CD45	BD	2D1	T200 family	1:2.5
CD90	BD	5E10	N-glycosylated GPI-linked membrane glycoprotein	1:10
CD105	Abcam	MEM229	Disulfide-linked glycoprotein homodimer	1:20
Isotype	BD	MOPC-21	(Not comfirmed)	1:10

Tabel 1.3 ICRS gross grading scale

Feature		Score	Animal No. 1		Animal No. 2	
			Control Site	Implanted site	Control Site	Implanted site
Coverage	>75% fill	4	2	3	4	4
	50-75% fill	3				
	25-50% fill	2				
	<25% full	1				
	No fill	0				
Neocartilage color	Normal	4	1	2	3	4
	25% yellow/brown	3				
	50% yellow/brown	2				
	75% yellow/brown	1				
	100%yellow/brown	0				
Defect margins	Invisible	4	1	2	3	3
	25% circumference visible	3				
	50% circumference visible	2				
	75% circumference visible	1				
	Entire circumference visible	0				
Surface	Smooth/level with normal	4	0	2	3	3
	Smooth but raised	3				
	Irregular 25-50%	2				
	Irregular 50-75%	1				
	Irregular >75%	0				
Average			1.0	2.25	3.25	3.5

Table 1.4 ICRS histological grading scale

Feature		Score	Animal No. 1		Animal No. 2	
			Control Site	Implanted site	Control Site	Implanted site
Surface	Smooth/continuous	3	0	3	3	3
	Discontinuities/irregulatrity	0				
Matrix	Hyaline	3	0	1	1	2
	Mixture; hyaline/fibrocartilage	2				
	Fibrocartilage	1				
	Fibrous tissue	0				
Cell distribution	Columnar	3	0	0	0	2
	Mixed/columnar clusters	2				
	Clusters	1				
	Individual cells/disorganized	0				
Viability of cell population	Predominantly viable	3	3	3	3	3
	Partially viable	1				
	<10% viable	0				
Subchondral bone	Normal	3	1	2	0	2
	Increased remodeling	2				
	Bone necrosis/granulation tissue	1				
	Detached/fractue/callus at base	0				
Cartilage mineralization (calcified cartilage)	Normal	3	0	3	3	3
	Abnormal/inappropriate location	0				
Average			0.67	2	1.67	2.5

Table 1.5 Summary of histological features

		Animal No. 1		Animal No. 2	
		Control site	Implanted site	Control site	Implanted site
Cartilage	Surface	Irregularity	Smooth	Smooth	Smooth
	Matrix	fibrous tissue	Fibrocartilage	Fibrocartilage	Mixture; hyaline/fibrocartilage (Transformation)
Subchondral bone		Granulation tissue	Increased remodelling	Detached (in the bottom half of the defect)	Increased remodelling (Endochondral ossification)

Tabel 1.6 ICRS gross grading scale

Feature		Score	Control Site	Implanted site
Coverage	>75% fill	4	4	4
	50-75% fill	3		
	25-50% fill	2		
	<25% full	1		
	No fill	0		
Neocartilage color	Normal	4	3	4
	25% yellow/brown	3		
	50% yellow/brown	2		
	75% yellow/brown	1		
	100%yellow/brown	0		
Defect margins	Invisible	4	1	1
	25% circumference visible	3		
	50% circumference visible	2		
	75% circumference visible	1		
	Entire circumference visible	0		
Surface	Smooth/level with normal	4	2	3
	Smooth but raised	3		
	Irregular 25-50%	2		
	Irregular 50-75%	1		
	Irregular >75%	0		
Average			2.5	3

Table 1.7 ICRS histological grading scale

	Feature	Score	Control Site	Implanted site
Surface	Smooth/continuous	3	3	3
	Discontinuities/irregulatrity	0		
Matrix	Hyaline	3	1	2
	Mixture; hyaline/fibrocartilage	2		
	Fibrocartilage	1		
	Fibrous tissue	0		
Cell distribution	Columnar	3	1	2
	Mixed/columnar clusters	2		
	Clusters	1		
	Individual cells/disorganized	0		
Viability of cell population	Predominantly viable	3	3	3
	Partially viable	1		
	<10% viable	0		
Subchondral bone	Normal	3	0	2
	Increased remodeling	2		
	Bone necrosis/granulation tissue	1		
	Detached/fractue/callus at base	0		
Cartilage mineralization (calcified cartilage)	Normal	3	3	3
	Abnormal/inappropriate location	0		
Average			1.83	2.5

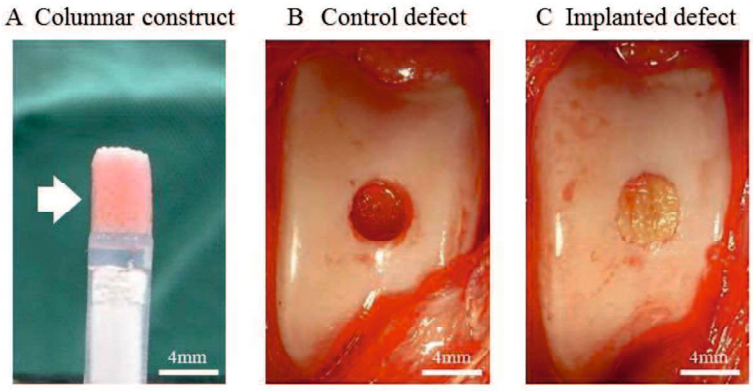

Figure 1.1 Surgical procedure.

A columnar construct (4 mm in diameter and 6 mm in height) for the implantation (A). A cylindrical osteochondral defect in each groove before implantation (B). The construct composed of about 760 spheroids of AT-MSCs was autografted into the osteochondral defect in the right hind limb (C). Nothing was implanted into the left limbs (control defects; B).

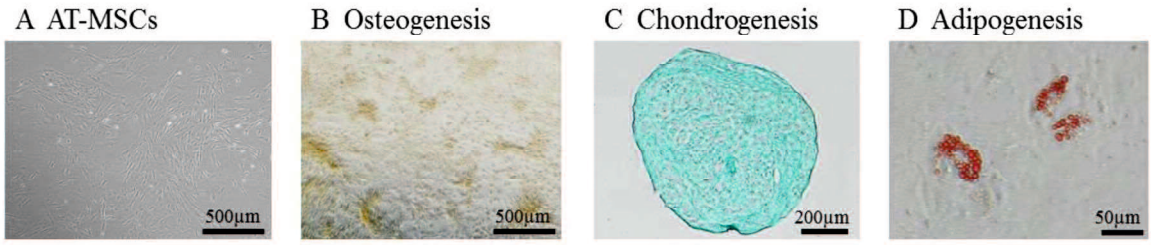

Figure 1.2 Representative images of special staining and RT-PCR results of tri-linage differentiation in AT-MSCs.

AT-MSCs adhering to the bottom of the culture dish were spindle-shaped (A). Following 2 weeks of osteogenic induction, MSCs also showed characteristics of the stroma, including staining with alizarin red, indicating the presence of calcium apatite crystals (B). Observation of the cell pellets that were induced by chondrogenic induction medium for 2 weeks showed a cartilage-like structure that was positively stained with alcian blue (C). Adipogenic induction of the MSCs resulted in adipocyte-like flattened cells with small lipid vesicles that stained positively with oil red O (D).

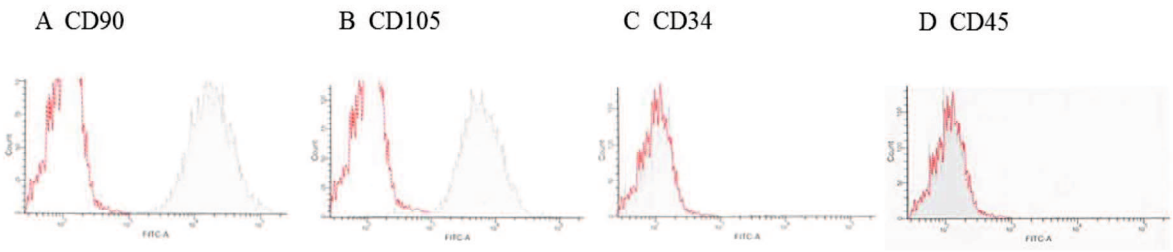

Figure 1.3 Flow cytometry results of immunological markers in AT-MSCs.
A strong shift in MFI was detected with antibodies against CD90 (A) and CD105 (B). Whereas, no signal reaction was detected with antibodies against CD34 (C) and CD45 (D).

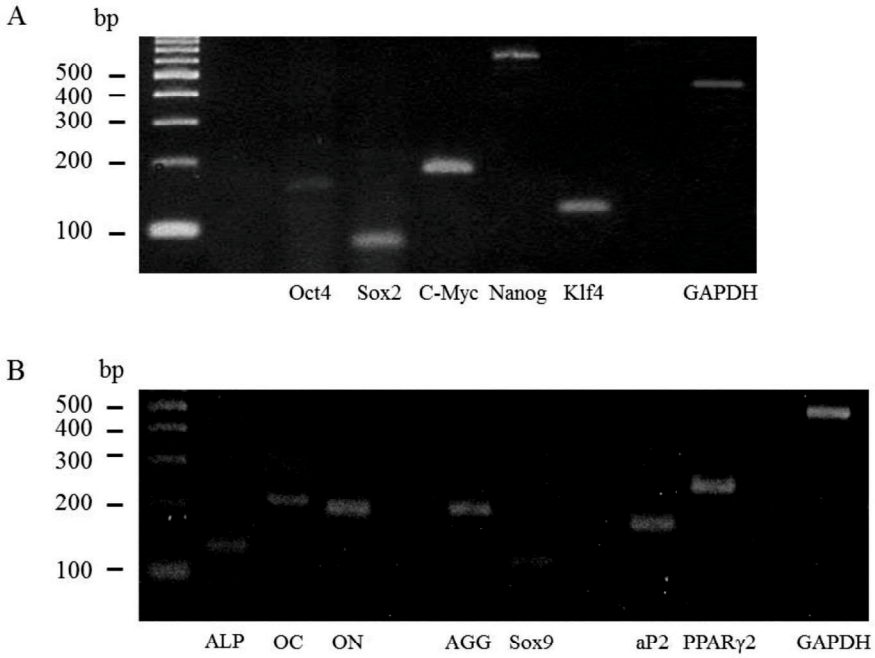

Figure 1.4 RT-PCR results of gene expression in AT-MSCs.

Premature gene expression in AT-MSCs (A) and specific marker gene expression in AT-MSCs induced by tri-linage differentiation medium (B) were confirmed.

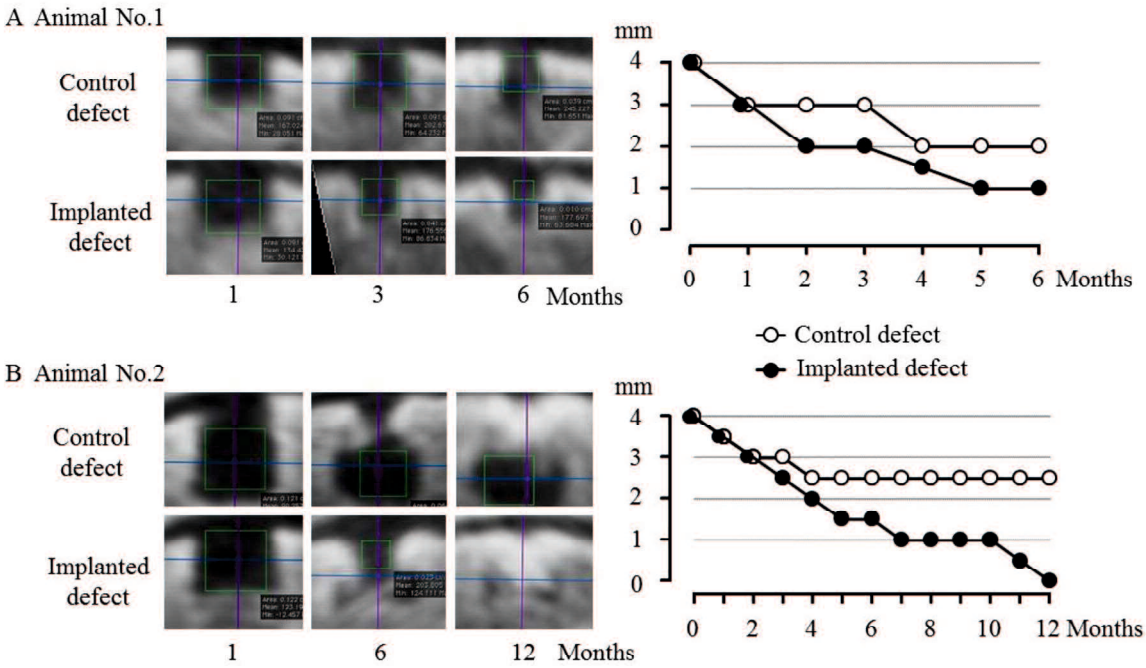

Figure 1.5 CT assessment of osteochondral defects.

Upper image shows one cross-section of the multi-planar reconstruction images 1, 3, and 6 months after the surgery in Animal No.1 (A). Lower image shows one cross-section of the multi-planar reconstruction images 1, 6, 12 months after the surgery in Animal No.2 (B). CT grade representing the radiolucent areas diminished earlier at the implanted defects in the both animals.

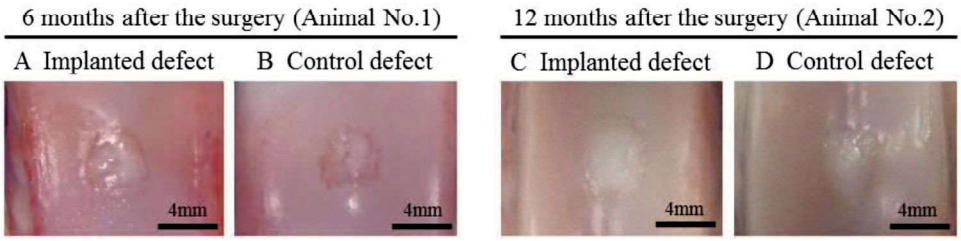

Figure 1.6 Macroscopic findings of the surface of the implanted and control sites.

In animal No. 1, the surface of the implanted defect was covered with the abundant cartilageous white tissues (A), whereas the cartilageous tissue was scarce and the surface was depressed in the control site (B). In animal No. 2, the surface was more uniformly covered with abundant cartilageous white tissues and the boundary to the surrounding normal cartilage was unclear in the implanted site (C), comparing to those of the control site (D).

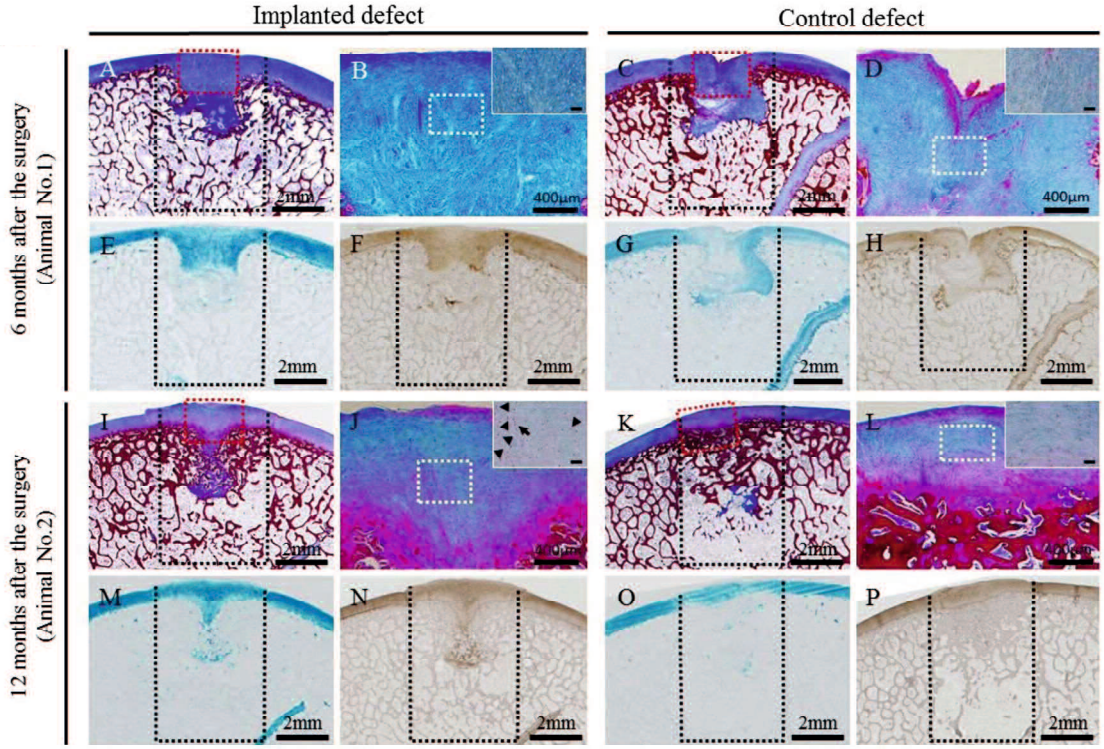

Figure 1.7 Histopathology of osteochondral defects using masson's trichrome, alcian blue and immunohistochemical staining of type II collagen.

In Animal No. 1, articular surface was smooth and fibrocartilage developed on the subchondral bone at the implanted site (A, B, E, F), whereas the surface was irregular and fibrous tissue lay over the subchondral bone at the control site (C, D, G, H). At the implanted site in Animal No.1, the subchondral bone was synmetrically reconstructed and was covered by matrix including hyaline cartilage, which was suggested by the clusters (arrowhead) and columnar clusters (arrow) of cells (I, J, M, N). On the other hand, smooth and continuous surface was restored due to fibrocartilage formation, but subchondral bone was absent in bottom half of the defect, at the control site in Animal No. 2 (K, L, O, P). Black dotted lines indicate the areas of osteochondral defects immediately after the surgery. The masson's trichrome staining sections (B, D, J, L) were enlarged from red dotted square in the images A, C, I, and K, respectively. The insert images in the sections B, D, J, and L were enlarged from white dotted square in the images B, D, J, and L, respectively. The bars in the insert images indicate 50 μm.

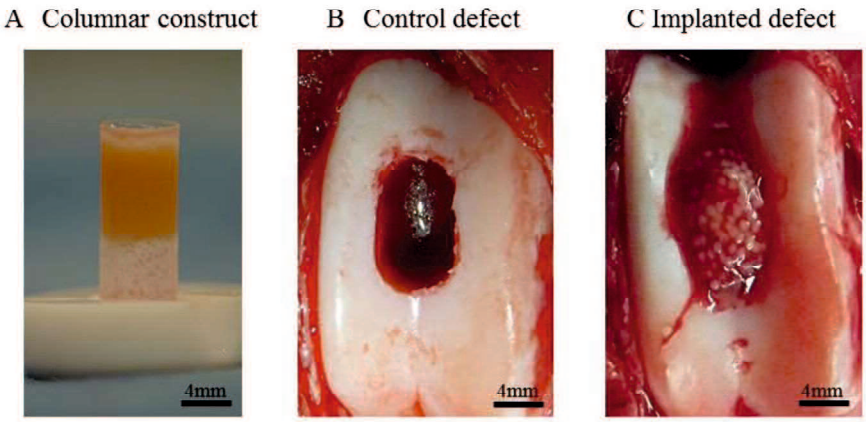

Figure 1.8 Surgical procedure.

A columnar construct (6 mm in diameter and 8 mm in height) composed of about 1150 spheroids of AT-MSCs (A). An elliptic cylindrical osteochondral defect in each groove (B). Two constructs were autografted into the defect of the right hind limb (C). No implantation was in the left limb (B).

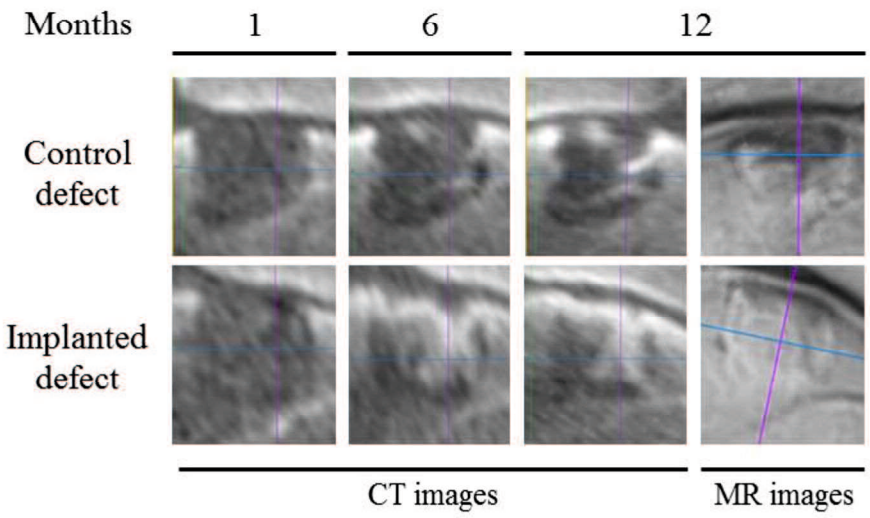

Figure 1.9　CT and MR assessment of osteochondral defects.
One cross-section of the multi-planar reconstruction images 1, 6, and 12 months after the surgery. In the implanted site, the radiopaque area gradually progressed, and filled throughout the osteochondral defect after 12 months. However, in the control site, the spread of radiopaque area was limited in the shallow layer, and no bone formation was in the deep layer. MR images in the implanted site showed that the signal pattern at the surface of articular cartilage was restored near to the normal pattern of surrounding sound cartilage, while the new bone formations under the cartilaginous tissue was incomplete. On the other hand, images in the control site showed that low intencity on the surface layer of the defect seemed to be fiblous tissue and high intencityon the deep layer seemed to be adipose tissue.

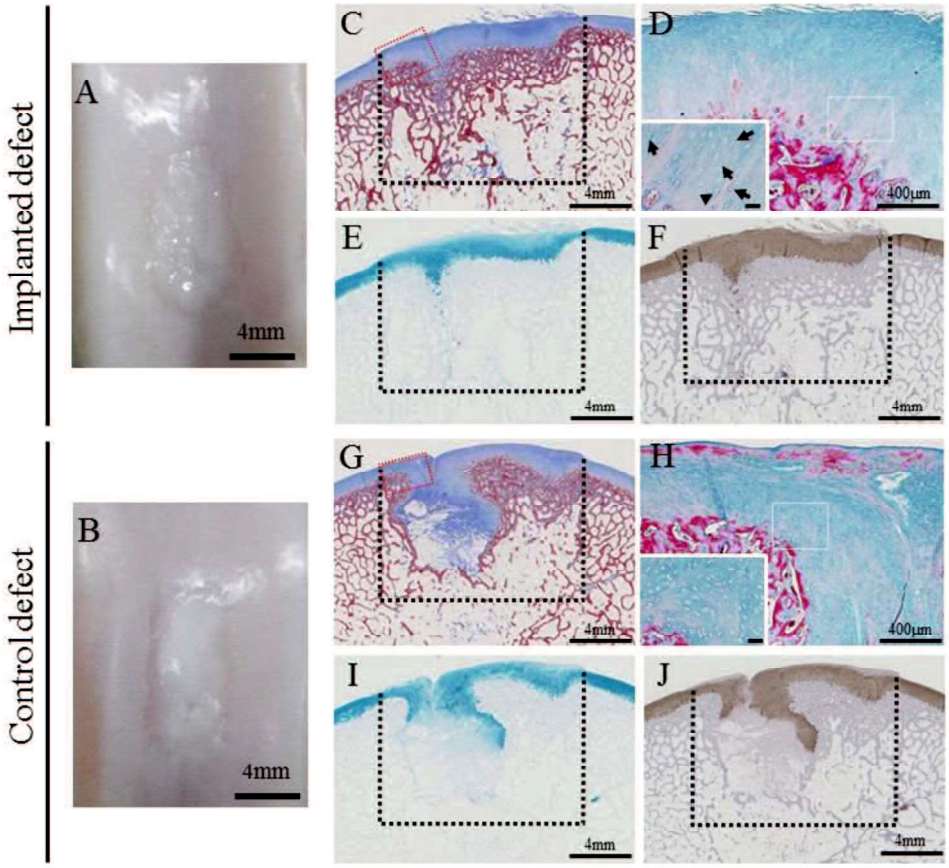

Figure 1.10 Macroscopic findings of the surface and histopathology of osteochondral defects at the implanted and control sites.

The surface was completely covered with abundant cartilageous white tissues. The boundary to the surrounding normal cartilage was not different between the implanted site (A) and the control site (B). At the implanted site, the restored subchondral bone was covered by mixture of hyaline/fibrocartilage, in which the clusters (arrowhead) and columnar clusters (arrow) of the cells were seen (C, D, E, F). In the control site, the surface was irregular, and the large fibrous tissue was presented in the subchondral (area no bone in bottom half of the defect (G, H, I, J). Black dotted lines indicate the areas of osteochondral defects immediately after the surgery. The images B and F are high power fields of red dotted square in the images A and E, respectively. The small images in the sections B and F were high power fields of white dotted squares in the respective images. The bars in the small images indicate 50 μm.

Chapter 2

Osteochondral regeneration on femoral medial condyle (load-bearing surface) using scaffold-free three-dimensional structure of swine adipose tissue-derived mesenchymal stem cells

2.1 Introduction

Osteoarthritis (OA), as defined as cartilage degradation and subchondral bone sclerosis/deformity, is slowly exacerbated not only following cumulative injuries to bone, cartilage, ligament, and the other joint structures (Mankin et al., 1982), but also due to many factors related to senescence, body mass index, and life-style (Ding et al., 2006). To restore joint structure and function in the late stages of OA, surgical strategies for reconstruction of both bone and cartilage have been investigated, some in clinical trials. A clinical report on osteochondral autografts (mosaicplasty) from non-load-bearing sites into the deteriorated sites (loading-bearing sites) showed favorable outcomes following surgery (clinical improvement in 79-94% of OA patients) (Szerb et al., 2005). However, with this therapeutic strategy, the loss of clinically sound cartilage is inevitable, and the obtainable autografts are limited by the large size of the osteochondral defects. Alternatively, a combination of artificial bone and autologous chondrocytes seeded onto a collagen scaffold has also shown favorable restoration of bone and cartilage (Funayama et al., 2008).

New bone can be produced following the implantation of bone filler materials (made of beta-tricalcium phosphate and/or hydroxyapatite) combined with or without bone-inducing substances, because crucial players in bone, the osteoclasts and osteoblasts, degrade the materials and generate the original bone matrix. On the other hand, articular cartilage has been shown to have a lower self-restorative capacity due to its avasculality and hypocellurarity that could also be inappropriate for degrading artificial meterials such as cell-scaffolds. The materials that persist in implanted sites for long period are unsuitable for regenerating articular cartilage consisting of the pure hyaline cartilage, and therefore, we hypothesize that scaffold-free cell implants are more

effective. Previous studies on autologous chondrocyte implantation have revealed problems such as isolation of a few chondrocytes from a small piece of normal cartilage (Fujisato et al., 1996), the small number of obtainable chondrocytes after in vitro culture (Fujisato et al., 1996), and dedifferentiation of chondrocytes during the culture passage (Diaz-Romero et al. 2005). To resolve these problems, studies on bone and cartilage regeneration using stem cells have recently been reported (Tatebe et al., 2005). Mesenchymal stem cells (MSCs) derived from bone marrow (BM), adipose tissue (AT), and synovium (SM) have been shown to differentiate into bone and cartilage in vitro (Pittenger et al., 1999; Zuk et al., 2002; Nimura et al., 2008). Among them, we expect that a therapeutic strategy using AT-MSCs would be acceptable for many OA patients. AT, which plays crucial roles in energy storage, shock absorbance, heat insulation, and endocrine function, might be unnecessary in OA patients with obesity and increased body mass index. If the AT that is eliminated to reduce a patient's weight can be utilised as a source of autologous MSCs, the regenerative strategy of bone and cartilage involving the use of AT-MSCs could be the most reasonable application for OA patients. It has been reported that AT-MSCs could little differentiate into chondrocytes (Nakamura et al., 2012). However, a recent study using rabbits and pigs presented bone and cartilage regeneration after implanting a scaffold-free three-dimensional (3D) construct of AT-MSCs into an osteochondral defect (Ishihara et al., 2014). These studies were designed to evaluate the autologous implantation in the non-load-bearing sites, where the osteochondral defects were generated subsequent to the mosaicplasty. Therefore, the aim of this study was to evaluate the regeneration of articular cartilage and subchondral bone after implanting a 3D construct of autologous AT-MSCs in the load-bearing site, where the osteocartilage may be mainly deteriorated in OA.

2.2 Materials & Methods

2.2.1 Animals

Five mini-pigs (Nippon Institute for Biological Science, Osaka, Japan), denoted animal Nos. 1 to 5 were used in this study. Their body weights and ages were 25.6 kg and 22 months (No.1), 25.4 kg and 22 months (No.2), 27.6 kg and 22 months (No.3), 25.6 kg and 22 months (No.4), and 26.0 kg and 22 months (No.5). And also, one male MMPigs (Fuji Micra, Shizuoka, Japan) designated Animal No.6 was used in this study. The body weight and age were 24.0 kg and 24 months. All procedures in this study were approved by the Animal Care and Use Committee of Kagoshima University (Approval No. A11037 and No. D13025).

2.2.2 Isolation and expantion of AT-MSCs

Fifteen to twenty grams (in Animal No. 1 to No. 5) and ten to fifteen grams (in Animal No. 6) of cervical adipose tissue per animal was aseptically obtained under general anesthesia. The adipose tissues were minced and digested for 90 min in phosphate-buffered saline (PBS) containing 0.1% collagenase type I (Collagenase Type I; Worthington Biochemical, Lake Wood, NJ). The digested cell suspensions were filtered through a 70-μm pore diameter membrane (BD, Franklin Lakes, NJ) and centrifuged at 160 × *g* for 5 min at room temperature. After decanting the supernatant, the pellet was rinsed with PBS and centrifuged. After decanting the supernatant, the pellet was resuspended and plated in a 150-cm^2 culture dish (Tissue Culture Dish ϕ 150; TPP, Trasadingen, Switzerland) in complete culture medium (CCM): Dulbecco's Modified Eagle's Medium (DMEM; Life technologies, Carlsbad, CA) containing 10% fetal bovine serum (FBS; Thermo Fisher Scientific, Waltham, MA) and 1%

antibiotic-antifungal preparation (100 U/mL Penicillin G, 100 μg/mL streptomycin, 0.25 μg/mL amphotericin B; Antibiotic-Antimycotic; Life technologies). Following incubation at 37 °C in 5% CO_2 for 7 days, the cells adhering to the bottom of the dish were washed with PBS and cultured in CCM. The medium was changed on the 7th day (D7) in Passage 0 (P0). The cells were harvested with 0.25% trypsin and 1mM ethylenediaminetetraacetate (Trypsin-EDTA; Life technologies, Carlsbad, CA) diluted by adding five volumes of PBS and centrifuged on the 10th day (D10). After decanting the supernatant, the pellet was rinsed with CCM, and the cells were replated at 5×10^5 cells in 150-cm^2 dishes and cultured for 6 days. The medium was changed every 3 days for 6 days in P1. This serial process of passaging was repeated until the analysis and the creation of a plug.

2.2.3 Preparation of 3D constructs of AT-MSCs

At least 1×10^8 AT-MSCs were used to produce an autologous construct for each of animal Nos. 1 to 5. The cells were inoculated into twenty 96-well plates (Sumitomo bakelite, Tokyo, Japan) with 5×10^4 cells per well. After the plates were incubated undisrupted for 48 h, the cells formed a spheroid with a diameter of approximately 700 μm in the bottom of the well. Approximately 1920 spheroids were placed into a cylindrical mold and incubated in CCM until implantation (7 days). When the mold was carefully removed, a columnar construct that was 6.3 mm in diameter and 6 mm in height appeared and was used for the subsequent autologous implantation (Figure 2.1A).

For animal No. 6, at least 1.5×10^8 AT-MSCs were used to produce an autologous construct. Approximately 2880 spheroids were placed into a cylindrical mold and

incubated in CCM until implantation (7 days). When the mold was carefully removed, a columnar construct that was 6.3 mm in diameter and 10 mm in height appeared and was used for the subsequent autologous implantation (Figure 2.9A). The general outline of this method of construction has been previously reported (Nakayama et al., 2013).

2.2.4 Implantation of the 3D constructs of AT-MSCs

The implant surgery was performed under general anesthesia using oxygen and isoflurane inhalation following pre-medication with sedatives and analgesics. Both femorotibial joints were incised from the outside, and the femoral medial condyle was exteriorized. Using a surgical trephine with an outer diameter of 6.8 mm, the articular cartilage and the subchondral bone were sawed to a depth of 6 mm in the center of the condyle in animal Nos. 1 to 5. By removing a column of cartilage and bone, a cylindrical osteochondral defect was created in each medial condyle (Figure 2.1B). A columnar construct (6.3 mm in diameter and 6 mm in height) composed of spheroids of AT-MSCs was autografted into the osteochondral defect in the right hind limb (Figure 1C), and nothing was implanted into the left limbs (control defects, Figure 2.1B).

Using a surgical trephine with an outer diameter of 6.8 mm, the articular cartilage and the subchondral bone were sawed to a depth of 10 mm in the center of the groove in animal No. 6. By removing a column of cartilage and bone, a cylindrical osteochondral defect was created in each medial condyle (Figure 2.9B). A columnar construct (6.3 mm in diameter and 10 mm in height) composed of spheroids of AT-MSCs was autografted into the osteochondral defect in the right hind limb (Figure 2.9C), and nothing was implanted into the left limbs (control defects, Figure 2.9B).

2.2.5 CT assessment of the osteochondral defects

The implants and the osteochondral defects were followed up every 3 months for 6 months (0, 3, and 6 months) after surgery using computed tomography (CT) scans of both stifles in animal Nos. 1 to No. 5. In animal No. 6, they were followed up every month for 12 months after surgery. As shown in the figures, longitudinal section images were obtained in the lateral views of the cylindrical defect with 0.5-mm slice thickness. The dimsension of the defect in each sectional image was measured, and these areas were integrally caluculated to a volume of the defect as a radiolucent volume (RV, mm^3)

2.2.6 MR assessment of the osteochondral defects

The implants and the osteochondral defects were followed up every 3 months for 6 months (0, 3, and 6 months) after surgery using magnetic resonance (MR) imaging of both stifles in Animal No. 1 to Noi. 5. In Animal No. 6, they were imaged at 12 months after surgery. The findings of MR images were also scored using a modified 2D-MOCART grading scale.

2.2.7 Pathological assessment of the ostechindral defects

All mini-pigs were euthanized 6 months after surgery, and the macroscopic findings were scored using the ICRS gross grading scale. Both distal femurs were fixed in 10% NBF for 2 weeks and then longitudinally sectioned parallel to the trochlear groove. The tissue was paraffin embedded following decalcification with formic acid for 1 week. Serial sections (3-μm thick) were placed on glass slides and evaluated with Masson's trichrome and safranine O staining. The histopathological findings were also scored using the ICRS histological grading scale.

The MMPig was euthanized 12 months after the surgery, and the macroscopic findings were scored using the ICRS gross grading scale (Table 2.2). Both distal femurs were fixed in 10% NBF for 1 week and then longitudinally sectioned parallel to the trochlear groove. The tissue was paraffin embedded following decalcification with formic acid for 1 week. Serial sections (3-μm thick) were placed on glass slides and evaluated with Masson's trichrome, and alcian blue staining, and immunohistochemistry using specific antibodies to collagen type II (Col-II; 1:100; Daiichi fin chemical, Takaoka, Japan) and ABC system (Vector Laboratories, Southfield, MI, USA). The histopathological findings were also scored using the ICRS histological grading scale (Table 2.3).

2.2.8 Statistical analysis

All numeric data are presented as the mean ± standard deviation (SD). The changes in RV in relation to the time course were analyzed using the paired t-test. The significant differences in the remaining percentages of RV, modified 2D-MOCART scores, and ICRS scores were analyzed between the implanted sites and the controls, using Student's t-test (Excel, Microsoft). Differences with $p < 0.05$ were considered to be statistically significant.

2.3 Results

2.3.1 CT images and radiolucent volume (RV) of the defect

In animal Nos. 1 to 5, a radiopaque area emerged from the boundary between the bone and the implant in the defects and increased more steadily upward and inward on the implanted sites than the control sites (Figure 2.2A,B,C,D,E). The average of RV (radiolucent volume) values in the both defects were significantly decreased at the 3rd (0.10 ± 0.04 and 0.12 ± 0.04 mm^3 in the implanted and the control sites, respectively) and the 6th months (0.06 ± 0.02 and 0.08 ± 0.03 mm^3 in the implanted and the control sites, respectively) after the surgery compared with those immediately after the surgery (at 0 month, 0.20 ± 0.04 and 0.17 ± 0.06 mm^3 in the implanted and the control sites, respectively). The RVs percentages at the 3rd and 6th months compaired with those at 0 month (that is, the remaining percentages of RV) were significantly decreased in the implanted defects (52.5 ± 16.5 and 30.2 ± 10.4 %, respectively), compared with the control defects (74.5 ± 8.0 and 50.5 ± 13.6 %, respectively) (Figure 2.2F).

In animal No. 6, a radiopaque area emerged from the boundary between the bone and the implant in the defects and increased more steadily upward and inward on the implanted site than the control sites (Figure 2.10A). The RVs in the both defects were significantly decreased at the 3rd and the 6th months after the surgery, compared with those immediately after the surgery. The RVs percentages at the 3rd, 6th, 9th, and 12th months against those at 0 month (that is remaining percentages of RV) were significantly decreased in the implanted defects (33.4, 23.0, 13.1, and 7.0 %, respectively), compared with the control defects (86.8, 66.9, 57.2 and 37.4 %, respectively) (Figure 2.10B).

2.3.2 MR images and modified 2D-MOCART scores of the defects

MR images in the implanted sites of animal Nos. 1, 3, and 4 showed that the signal pattern at the surface of the articular cartilage was restored near to the normal pattern of the surrounding sound cartilage, whereas the formation of new bone under the cartilaginous tissue was incomplete (Figure 2.3A,C,D). High signal intensity indicated that AT predominantly occupied the subchondral area in the implanted sites of animal Nos. 2 and 5 (Figure 2.3B,E). There were significant differences in the outcome measures such as defect fill (8.0 ± 2.4 and 5.0 ± 0.0 in the implanted and control sites, respectively), cartilage interface (6.0 ± 4.9 and 0.0 ± 0.0 in the implanted and control sites, respectively), and signal intensity (5.0 ± 4.4 and 0.0 ± 0.0 in the implanted and control sites, respectively) between the implanted and the control sites (Figure 2.4). The scores of surface ($p = 0.06$), cartilage structure, subchondral lamina and bone, and adhesion ($p = 0.34$) did not differ between both sites (Figure 2.4). Accordingly, the total scores of the modified 2D-MOCART system were significantly increased in the implanted sites (36.0 ± 17.8) compared with the controls (15.0 ± 0.0) (Figure 2.4).

In animal No. 6, MR images in the implanted site showed that the signal pattern at the surface of the articular cartilage was restored near to the normal pattern of surrounding sound cartilage, whereas the formation of new bone under the cartilaginous tissue was incomplete (Figure 2.10A). On the other hand, MR images of the control site showed that the irregularity pattern at the surface of the articular cartilage, and high signal intensity indicating AT predominantly occupied the deep of subchondral area (Figure 2.10A). There were significant differences in the outcome measures such as defect fill (20 and 10 in the implanted and control sites, respectively), cartilage interface

(10 and 0 in the implanted and control sites, respectively), and signal intensity (10 and 0 in the implanted and control site) between the implanted and control site (Table 2.1). The scores of surface, Adhesion, and effusion differ between both sites by five points (Table 2.1). Accordingly, the total scores of the modified 2D-MOCART system were significantly increased in the implanted sites (55) compared with the controls (10) (Table 2.1).

2.3.3 Macroscopic appearance, histopathology, and ICRS scores of the defects

Gross pathology in the implanted sites of animal Nos. 1, 3, and 4 showed higher scores at the points of cartilage including the coverage, the smooth surface, disappearing margin, and the color (Figure 2.5F,H,I). However, there are no significant differences in the outcome measures of ICRS gross scores such as coverage ($p = 0.13$), neocartilage color ($p = 0.13$), defect margin ($p = 0.37$), and surface ($p = 0.09$) between the implanted and the control sites (Figure 2.6). Accordingly, the average gross scores did not significantly differ between the sites (2.3 ± 1.5 and 1.0 ± 0.7 in the implanted and the control sites, respectively) (Figure 2.6). Histopathological findings in animals Nos. 1, 3, and 4 indiated the smooth coverage containing cartilage matrix positively stained by safranine O and the subchondral bone formation in the implanted sites (Figure 2.7A,C,D,F,H,I), whereas a deeply recessed surface and a lower rate of bone formation were observed in the control defects (Figure 2.7K,M,N,P,R,S). The ICRS histologic scores at the points except for subchondral bone were higher in the implanted sites than the control sites in animal Nos. 1, 3, and 4. Animal Nos. 2 and 5 showed that the cartilaginous smooth coverage as well as the subchondral bone did not progress in both

defects (Figure 2.7B,E,G,J,L,O,Q,T), therefore the scores at all points did not differ between the defects. The scores of the histologic outcome measures such as surface, matrix, cell distribution, viability of the cell population, and cartilage mineralization (except for the subchondral bone ($p = 0.14$)) were significantly higher in the implanted sites than those in the control sites (Figure 2.8). The average histological scores were also significantly higher in the implanted sites (1.7 ± 1.0) than in the control sites (0.3 ± 0.2) (Figure 2.8).

In animal No. 6, gross pathology in the implanted sites showed higher scores at the points of cartilage including the coverage, the smooth surface, disappearing margin, and the color (Figure 2.11). However, there are differences (which are not significantly) in the outcome measures of ICRS gross scores such as coverage, neocartilage color, defect margin, and surface between the implanted and the control sites (Table 2.2). Accordingly, the averages of gross scores did differ (which are not significantly) between the sites (3.3 and 1.3 in the implanted and the control sites, respectively) (Table 2.2). Histopathological findings indicated the smooth coverage containing cartilage matrix positively stained by alcian blue and the subchondral bone formation in the implanted sites, whereas a deeply recessed surface and a lower rate of bone formation were observed in the control defects (Figure 2.11). The ICRS histologic scores at the points of cartilage matrix, chondrocyte distribution, subchondral bone, and cartilage mineralization were higher in the implanted sites than the control site (Table 2.3). The average histological scores were also significantly higher in the implanted sites (2.2) than in the control sites (0.6) (Table 2.3).

2.4 Discussion

A radiopaque area emerged from the boundary between the implant and the bone defect, and the RVs in both defects were significantly decreased 3 and 6 months after the surgery, compared with those immediately after the surgery. The results suggest that the subchondral bone formation naturally progressed in both osteochondral defects regardless of AT-MSCs implantation. However, the ratios (%) of RVs at 3rd and 6th months after the surgery compaired with those at 0 month were significantly lower in the implanted sites than in the controls. This indicates that the increased radiopaque area after the surgery could be larger in the implanted sites than in the controls, and that the subchondral bone formation would be increased by the AT-MSCs implantation. The implantation of a scaffold-free 3D construct of AT-MSCs could be a promising medical strategy for the regeneration of the subchondral bone lost in the clinical cases of OA. As presented in this study, the significant effects on bone formation were confirmed 3 months after the implantation using a quantitative analysis of RV in the CT images. On the other hand, given that RVs percentages at the 6th month after the surgery were 30.2±10.4% and 50.5±13.6% in the implanted and control defects, respectively, the subchondral bone formation was not completed for 6 months in this study. We also have a preliminary data showing lower percentages of RV persisting 12 months after the surgery (7.0% and 37.4% in the implanted and the control defects, respectively) (Figure 2.10). Given these results, we speculate that the subchondral bone regeneration after the AT-MSC implantation progresses over 1 year based on the size of this defect (diameter of 6.8 mm and height of 5 mm).

Proton density (PD) - MR images 6 months after the surgery demonstrated that, in 3 of the animals (Nos. 1, 3, and 4), the double structure of the superficial and deep

cartilage layers showing the high and the low signal layers, respectively, was nearly restored to that of the surrounding sound cartilage in the implanted sites, but not in the controls. The cartilage regeneration suggest by the MR imaging findings was correspondingly defined based on the higher gross scores of the coverage, the smooth surface, the disappearing margin, and the color in the implanted sites of these 3 animals. Similarly, in the other animals (Nos. 2 and 5), as their MR images lacked the signal pattern specific to articular cartilage, the cartilage scores were degraded in the gross pathology. Considering these results, MR imaging could be very helpful for speculating about cartilage regeneration by implanting a scaffold-free 3D construct of AT-MSCs. Recent studies have suggested that PD-MR imaging would be feasible for assessing injuries and matrix degradation in articular cartilage (Rehnitz et al., 2014). Some scaffolds, which can be detectable using MR imaging might conceivably mask the cartilage regeneration. Although MR imaging might not replace arthroscopy as the gold standard for cartilage evaluation, rapidly advancing MR imaging technology would be a powerful complementary tool. The significantly higher total scores with the modified-MOCART system in the implanted defect as presented here suggest that MR imaging could become a non-invasive approach to the examination of cartilage regeneration using a scaffold-free 3D construct of AT-MSCs. The MR imaging also provided insight into the osteogenesis or the adipogenesis occuring under the new cartilaginous tissues. The undesirable adipogenesis in the subchondral area after the implantation could be detectable using MR imaging, although we do not have a clear answer regarding whether MR imaging is more effective for speculating about the subchondral bone formation compared with the CT imaging.

Histologically, in 3 animals (Nos. 1, 3, and 4), the smooth coverage containing the cartilage matrix was positively stained with safranine O, and subchondral bone

formation occurred in the implanted sites, whereas a deeply recessed surface and lower levels of bone formation were observed in the control defects. The other animals (Nos. 2 and 5) showed that neither the cartilaginous smooth coverage nor the subchondral bone was formed in both defects. Consistent with the statistical analysis of the animal data, not only the individual histological scores such as surface, matrix, cell distribution, viability of cell population, and cartilage mineralization, but also the average scores were higher in the implanted sites compared with the control sites. The significant differences were conclusive evidence in support of our speculation that a scaffold-free 3D construct of AT-MSCs can possibly achieve osteochondral regeneration in the future. However, the reason why neither the cartilaginous coverage nor the subchondral bone was regenerated in the implanted defects of animal Nos. 2 and 5. We speculated that the result could be due to defluxion of the AT-MSC constructs from the osteochondral defects in the early phase of post-operation. As mentioned in the preceding section, a 3D construct was accomplished by merging approximately 760 spheroids including 5×10^4 AT-MSCs individually. We suppose that the indissoluble merge between some spheroids might contribut to the fragility of the construct. Although the fragility has not yet been quantified, the vulnerable construct could be deformed during the surgery. As the constructs were implanted into the osteochondral defects in the femoral medial condyle, in this study, we cannot rule out the possibility of defluxion of the AT-MSC spheroids or constructs from the osteochondral defects in the early post-operative phase due to the movements of the joint.

Although further studies might be required, we conclude that implantation of a scaffold-free 3D construct of AT-MSCs into an osteochondral defect regenerates the original structure of the cartilage and subchondral bone.

Tabel 2.1 Modified 2D-MOCART scores

Feature		Score	Control Site	Implanted site
Defect fill	Complete	20	10	20
	Hypertrophy	15		
	Incomplete > 50 %	10		
	Incomplete < 50 %	5		
	Subchondral bone expose	0		
Cartilage interface	Complete	15	0	10
	Demarcating border visible	10		
	Defect visible < 50 %	5		
	Defect visible > 50 %	0		
Surface	Surface intact	10	0	5
	Surface damaged < 50 % of depth	5		
	Surface damaged > 50 % of depth	0		
Adhesion	Yes	5	0	5
	No	0		
Structure	Homogenous	5	0	0
	Inhomogenous or cleft formation	0		
Signal intensity	Normal	30	0	10
	Nearly normal	10		
	Abnormal	0		
Subchondral Lamina	Intact	5	0	0
	Not intact	0		
Sabchondral bone	Intact	5	0	0
	Granulation tissue, cyst, sclerosis	0		
Effusion	No effusion	5	0	5
	Effusion	0		
Average (0-100)			10	55

Tabel 2.2 ICRS gross grading scale

	Feature	Score	Control Site	Implanted site
Coverage	>75% fill	4	2	4
	50-75% fill	3		
	25-50% fill	2		
	<25% full	1		
	No fill	0		
Neocartilage color	Normal	4	1	3
	25% yellow/brown	3		
	50% yellow/brown	2		
	75% yellow/brown	1		
	100%yellow/brown	0		
Defect margins	Invisible	4	1	3
	25% circumference visible	3		
	50% circumference visible	2		
	75% circumference visible	1		
	Entire circumference visible	0		
Surface	Smooth/level with normal	4	1	3
	Smooth but raised	3		
	Irregular 25-50%	2		
	Irregular 50-75%	1		
	Irregular >75%	0		
Average			1.3	3.3

Table 2.3 ICRS histological grading scale

Feature		Score	Control Site	Implanted site
Surface	Smooth/continuous	3	0	0
	Discontinuities/irregulatrity	0		
Matrix	Hyaline	3	1	2
	Mixture; hyaline/fibrocartilage	2		
	Fibrocartilage	1		
	Fibrous tissue	0		
Cell distribution	Columnar	3	0	2
	Mixed/columnar clusters	2		
	Clusters	1		
	Individual cells/disorganized	0		
Viability of cell population	Predominantly viable	3	3	3
	Partially viable	1		
	<10% viable	0		
Subchondral bone	Normal	3	0	3
	Increased remodeling	2		
	Bone necrosis/granulation tissue	1		
	Detached/fractue/callus at base	0		
Cartilage mineralization (calcified cartilage)	Normal	3	0	3
	Abnormal/inappropriate location	0		
Average			0.6	2.2

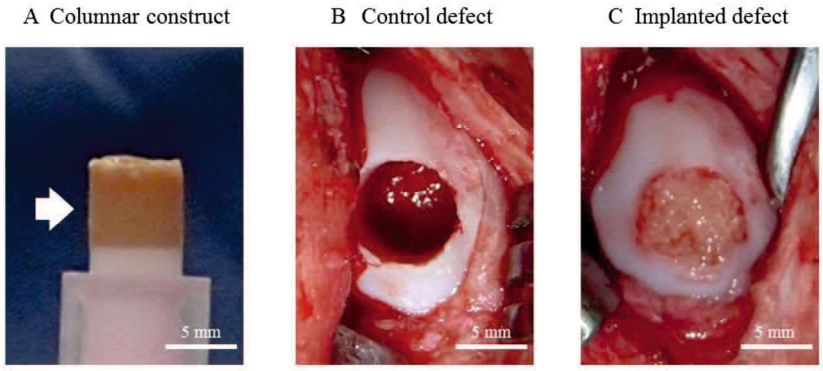

Figure 2.1 Surgical procedure.

A columnar construct (6.3 mm in diameter and 6 mm in height) for the implantation (A). A cylindrical osteochondral defect in each medial condyle before implantation (B). The construct composed of about 1920 spheroids of AT-MSCs was autografted into the osteochondral defect in the right hind limb (C). Nothing was implanted into the left limbs (control defects; B).

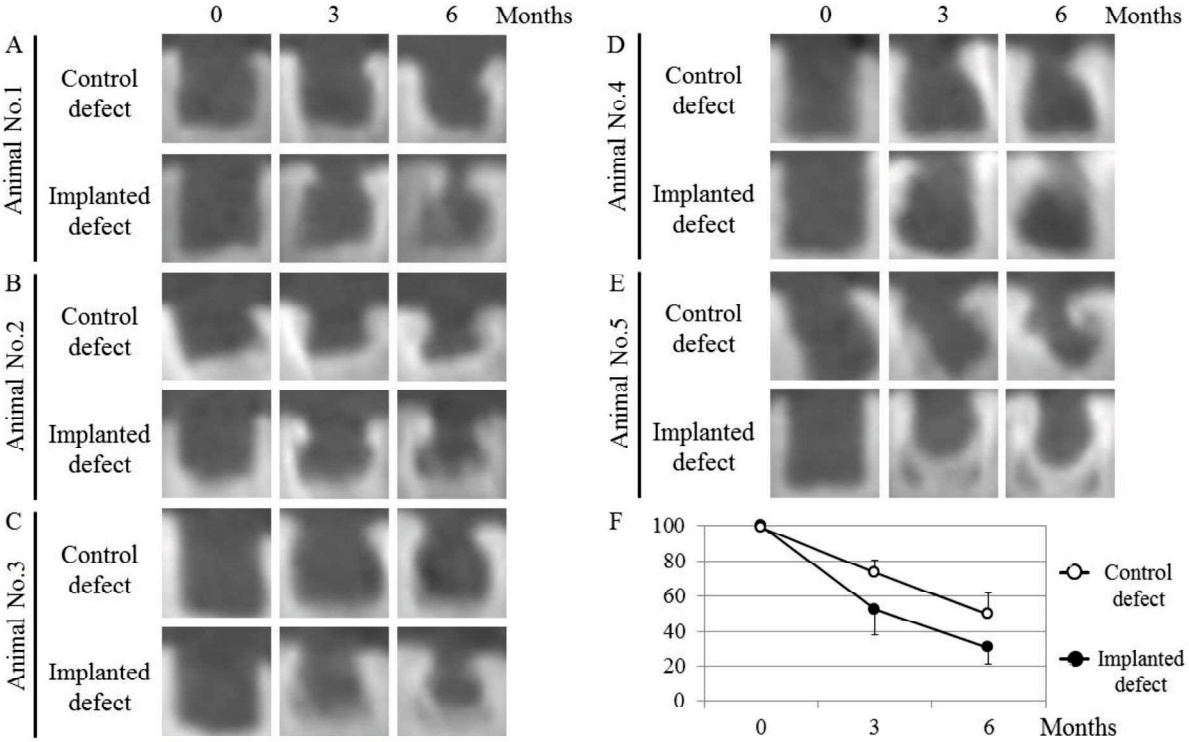

Figure 2.2 CT assessment of osteochondral defects.

CT images show one cross-section of the multi-planar reconstruction images 1, 3, and 6 months after the surgery in Animal No.1 (A), Animal No.2 (B), Animal No.3 (C), Animal No.4 (D), Animal No.5 (E). Line graph shows the averages of RV (radiolucent volume) percentages in the both defects (F). The averages at the 3rd and 6th months against those at 0 month were significantly decreased in the implanted defects (52.5 ± 16.5 and 30.2 ± 10.4 %, respectively), comparing to the control defects (74.5 ± 8.0 and 50.5 ± 13.6 %, respectively).

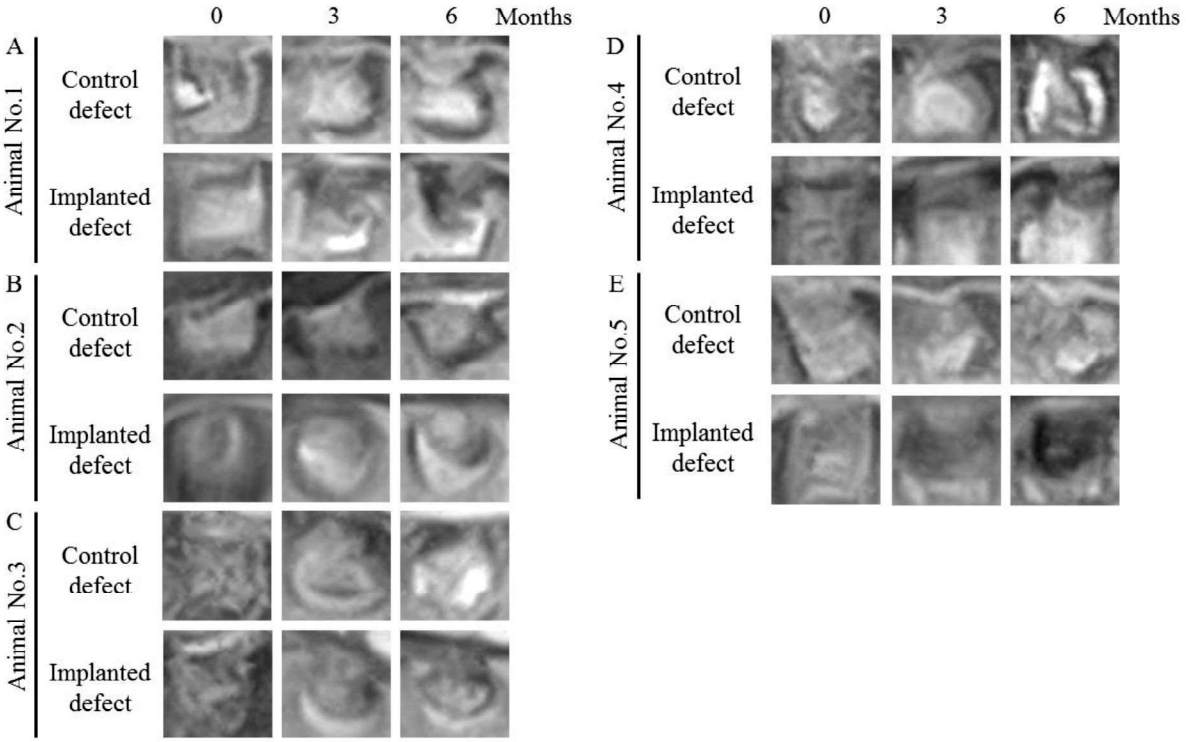

Figure 2.3 MR images of osteochondral defects.

CT images show one cross-section of the multi-planar reconstruction images 1, 3, and 6 months after the surgery in Animal No.1 (A), Animal No.2 (B), Animal No.3 (C), Animal No.4 (D), Animal No.5 (E). MR images in the implanted sites of animal No 1, 3, and 4 showed that the signal pattern at the surface of articular cartilage was restored near to the normal pattern of surrounding sound cartilage, while the new bone formations under the cartilaginous tissue was incomplete. High signal intensity indicating AT predominantly occupied the subchondral area in the implanted sites of animal No. 2 and 5.

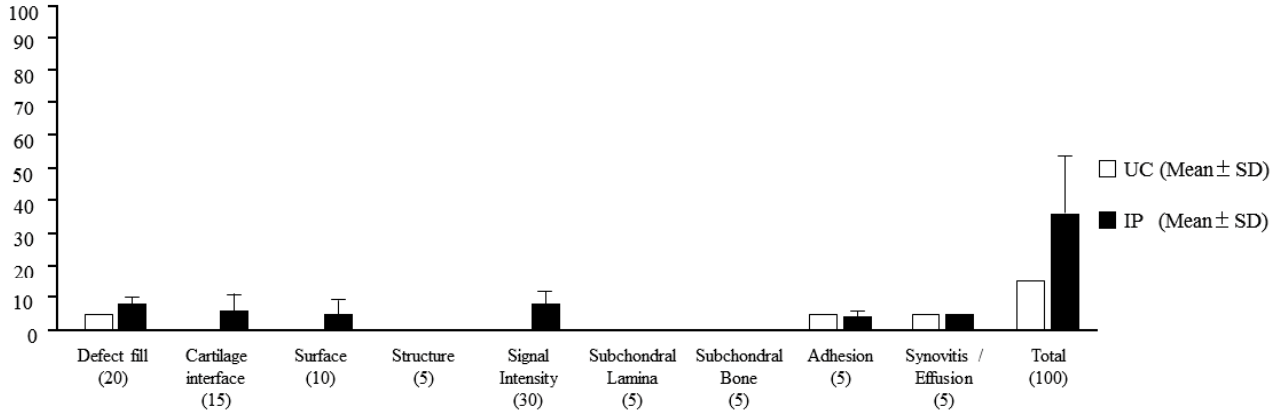

Figure 2.4 Modified 2D-MOCART scores of osteochondral defects.

There are significant differences in the outcome measures such as defect fill (8.0 ± 2.4 and 5.0 ± 0.0 in the implanted and the control sites, respectively), cartilage interface (6.0 ± 4.9 and 0.0 ± 0.0 in the implanted and the control sites, respectively), and signal intensity (5.0 ± 4.4 and 0.0 ± 0.0 in the implanted and the control sites, respectively) between the implanted and the control sites. The scores of surface ($p = 0.06$), cartilage structure, subchondral lamina and bone, and adhesion ($p = 0.34$) were not different between the both sites. Accordingly, the total scores of modified 2D-MOCART system were significantly increased in the implanted sites (36.0 ± 17.8) comparing to the controls (15.0 ± 0.0).

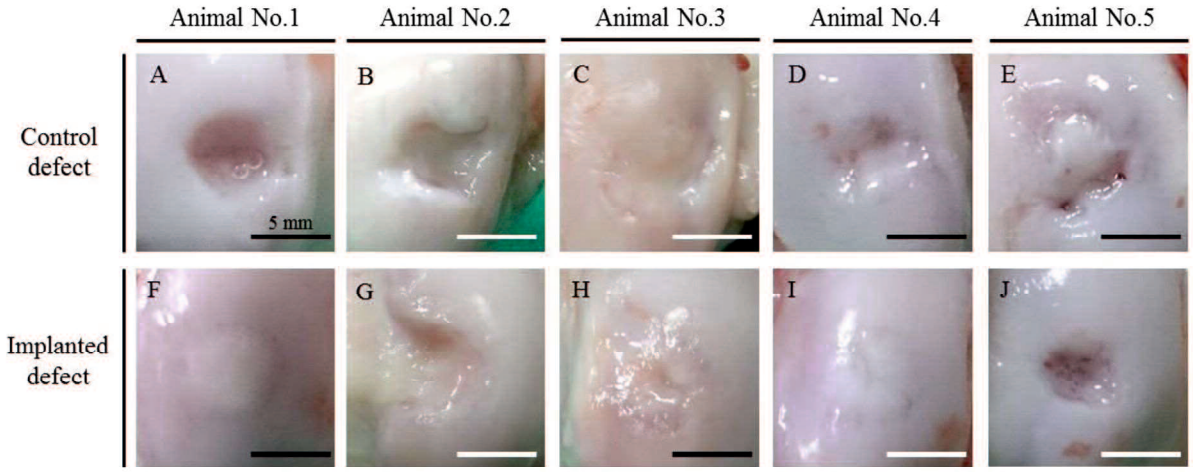

Figure 2.5 Macroscopic findings of the surface of the implanted and control sites.

In animal No. 1, 3, and 4, the surfaces of the implanted defects were covered with the abundant cartilageous white tissues (F, H, I), while the surfaces of the implanted defets were depressed and the cartilaginous tissues were scarce in animal No. 2 and 5(G, J). Furthermore, synovium adhered to the defect in animal No.2 (G). On the other hand, the defects of the control sites were lagely depressed in all animals (A, B, C, D, E).

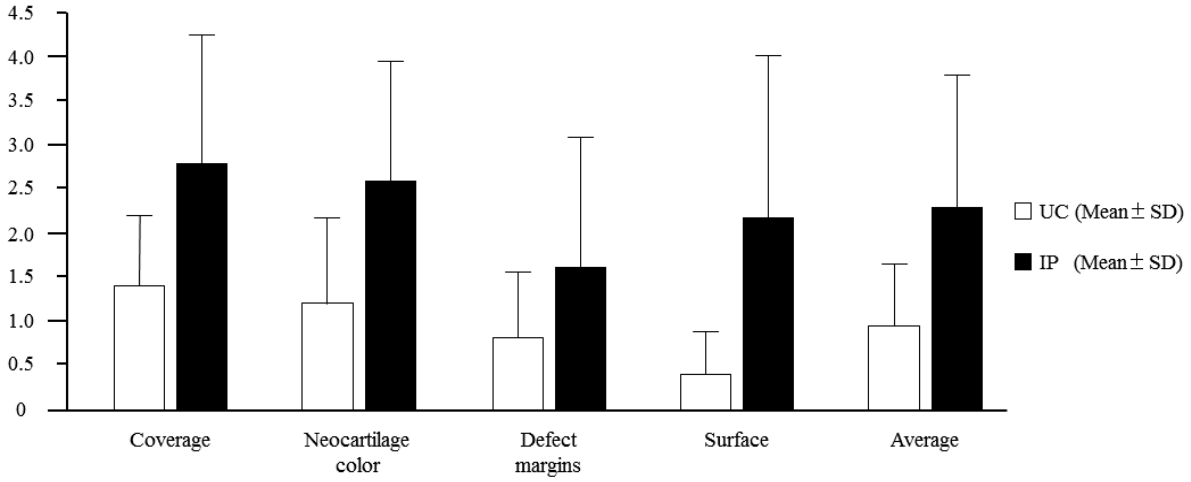

Figure 2.6 Macroscopic scores of the implanted and control sites with ICRS gross grading scale

Gross pathology in the implanted sites of animal No 1, 3, and 4 showed higher scores at the points of cartilage including the coverage, the smooth surface, disappearing margin, and the color. However, there are no significant differences in the outcome measures of ICRS gross scores such as coverage ($p = 0.13$), neocartilage color ($p = 0.13$), defect margin ($p = 0.37$), and surface ($p = 0.09$) between the implanted and the control sites. Accordingly, the averages of gross scores were not significantly different between the sites (2.3 ± 1.5 and 1.0 ± 0.7 in the implanted and the control sites, respectively).

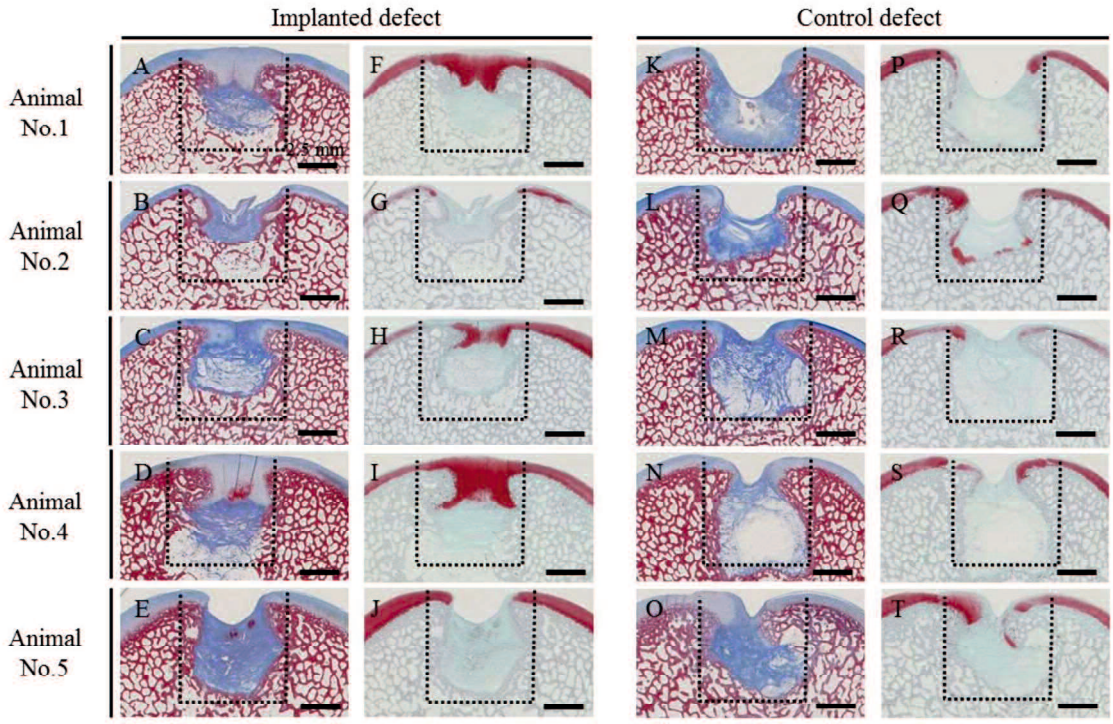

Figure 2.7 Histopathology of osteochondral defects using masson's trichrome, alcian blue and immunohistochemical staining of type II collagen.

In animal No 1, 3, and 4, smooth coverage containing cartilage matrix positively stained by safranine O and the subchondral bone formation were going on at the implanted sites (A, C, D, F, H, I), while that the deeply recessed surface and the lower bone formation were left at the implanted site in animal No.2 and 5 (B, E, G, J). At the control site, the surface was irregular and fibrous tissue (which is not stained by safranine O) lay over the subchondral bone at the control site (K, L, M, N, O, P, Q, R, S, T). Black dotted lines indicate the areas of osteochondral defects immediately after the surgery.

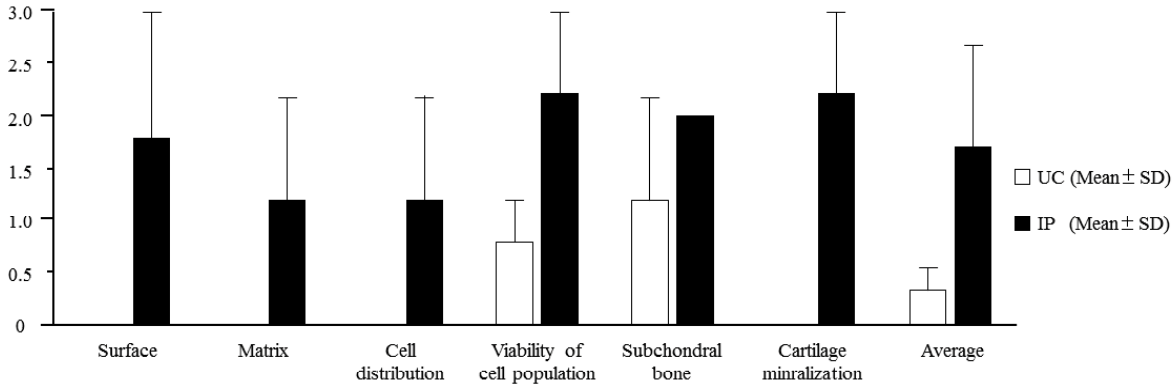

Figure 2.8 Maicroscopic scores of the implanted and control sites with ICRS histological gradig scale

The ICRS histologic scores at the points except for subchondral bone were higher in the implanted sites than the control sites in animal No 1, 3, and 4. Animal No 2 and 5 showed that the cartilagenous smooth coverage as well as the subchondral bone were not progressed in the both defects, therefore the scores at the all points were not different between the both defects. The scores of the histologic outcome measures such as surface, matrix, cell distribution, viability of cell population, and cartilage mineralization (except for the subchondral bone ($p = 0.14$)) were significantly higher in the implanted sites than those in the control sites. The average of histological scores was also significantly higher in the implanted sites (1.7 ± 1.0) than the control sites (0.3 ± 0.2).

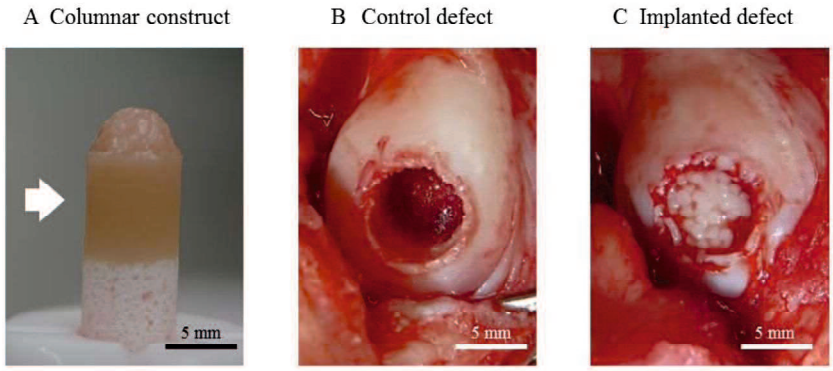

Figure 2.9 Surgical procedure.

A columnar construct (6.3 mm in diameter and 10 mm in height) for the implantation (A). A cylindrical osteochondral defect in each medial condyle before implantation (B). The construct composed of about 2880 spheroids of AT-MSCs was autografted into the osteochondral defect in the right hind limb (C). Nothing was implanted into the left limbs (control defects; B).

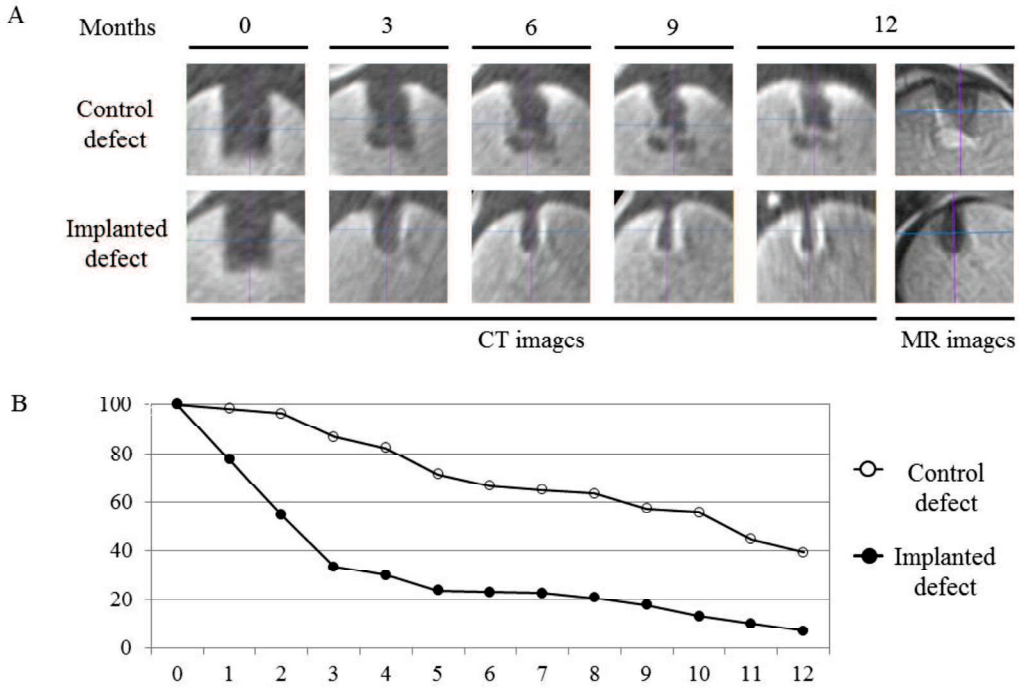

Figure 2.10 CT assessment and MR images of osteochondral defects.

A radiopaque area emerged from the boundary between the bone and the implant in the defects and increased more steadily upward and inward on the implanted site than the control sites (A). MR images in the implanted site showed that the signal pattern at the surface of articular cartilage was restored near to the normal pattern of surrounding sound cartilage, while the new bone formations under the cartilaginous tissue was incomplete (A). On the other hand, MR images of the control site showed that the irregularity pattern at the surface of articular cartilage, and high signal intensity indicating AT predominantly occupied the deep of subchondral area (A). The percentages of RVs at the 3rd, 6th, 9th, and 12th months against those at 0 month (that is remaining percentages of RV) were significantly decreased in the implanted defects (33.4, 23.0, 13.1, and 7.0 %, respectively), comparing to the control defects (86.8, 66.9, 57.2 and 37.4 %, respectively) (B).

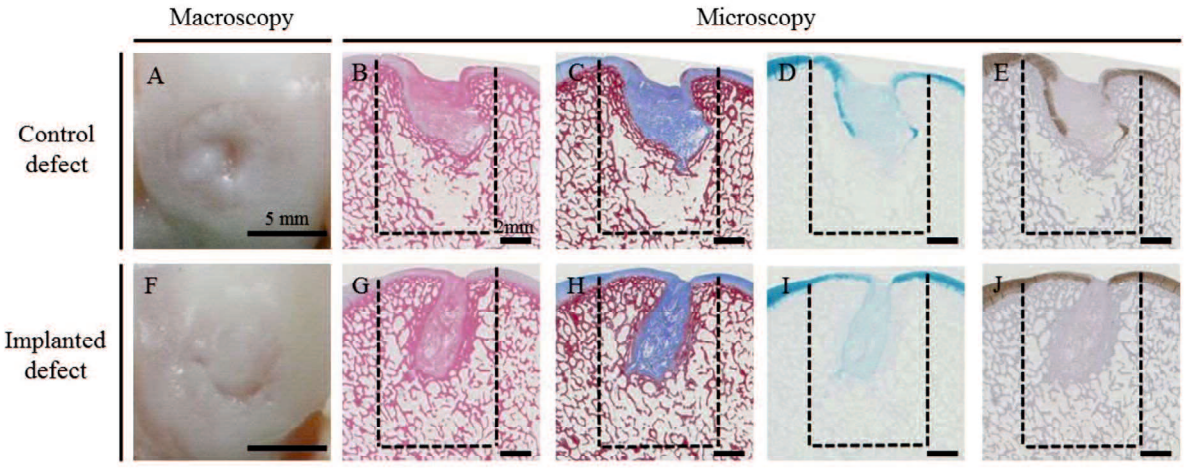

Figure 2.11 Macroscopic findings of the surface and histopathology at osteochondral defects on the implanted and control sites.

Gross pathology showed that the surface of the implanted defect was covered with the abundant cartilageous white tissues, but the fissure was still observed (F). On the other hand, the surface of the control site was depressed and the circumferrance was also visible (A). Histopathology presented that the smooth coverage containing cartilage matrix positively stained by alcian blue and immunohistochemistry with type II collagen (I, J). And the subchondral bone formation was going on in the implanted sites (G, H), while that the deeply recessed surface and the lower bone formation were left in the control defects (B, C, D, F).

Chapter 3

Characteristics of equine mesenchymal stem cells derived from synovial fluid

3.1 Introduction

Arthroscopic surgery to remove osteochondral fragments and to curette the surrounding degenerative cartilage has been accepted worldwide in Thoroughbred horses with intra-articular fractures (IAF) and osteochondrosis dissecans (OCD). Post-operative cartilage defects spontaneously recover with fibrous cartilage, but this is not favourable compared to hyaline cartilage because of poor lubrication, abrasion resistance and impact absorption. To repair defects with original hyaline cartilage, cartilage regeneration using mesenchymal stem cells (MSCs) derived from bone marrow (BM) (Arnhold et al., 2007) or adipose tissue (AT) (Braun et al., 2010) has been investigated. The cells obtained from these tissues are multipotent and can differentiate into cartilage (Vidal et al., 2008), bone (Toupadakis et al., 2010), adipose (Vidal et al., 2011), neuronal (Kang et al., 2004; Jansen et al., 2010), myocardial (Lee et al., 2009; Palpant et al., 2010; Young et al., 2011), and hepatic (Taléns-Visconti et al., 2006; Stock et al., 2008; Lee et al., 2012) cells in humans or animals.

We have also attempted to regenerate original tissues, including repair of osteochondral deficits, by transplanting AT-derived MSCs (AT-MSCs) experimentally created in other animal species. The advantage of AT-MSCs is the abundance of MSCs that are found per unit weight of the tissue (Burk et al., 2013); however, we believe that a therapeutic strategy using AT-MSCs may be unacceptable in racehorse practice, because of the lower somatic fat amounts in Thoroughbred horses compared to Standardbred horses (Kearns et al., 2001). BM-derived MSCs (BM-MSCs), which may be susceptible to osteogenic induction (Burk et al., 2013), are another option for regenerating bone and cartilage in equine animals (Ranela et al., 2012). However, paracentesis to aspirate BM is invasive and must be done with extreme care to avoid

contamination (Vidal et al., 2007). Ideally, all steps from collection to implantation of stem cells must minimise contamination and be minimally invasive for horses. Other sources, such as umbilical cord tissue (UCT), umbilical cord blood (UCB) and peripheral blood that can also be obtained less invasively, are of interest for MSC therapy in horses (Carrade et al., 2011; Dhar et al., 2012; Burk et al., 2013). Method for the long-term preservation of UCT and UCB should be established.

Research in cartilage regeneration has played a leading part in tissue engineering, and futuristic technology to directly reprogram differentiated skin fibroblasts into chondrocyte-like cells without going through induced pluripotent stem cells has already been developed (Yin et al., 2010). Also, excellent clinical outcomes have been reported following treatment of cartilage deficits using stem cells derived from another source such as the synovium and synovial fluid (SF) (Nimura et al., 2008; Lee et al., 2011; Sekiya et al., 2012). Synovium-derived MSCs from humans with osteoarthritis can be cultured in vitro, plentiful numbers of cells settle on defective parts of the articular surface approximately 10 min after arthrotomy, and a few months later, recovery of hyaline cartilage can be seen with arthroscopy (Lee et al., 2011; Suzuki et al., 2012).

Stem cells are known to be increased in SF of human patients with joint disease and injury (Jones et al., 2004; Morito et al., 2008); these authors have suggested that the stem cells are released from the synovium into the SF. Improved clinical outcomes have been reported following treatment of cartilage deficits in human beings using MSCs derived from the synovium and SF (Nimura et al., 2008; Lee et al., 2011; Sekiya et al., 2012; Suzuki et al. 2012). If MSCs can be isolated from SF and expanded over a short time period after a racehorse is injured, they may be useful as a new strategy for cartilage regeneration. We hope to design a less invasive protocol using SF-derived MSCs (SF-MSCs) for use in regenerative therapy to repair cartilage deficits after

arthroscopic surgery in racehorses with IAF and OCD.

The aims of this study were to investigate the proliferative capacity, phenotypic characteristics, and multi-potency of cells in the SF associated with intra-articular injury and synovitis, and to provide a new strategy for regenerating lost cartilage with SF-MSCs.

3.2 Materials & Methods

3.2.1 Animals & Samples

Eleven Thoroughbred horses with IAF or OCD were used to obtain and cultured diseased SF samples (Table 3.1). Another nine diseased and nine normal horses were used to compare the number of MSCs included in additional SF samples (Table 3.2). All procedures were approved by the Animal Care and Use Committee of Kagoshima University (Approval No. A11029 and No. A11037).

3.2.2 Isolation and expansion of equine MSCs

3.2.2.1 Collection of SF from animals

SF (3 to 4 ml per joint) was collected aseptically from carpal, fetlock, or tarsal joints of the 11 Thoroughbred horses at the time of arthroscopic surgery (Table 3.1). SF samples were also obtained from nine diseased and nine normal Thoroughbred horse joints to compare the number of MSCs in the SF (Table 3.2).

3.2.2.2 Collection of AT and BM from animals

AT and BM were collected from two other horses (a male 10 years old and a female 3 years old) that were free of any joint diseases.

3.2.2.3 Isolation and expansion of stromal cells from SF

SF was diluted with five volumes of phosphate-buffered saline (PBS), filtered through a 70-μm nylon filter (Cell Strainer; BD, Franklin Lakes, NJ) to remove debris and centrifuged at 160 × *g* for 5 min at room temperature. After decanting the supernatant, the pellet was resuspended and plated in a 25-cm^2 culture flask in complete

culture medium (CCM): Dulbecco's Modified Eagle's Medium (DMEM; Life Technologies, Carlsbad, CA), 10% foetal bovine serum (FBS; Thermo Scientific, Waltham, MA, USA) and 1% antibiotic-antifungal preparation (100 U/mL Penicillin G, 100 μg/mL streptomycin, 0.25 μg/mL amphotericin B; Antibiotic-Antimycotic; Life Technologies). After incubation at 37°C under 5% CO_2 for 9 days, the cells adhering to the bottom of the flask were washed with PBS and harvested as described below. The medium was changed on day 4 and 7 (D4 and D7; Passage 0; P0). The number of colonies was counted at P0 in the 18 SF samples from the nine diseased and nine normal horse joints (Table 3.2).

Cultured cells were harvested with 0.05% trypsin and 0.2 mM ethylene diamine tetraacetic acid (Trypsin-EDTA; Life Technologies) and centrifuged. After decanting the supernatant, the pellet was rinsed with CCM and the cells were replated at 1×10^6 cells in 150-cm^2 dishes and cultured for 9 days. The medium was changed every 3 days for 9 days (P1). This serial process of passaging was repeated to obtain $> 1 \times 10^7$ cells for reverse transcription (RT)-PCR and flow cytometry. The total number of cells was determined with a cell counter at every passage from P1 to determine the proliferation rates, which were calculated as the cell doubling number, cell doubling time and daily duplication rate using the following formulas:

Cell doubling number = ln(final number of cells/initial number of cells)/ln(2)

Cell doubling time = Cell culture time/cell doubling number

Daily duplication rate = Cell doubling number/cell culture time

= 1/cell doubling time

Premature marker gene expression, immunological surface markers, and multi-potency of the cells were analysed at the fifth passage (P5). Normal SF-MSCs were analysed at P6, when sufficient numbers of cells were obtained.

3.2.2.4 Isolation and expansion of stromal cells from AT and BM

AT (25-30 g) were obtained from the gluteal subcutis using liposuction after horses were sedated by IV injection with 4 μg/kg medetomidine HCl (Domitor, Zenoaq, Fukushima, Japan) and 10 μg/kg butorphanol tartrate (Vetorphale, Meiji Seika, Tokyo, Japan). After subcutaneous injection of 100-200 ml liposuction solution through a 10 mm skin incision, AT was aspirated with a probe (Collection Cannula, 14 G, length 30 cm; Cytori, San Diego, CA) connected to a 50 ml syringe. The liposuction solution was physiological saline (Otsuka Normal Saline, Otsuka, Tokyo, Japan) containing 400 μg/mL lignocaine HCl and 0.4 μg/mL adrenaline (Xylocaine injection 1% with Epinephrine, AstraZeneca, London, U.K.). This procedure was repeated 10 times. The aspirated AT was digested with a 2 × volume of PBS containing 0.1% collagenase at 37 °C for 90 min, filtered a 70 μm nylon filter (Cell Strainer, BD), and centrifuged at 160 × *g* for 5 min at room temperature. The pellet was re-suspended in CCM. Following incubation at 37 °C in 5% CO_2 for 9 days, the cells adhering to the bottom of the flask were washed with PBS and harvested. The medium was changed on the sixth day (D6; P0).

BM (30-35 ml) were collected from the fifth segment of the sternum by needle core biopsy under local anaesthesia with 20 mg/mL lignocaine HCl (Xylocaine Injection 2%, AstraZeneca) and medication with the same sedatives and analgesics as used for AT collection. A bone marrow biopsy needle (11 G, length 10.2 cm; Angiotech, Vancouver, Canada) was inserted through a 10 mm skin incision and through the subcutis and muscle. BM was aspirated with a 20 ml syringe containing 5000 IU heparin and then immediately re-suspended in CCM. Following incubation at 37°C under 5% CO_2 for 9 days, the cells adhering to the bottom of the flask were washed with PBS and harvested

as described below. The medium was changed on the sixth day (D6; P0).

AT-derived and BM-derived stromal cells were harvested with 0.05% trypsin and 0.2mM EDTA and centrifuged. The pellet was rinsed with CCM and the cells were replated at 1×10^6 cells in 150-cm^2 dishes and cultured for 6 days. The medium was changed on the third day for 6 days (P1). This serial process of passaging was repeated until surface markers analysis.

3.2.3 Analysis of premature marker genes with RT-PCR

Total RNA from the cultured cells was isolated using the mirVana miRNA Isolation Kit (Life Technologies) and converted to cDNA by RT using the TaKaRa RT-PCR system (PCR Thermal Cycler MP, Takara Bio, Otu, Japan) and RT-PCR kit (ReverTra Dash, Toyobo, Osaka, Japan), with a 20 min incubation at 42 °C, followed by a 5 min incubation at 99 °C to inactivate the RT. The PCR primers and the expected sizes of products for homeobox protein Nanog (NANOG) and sex determining region Y-box 2 (SOX-2) are summarised in Table 3.3. PCR amplification was performed with the following conditions: 30 cycles of 98 °C for 10 s, individual annealing temperature for 2 s (Table 3.3), and 74 °C for 15 s. The reaction products were separated with electrophoresis on a 1.5% agarose gel (Agarose WP; Wako Pure Chemical Industries, Osaka, Japan) and the expression of premature marker genes was determined based on the expected size of the bands labelled with SYBR green (Takara Bio).

3.2.4 Analysis of immunological surface markers with flow cytometry

Cells (1×10^4) were resuspended in 500 μl staining buffer (SB; PBS containing

1% FBS) and incubated for 30 min at 4 °C with 20 μg/ml antibodies that recognise CD11a/18, CD34, CD44, CD45, CD90, CD105, major histocompatibility complex (MHC) class I, and II, with reference to the manufacturers' or producers' instructions (Table 3.4). Prior to incubation with cells, the antibodies against CD11a/18, CD44, and MHC class I (MHC-I) and MHC-II were coupled with secondary antibodies conjugated to fluorescein isothiocyanate (FITC). Non-specific FITC mouse immunoglobulin G1κ (BD) was used as a negative control. FITC-labelled cells were washed with SB and resuspended in 500 μl SB for fluorescence-activated cell sorting (FACS) analysis. Cell fluorescence was evaluated as a strong shift in the mean fluorescence intensity (MFI) by flow cytometry using a FACS Aria II instrument (BD). The data were analysed using FACS Diva software (BD).

3.2.5 Analysis of differentiation along specific lineages (osteogenic, chondrogenic, adipogenic, and tenogenic differentiation)

3.2.5.1 Osteogenic differentiation assay

To investigate osteogenic differentiation, the cells were plated in 6-well plates (6 Well Plate-N, Nest Biotech, Wuxi, China) in CCM at an initial density of 2.5×10^3 cells/cm^2. After 24 h of incubation, CCM was replaced with special osteogenic induction medium (Differentiation Basal Medium-Osteogenic, Lonza, Walkersville, MD) supplemented with 100μM ascorbic acid, 10mM β-glycerophosphate and 1μM dexamethasone. After 2 weeks in induction medium, total RNA from the plate-cultured cells was prepared as described above, and expression of osteoblast-specific genes runt-related transcription factor 2 (RUNX-2), alkaline phosphatase (ALP), and

osteocalcin (OC) were analysed. PCR primers, amplification conditions and the expected size of the products are summarised in Table 3.3. Negative controls for RT-PCR products were obtained from SF derived stromal cells that were not placed in induction medium (data not shown).

3.2.5.2 Chondrogenic differentiation assay

Chondrogenic differentiation was induced in pellet cultures as well as dish cultures for 2 weeks. Cells (5×10^5) were resuspended in a 15 ml culture tube (SuperClear Centrifuge Tubes, Labcon, Petaluma, CA) in 500µl chondrogenic induction medium (Differentiation Basal Medium-Chondrogenic, Lonza) supplemented with 4.5 g/l $_D$-glucose, 350 µM $_L$-proline, 100 nM dexamethasone and 0.02 g/l transforming growth factor (TGF)-β3. Another aliquot of 5×10^4 cells was resuspended in 6-well plate (6 Well Plate-N, Nest Biotech) in 2 ml induction medium, which was replaced three times per week, similar to osteogenic induction. Two weeks later, total RNA from the dish-cultured cells was prepared, as described above, and expression of chondrogenic marker genes, including sex determining region Y-box 9 (SOX-9), type II collagen (COL-II), and aggrecan (AGG) was examined (Table 3). Furthermore, production of mucopolysaccharide in the chondrogenic extracellular matrix was stained with Alcian blue in 6-well plates. The differentiated cells were fixed onto the culture plate by methanol and then treated with 3% acetic acid. The plates onto which the cells adhered were stained with Alcian blue (pH 2.5) for 90 min.

At the same time, cell aggregates were fixed with 10% neutral buffered formalin, dehydrated in graded series of ethanol, embedded in paraffin, and cut 5 µm thick sections with a microtome. The sections were mounted and dried on glass slides. After dehydration with methanol and treatment with 3% acetic acid, cell aggregates were

stained with Alcian blue (pH 2.5) for 90 min to detect cartilage-specific proteoglycans, then counterstained with Mayer's haematoxylin. The sections were also analysed immunohistochemically with an antibody against cartilage oligomeric matrix protein (COMP; catalogue number ab91354, Abcam, Cambridge, UK). Following deparaffinisation and rehydration, the sections were treated with blocking buffer (0.01 M PBS containing 0.25% casein) and then incubated with primary antibody (diluted 1:100 in blocking buffer) overnight. The slides were incubated with secondary biotinylated goat anti-rabbit IgG (Polyclonal Goat Anti-Rabbit Immunoglobulins/Biotinylated; catalogue number E0432, DakoCytomation, diluted 1:300, Glostrup, Denmark), for 30 min. Secondary antibodies were labelled with avidin-biotin-horseradish peroxidase complex (VECTASTAIN ABC Standard Kit; Vector Laboratories, Southfield, MI) and visualised after treatment with 3, 3'-diaminobenzine.

3.2.5.3 Adipogenic differentiation assay

Adipogenic differentiation was induced when cells reached a density of 1.5×10^3 cells/cm^2 on 6-well plates (6 Well Plate-N, Nest Biotech) in basal medium. After pre-incubation for 24 h, CCM was replaced with adipogenic induction medium (Lonza) supplemented with 4.5 g/l $_D$-glucose, 100 µM indomethacin, 10 µg/mL insulin, 0.5 mM 3-isobutyl-1-methylxanthine, 1 µM dexamethasone and 5% rabbit serum. Seven days later, total RNA from the cells was isolated as described above and evaluated for expression of the adipogenic marker gene peroxisome proliferator activated receptor γ2 (PPARγ2) (Table 3.3). Adipocyte-specific intracellular lipids were stained with oil red O.

3.2.5.4 Tenogenic differentiation assay

Tenogenic differentiation was induced when cells reached a density of 1.5×10^3 cells/cm^2 on 6-well plates (6 Well Plate-N, Nest Biotech) in CCM. After incubation for 24 h, bone morphogenetic protein (BMP) 12 (BMP-12; BioVison, San Francisco, CA) was added to CCM for tenogenic induction. Following 2 weeks in induction medium, total RNA from the dish-cultured cells was prepared as described above, and expression of scleraxis (SCX) and tenascin C (TEN-C) as tenocyte- and tenogenesis-specific genes were analysed (Table 3.3).

3.2.6 Statistical analysis

All quantitative group data are shown as the average ± standard deviation (SD). The all statistical differences in this study were analysed with the Student's t-test (Excel; Microsoft). Differences of $P < 0.01$ were considered to be statistically significant.

3.3 Results

3.3.1 Isolated colonies of stromal cells from SF

SF-derived MSCs adhering to the bottom of the culture flask were spindle-shaped and present as a minority of cell components. At P0, the total number of colonies of SF-MSCs from diseased joints (62-364 colonies) was significantly (P = 0.001) larger than the number from normal joints (0-21 colonies) (Table 3.2).

3.3.2 Proliferation of stromal cells from SF

SF-MSCs isolated from diseased joints proliferated well to 1×10^6 at P3 and 1×10^7 cells at P4 (Figure 3.1A). Total cell doubling numbers were 1.81 ± 0.94, 3.93 ± 1.11, and 5.83 ± 0.54 at P2, P3 and P4, respectively (Figure 3.1B). Cell doubling times of SF-MSCs (8.62 ± 8.62, 6.60 ± 5.33, and 5.27 ± 2.91 at P2, P3, and P4, respectively; Figure 3.1C) were longer, compared to AT-MSCs (6.84, 3.17, and 4.85 at P1, P2 and P3, respectively) and BM-MSCs (3.96, 2.54, and 2.84 at P1, P2, and P3, respectively). Daily duplication rates were 0.20 ± 0.11, 0.23 ± 0.12 and 0.25 ± 0.11 at P2, P3, and P4, respectively (Figure 3.1D). AT-MSCs and BM-MSCs could be transferred repeatedly to the next passage at intervals of 6 days, whereas the interval was 9 days in SF-MSCs. However, the doubling times of SF-MSCs were not statistically different from those of AT-MSCs and BM-derived MSCs (BM-MSCs) (Figure 3.2).

3.3.3 Expression of premature marker genes of stromal cells from SF

The expression of NANOG and SOX-2 in SF-MSCs was confirmed by RT-PCR

(Figure 3.3A).

3.3.4 Expression of immunological cell-surface markers of stromal cells from SF

The expression of immunological markers in SF-MSCs is shown in Figure 3.4 and tabulated in Table 3.5. More than 90% of cells were positive for CD44, CD90 and MHC-I (Figure 3.4C,E,G and Table 3.5) and 60-80% of cells were positive for CD11a/18, CD105 and MHC-II, overlapping with the negative control (Figure 3.4A,F,H and Tabel 3.5), whereas no signal was detected with antibodies against CD34 and CD45 (Figure 3.4B,D and Tabel 3.5). Equine mononuclear blood cells were positive for CD34 and CD45 (Figure 3.5), as previously reported (Barberini et al., 2014; Mohanty et al., 2014). No statistical difference in flow cytometry was observed between the SFs from the normal and diseased joints (P values of CD11a/18, CD34, CD44, CD45, CD90, CD105, MHC-I, and MHC-II were 0.013, 0.714, 0.7, 0.768, 0.317, 0.372, 0.639, and 0.45, respectively). The results of SF-MSCs corresponded to those of AT-MSCs and BM-MSCs (Figure 3.6).

3.3.5 Evaluation of differentiation along specific lineages (osteogenic, chondrogenic, adipogenic, and tenogenic differentiation)

3.3.5.1 Osteogenic differentiation

After 2 weeks of osteogenic induction, SF-MSCs aggregated and contracted to form a colony, and expression of RUNX-2, ALP, and OC (Figure 3.3B). These cells

clasters produced a specific matrix, including calcium apatite crystals, which stained positively with alizarin red (Figure 3.7A, negative control is shown in Figure 3.8A).

3.3.5.2 Chondrogenic differentiation

The plate culture of SF-MSCs in chondrogenic induction medium induced a change in cell shape to a 'stone-wall' structure, followed by formation of a gelatinous monolayer sheet that was stained intensely with Alcian blue (Figure 3.7C, negative control is shown in Figure 3.8C). Blue sheets were also formed by chondrogenic induction of SF-MSCs at P10 (Figure 3.9A) and SF-MSCs from normal joints (Figure 3.9B) as well. However, AT-MSCs and BM-MSCs formed no blue gelatinous sheets following chondrogenic induction (Figure 3.9C,D). RT-PCR revealed elevated expression of marker genes specific for chondrogenesis, including SOX-9, COL-II, and AGG (Figure 3.3D). Histological observation of the cell pellets showed a hyaline cartilage-like structure that was positively stained with Alcian blue (Figure 3.7D, negative control is shown in Figure 3.8D) and that abundantly expressed cartilage-specific molecules such as COMP in the extracellular matrix (Figure 3.10).

3.3.5.3 Adipogenic differentiation

Adipogenic induction of the MSCs resulted in adipocyte-like flattened cells with small lipid vesicles that stained positively with oil red O (Figure 3.7B, negative control is shown in Figure 3.8B). RT-PCR revealed the expression of adipogenic marker genes such as PPAR-γ2 (Figure 3.3C).

3.3.5.4 Tenogenic differentiation

Tenogenic induction of the MSCs resulted in elongated cells with parallel to each

others. RT-PCR revealed the expression of tenogenic marker genes, such as SCX and TEN-C (Figure 3.3E).

3.4 Discussion

Implantation of autologous cells with or without artificial scaffolds has led to regeneration of hyaline cartilage at osteochondral defects associated with human and equine osteoarthritis. Although BM-MSCs and AT-MSCs can be differentiated into chondrogenic cells (Ranela et al., 2012; Xie et al., 2012), the clinical safety and invasiveness must be improved for widespread use in equine practice. Not only must the safety of the culture media and supplements be considered with no infectious contamination similar to human medicine, but also the surgical invasiveness involved in the collection and implantation of the MSCs should be also decreased as much as possible. If possible, intact tissues such as BM and AT should not be used to obtain MSCs, and any other invasive procedures in addition to the arthroscopic surgery should be minimised to injured joints in racehorses.

In the present study, equine SF from joints with osteochondral fragments included spindle-shaped cells that adhered to the culture dish and proliferated to form colonies; these findings correspond to the distinctive features of human MSCs (Friedenstein et al., 1976). Previously defined markers for MSCs, in which CD44, CD90, and CD105, but not CD34 and CD45, are epressed (Morito et al., 2008; Sekiya et al., 2012), waere identical in the cells derived from equine SF, as well as equine AT-MSCs and BM-MSCs, in the present study. In addition to these results, the ablitiy of these cells to differentiate into osteoblasts, chondrocytes, adipocytes, and tenocytes was also a feature of equine SF-MSCs, as well as equine AT-MSCs and BM-MSCs. If we can efficiently and effectively isolate and increase the number of cells, SF could be a useful source of equine MSCs for equine cartilage regeneration, since arthrocentesis to collect SF is less invasive and has a lower risk of contamination with infectious agents, compared to

collection of BM or AT.

In this study, we used SF from injured joints, which produced small numbers of colonies of MSCs at P0 and reached a total number of over 1×10^5 cells at P1. In a human study, MSCs were detected at very low densities in SF from normal volunteers, but increased with the grade of osteoarthritis (Sekiya et al., 2012). In the present study, we showed that the number of colonies of SF-MSCs at P0 was significantly increased in SF from diseased joints compared to normal joints. Since fewer MSCs are present in normal SF, the increased numbers of the cells in SF from diseased or injured joints suggest that SF-MSCs could play a role in the process of degradation, repair and regeneration of damaged cartilage. MSCs can be guided to migrate from their niche, home to the site of damaged tissue, and be induced to undergo chondrogenesis by chemokines such as TGF-β3 and stromal derived factor-1β (Mendelson et al., 2011). When partial thickness defects in the articular cartilage form, a continuous layer extending from the synovial membrane, which contributes to cartilage repair, is observed (Hunziker et al., 1996). Another report suggested that synovium-derived MSCs may be a superior cell source for autologous transplantation for cartilage regeneration (Sakaguchi et al., 2005).

In our study, chondrogenic dish culture of either diseased or normal SF-MSCs induced a change in the cell shape into a ‘stone-wall’ structure, followed by formation of a gelatinous monolayer sheet that was intensely stained with Alcian blue. However, chondrogenic induction of AT-MSCs and BM-MSCs resulted in no blue gelatinous sheet. This result is suggestive of the superiority of SF-MSCs, which may be more susceptible to generatinge cartilage matrix during chondrogenic differentiation compared to AT-MSCs or BM-MSCs. Therefore, a serial cartilage therapeutic strategy in which SF-MSCs are temporarily cultured in vitro and then returned to the diseased or injured

joint is logical.

On the basis of morphology and gene profile, SF-MSCs were more similar to synovium-derived MSCs than to BM-MSCs (Sekiya et al., 2012). A previous paper suggested that human SF-MSCs are released from the synovium in association with joint insults (Nimura et al., 2008); thus, we also speculate that equine SF-MSCs may be released from the synovium, especially in OCD cases. However, we do not deny that, in fracture cases, MSCs derived from BM at the broken part of a cancerous bone may be included because of the reddish SF frequently obtained at the time of arthroscopic surgeries. Although a previous study reported that α3/β1 integrin is a specific marker of SF-MSCs (Shimaya et al., 2010), we have not yet examined the presence of this molecule on the MSCs. Another study suggested that protein gene product 9.5 (PGP9.5) may be specific to synovial cells (Kitamura et al., 1999); however, we have no useful data indicating the expression of this molecule SF-MSCs. Future studies examining a specific marker of MSCs are needed to identify equine SF-MSCs released from the synovium, or to discriminate BM cells that are included in the SF.

We propose a therapeutic strategy using SF-MSCs for cartilage regeneration following arthroscopic surgery in racehorses with IAF and OCD as follows: (1) preparation of over 10^7 MSCs in a short period; and (2) less invasive implantation of the MSCs into the cartilage defects. As shown here, 4-5 weeks (at passage 3 or 4) were required to obtain $> 1 \times 10^7$ MSCs from 3-4 ml SF. Compared to AT-MSCs and BM-MSCs, the cell doubling time of SF-MSCs was also longer. Nine days were needed until the next passage for SF-MSCs, whereas only 6 days were required to the next passage for AT-MSCs and BM-MSCs. The slower growth rate may indicate the inferiority of SF-MSCs relative to the other cell sources. Therefore, for SF-MSCs to be implanted at the time of the arthroscopic surgery, the SF should be collected

approximately 1 month before the surgery. To reduce the period of cell preparation, we will need to collect more SF using joint irrigation and other methods. Furthermore, a less invasive procedure for obtaining synovium should be investigated for clinical use. In a previous experiment, the cartilage defects on which a high-density suspension of synovium-derived MSCs was directly implanted during arthrotomy showed good cartilage regeneration (Koga et al., 2008). Also, less invasive arthroscopic surgery to implant them should be investigated for equine practice.

Our results suggest that equine SF might be a superior source of MSCs for cartilage regeneration, but more definitive results would be needed to conclude that SF-MSCs could be suitable for generating cartilage matrix during chondrogenic differentiation compared to AT-MSCs or BM-MSCs.

Table 3.1 Profiles of the synovial fluid (SF) samples.

Sample number	Age (years)	Sex	Disease	Diseased site (limb/joint)	Period of clinical onset (weeks)
01	3	F	IAF	RF/Carpus	2
02	2	F	IAF	RF/Fetlock	4
03	2	F	IAF	LF/Fetlock	4
04	1	F	IAF	LH/Tarsus	3
05	1	F	OCD	LH/Tarsus	3
06	3	M	IAF	RF/Carpus	2
07	3	F	IAF	RF/Carpus	2
08	3	M	IAF	RF/Carpus	2
09	3	M	IAF	RF/Carpus	2
10	6	M	IAF	RH/Tarsus	2
11	1	F	OCD	LH/Tarsus	No signs

SF samples were aseptically obtained from carpal, fetlock or tarsal joints of 11 Thoroughbred horses with IAF or OCD.

M, male; F, female; IAF, intra-articular fractures; OCD, osteochondritis dissecans; RF, right forelimb; LF, left forelimb; RH, right hind limb; LH, left hind limb.

Table 3.2 Colonies of normal and diseased equine synovial fluid (SF) derived mesenchymal stem cells at passage 0.

Source of stem cells	Sample number	Disease	Limb/Joint	Colonies at passage 0	Mean ± standard deviation	*P* value
SF from diseased joints	D1	IAF	RF/Carpus	73	166.9 ± 100.9	0.001
	D2	IAF	RF/Carpus	62		
	D3	IAF	LF/Carpus	94		
	D4	IAF	RF/Carpus	121		
	D5	IAF	LF/Carpus	364		
	D6	IAF	RF/Carpus	271		
	D7	OCD	RH/Tarsus	161		
	D8	IAF	RF/Carpus	136		
	D9	IAF	RF/Carpus	220		
SF from normal joints	N1	ND	LF/Carpus	10	8.3 ± 6.5	
	N2	ND	LF/Carpus	21		
	N3	ND	LF/Carpus	10		
	N4	ND	RF/Carpus	5		
	N5	ND	LF/Carpus	6		
	N6	ND	LH/Tarsus	3		
	N7	ND	RF/Carpus	5		
	N8	ND	RH/Tarsus	0		
	N9	ND	LF/Carpus	13		

SD, standard deviation; IAF, intra-articular fractures; OCD, osteochondritis dissecans; ND, no data; RF, right forelimb; LF, left forelimb; RH, right hind limb; LH, left hind limb.

Table 3.3 Primers' sequence, annealing temperature and fragment size of RT-PCR for premature, osteogenic, chondrogenic, adipogenic and tenogenic genes.

Marker	Gene	Sequence (Forward/Reverse)	Annealing temperature (°C)	Fragment (base pairs)
Premature	NANOG	5'-TACCTCAGCCTCCAGCAGAT-3'	58.0	190
		5'-CATTGGTTTTTCTGCCACCT-3'		
	SOX-2	5'-TGGTTACCTCTTCCTCCCACT-3'	58.0	179
		5'-GGGCAGTGTGCCGTTAAT-3'		
Osteogenesis	RUNX-2	5'-TGTCATGGCGGGTAACGAT-3'	61.3	107
		5'-TCCGGCCCACAAATCTCA-3'		
	ALP	5'-GCTGGGAAATCCGTGGGCATTGTG-3'	64.3	81
		5'-CGGCAGAGTGGGCGTAGG-3'		
	OC	5'-GAGGGCAGTGAGGTGGTGAAG-3'	63.3	152
		5'-CTCCTGGAAGCCGATGTGGTC-3'		
Chondrogenesis	SOX-9	5'-AGTACCCGCACCTGCACAAC-3'	50.0	79
		5'-CGCTTCTCGCTCTCGTTCAG-3'		
	COL-2	5'-GCTTCCACTTCAGCTATGGA-3'	56.9	256
		5'-TGTTTCGTGCAGCCATCCTT-3'		
	AGG	5'-TGCACAGACCCCGCCAGCTA-3'	51.4	339
		5'-GTCTCTAAACTCAGTCCACG-3'		
Adipogenesis	PPARγ2	5'-GTCTCATAACGCCATCAGGTTTG-3'	50.0	180
		5'-GCCCTCGCCTTCGCTTTG-3'		
Tenogenenesis	SCX	5'-TCTGCCTCAGCAACCAGAGA-3'	58.0	59
		5'-TCCGAATCGCCGTCTTTC-3'		
	TEN-C	5'-GATCTTCACTTCCCTACCAACG-3'	58.0	70
		5'-CTCATCCAGCATGGGGTC-3'		
Housekeeping	GAPDH	5'-ACCACAGTCCATGCCATCAC-3'	60.0	450
		5'-TCCACCACCCTGTTGCTGTA-3'		

NANOG, homeobox protein NANOG; SOX-2, sex determining region Y-box 2; GAPDH, glyceraldehyde-3-phosphate dehydrogenase; ALP, alkaline phosphatase; OC, osteocalcin; SOX-9, sex determining region Y-box 9; COL-II, type II collagen; AGG, aggrecan; PPARγ2, peroxisome proliferator activated receptor γ2; SCX, scleraxis; TEN-C, tenascin C.

Table 3.4 Antibodies for analysing the specific molecular markers on the cell surface.

Antibody	Company	Clone	Epitope	Dilution
CD11a/CD18	Gifted	CZ3.2, 117, 2E11, B10	Not confirmed	1:10
CD34	BD Bioscience	581/CD34	O-glycosylated transmembrane glycoprotein	1:5
CD44	AbD Serotec	CVS18	Not confirmed	1:10
CD45	BD Bioscience	2D1	T200 family	1:2.5
CD90	BD Bioscience	5E10	Not confirmed	1:10
CD105	AbD Serotec	SN6	Glycoprotein homodimer	1:10
MHC class I	Gifted	CZ3, 117,1B12, C11	Not confirmed	1:10
MHC class II	Gifted	CZ11, 130, 8E8, D9	Not confirmed	1:10
Isotype control	BD Bioscience	MOPC-21	Not confirmed	1:10

MHC, major histocompatibility complex.

Table 3.5 Percentages (%) of positive cells to specific molecular markers in the flow cytometry.

	Diseased SF-MSCs	Normal SF-MSCs	BM-MSCs	AT-MSCs
CD11a/CD18	73.7±2.3	61.6±3.2	80.1±1.1	79.6±5.5
CD34	0.3±0.2	0.3±0.2	0.4±0.1	1.0±0.2
CD44	98.1±0.6	97.9±0.5	96.8±0.0	95.6±2.4
CD45	0.2±0.1	0.2±0.1	0.4±0.1	1.0±0.8
CD90	99.0±0.4	96.0±3.7	98.5±0.7	98.7±0.8
CD105	73.5±6.0	77.9±1.6	50.2±27.2	77.1±14.5
MHC-1	94.6±3.3	95.9±1.6	90.8±6.5	94.5±2.6
MHC-II	71.9±4.1	74.9±3.0	78.1±3.9	79.3±7.7

SF, synovial fluid; BM, Bone marrow; AT, adipose tissue; MSCs, mesenchymal stem cells; MHC, major histocompatibility complex.

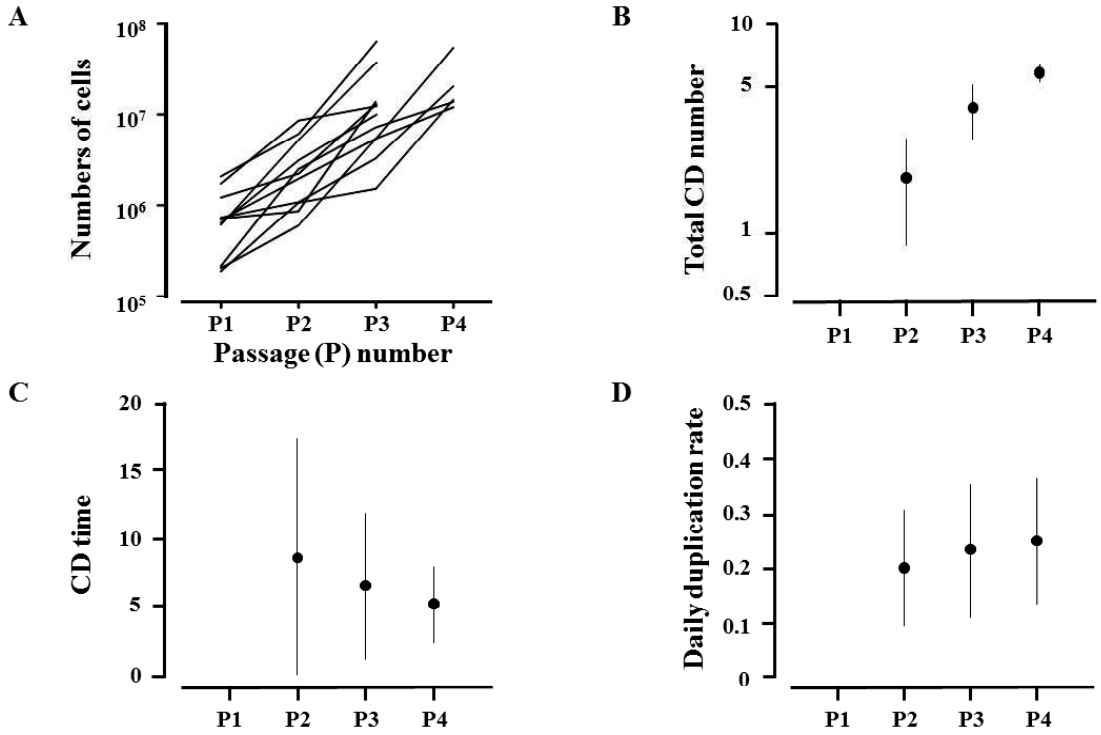

Figure 3.1 Growth curves (A), total cell doubling numbers (B), and cell doubling time (C), and daily duplication rate (D) of SF-MSCs from P0 to P4 collected from 11 horses. Six samples produced over 1 x 10^7 cells at P3 and five required about 6 weeks to reach > 1 x 10^7 cells (at P4). SF, synovial fluid; MSCs, mesenchymal stem cells; SF-MSCs, synovial fluid-derived mesenchymal stem cells; CD number = ln(Nf/Ni)/ln(2); CD, cell doubling; Nf, final number of cells; Ni, initial number of cells; CD time = cell culture time/CD number.

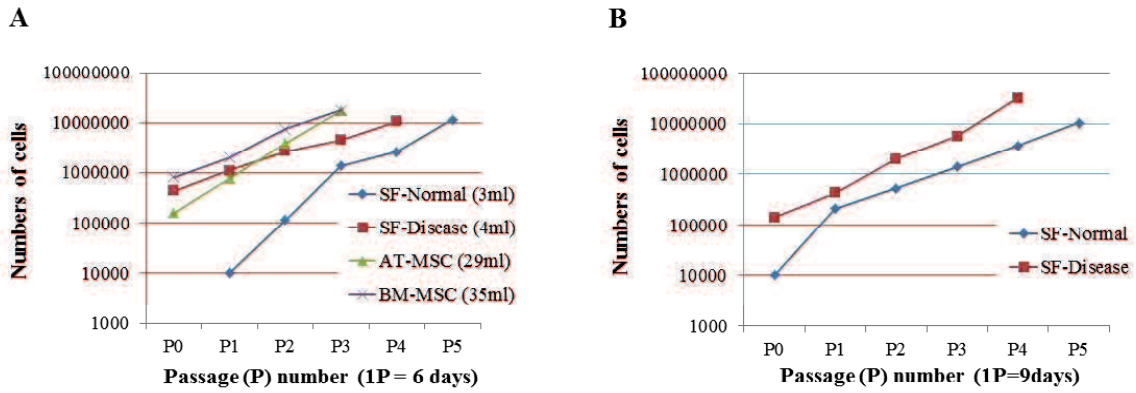

Figure 3.2 Growth curves of synovial fluid-derived mesenchymal stem cells (SF-MSCs), adipose tissue-derived MSCs (AT-MSCs) and bone marrow-derived MSCs (BM-MSCs). AT-MSCs and BM-MSCs could be repeatedly transferred to the next passage at intervals of 6 days, whereas SF-MSCs were transferred at intervals of 9 days. However, the cell doubling times of SF-MSCs (8.62 ± 8.62 days, 6.60 ± 5.33 days and 5.27 ± 2.91 days at P2, P3 and P4, respectively) were not statistically different from those of AT-MSCs (3.92 ± 0.04 days, 2.76 ± 0.23 days (P = 0.061) and 2.98 ± 0.14 days (P = 0.058) at P1, P2 and P3, respectively) and BM-derived MSCs (BM-MSCs) (6.55 ± 0.28 days, 3.55 ± 0.38 days (P = 0.099) and 4.70 ± 0.15 days (P = 0.286) at P1, P2 and P3, respectively).

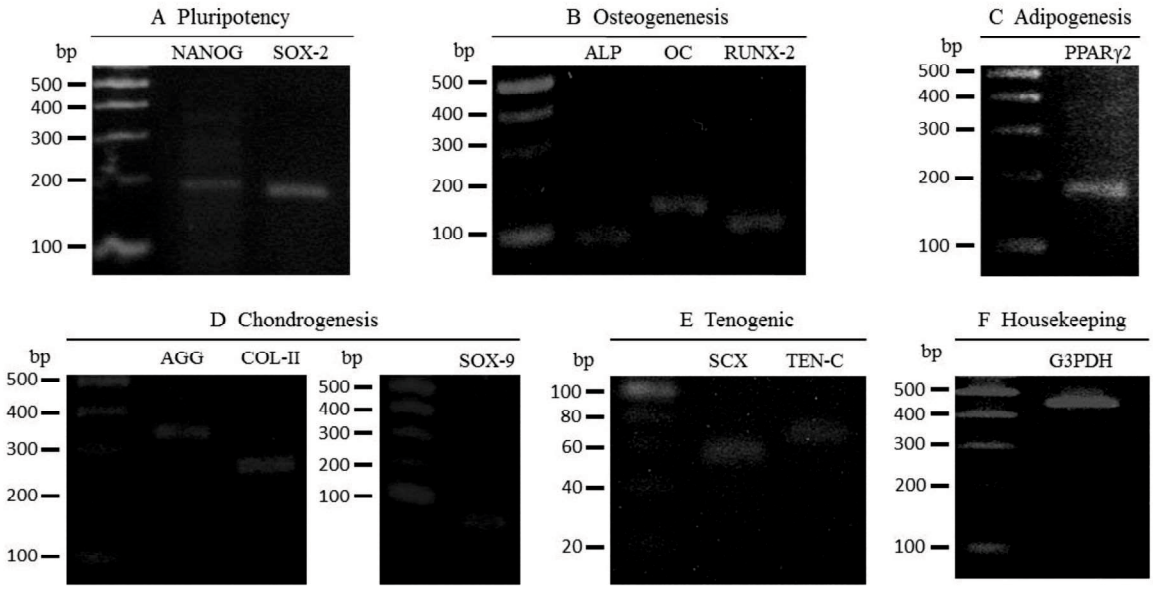

Figure 3.3 Results of RT-PCR using specific marker genes of premature, osteogenic, chondrogenic, adipogenic and tenogenic differentiation. Nanog, homeobox protein NANOG; Sox2, sex determining region Y-box 2; Runx2, runt-related transcription factor 2; ALP, alkaline phosphatase; OC, osteocalcin; Sox9, sex determining region Y-box 9; Col2, type II collagen; Agg, aggrecan; PPARγ2, peroxisome proliferator activated receptor γ2; Scx, scleraxis; TenC, tenascin C; G3PDH, glyceraldehyde-3-phosphate dehydrogenase.

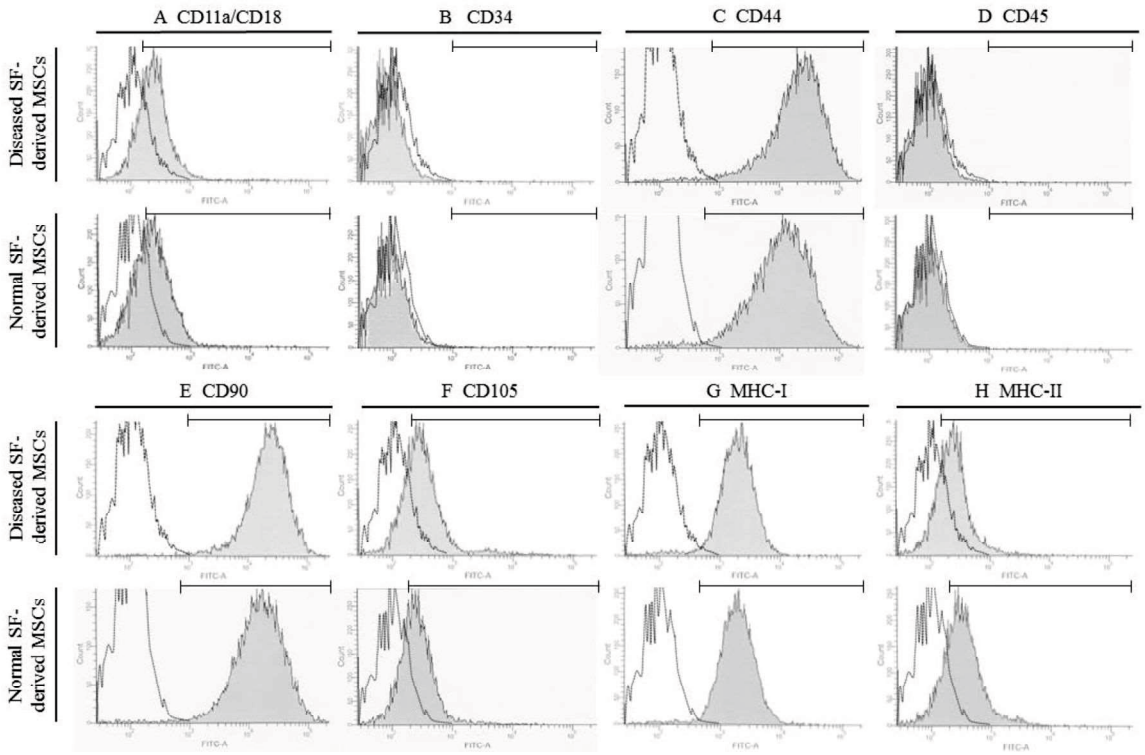

Figure 3.4 Results of flow cytometry using immunological markers on the SF-MSCs from normal and diseased joints. A strong shift in MFI was detected with antibodies against CD44 (C), CD90 (E), and MHC class I (G); a positive signal with antibodies against CD11a/18 (A), CD105 (F), and MHC class II (H) partially overlapped with the negative control; no positive signal was detected with antibodies against, CD34 (B) and CD45 (D). The dotted line represents the negative control. A horizontal line in individual histograms indicates the population of the positive cells. SF, synovial fluid; MSCs, mesenchymal stem cells; SF-MCSs, synovial fluid-derived mesenchymal stem cells; MHC, major histocompatibility complex.

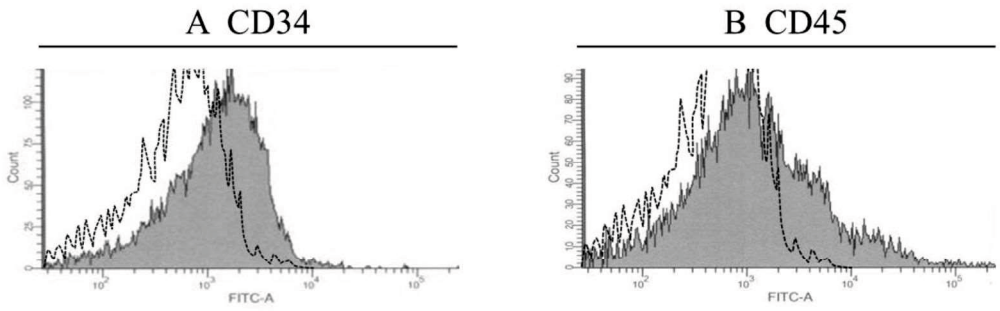

Figure 3.5 Results of flow cytometry using specific antibodies against CD34 (A) and CD45 (B) on equine mononuclear blood cells. Positive reactions of these antibodies were determined as previously reported (Barberini et al., 2014; Mohanty et al., 2014).

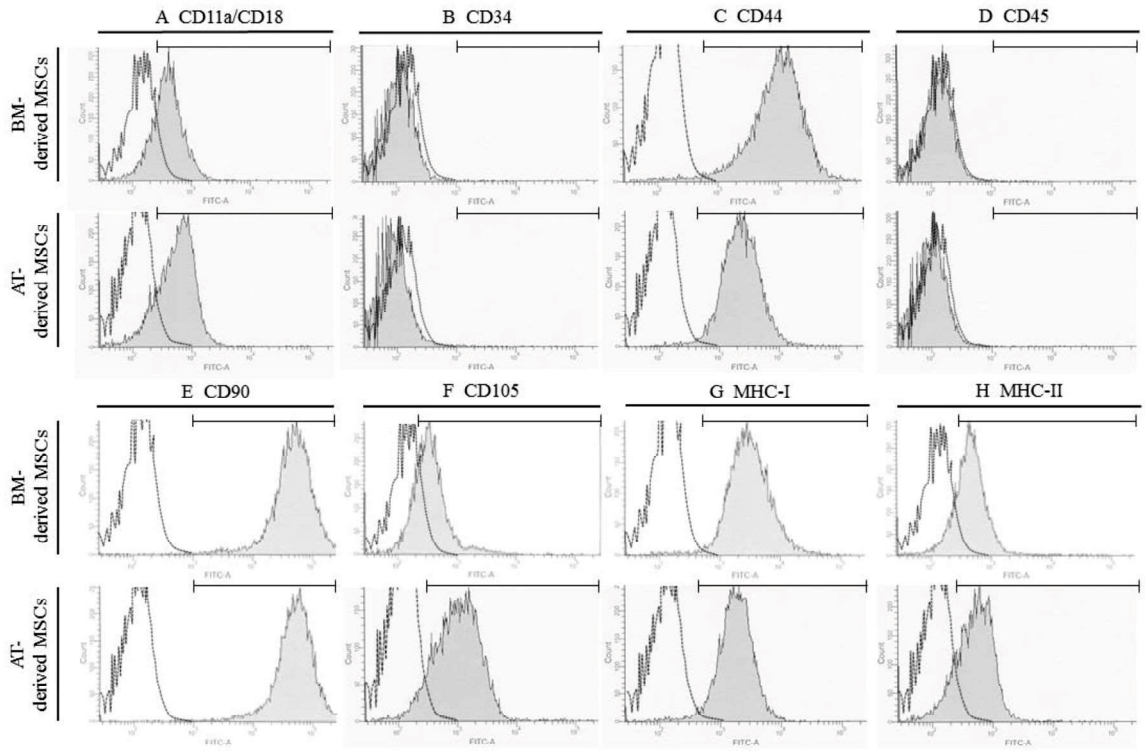

Figure 3.6 Results of flow cytometry using the same markers on the AT- and BM-MSCs. The dotted line represents the negative control. A horizontal line in individual histograms indicates the population of the positive cells. The signal patterns were corresponding to those in SF-MSCs. AT, adipose tissue; BM, bone marrow; SF, synovial fluid; MSCs, mesenchymal stem cells; AT-MSCs, adipose tissue-derived mesenchymal stem cells; BM-MSCs, bone marrow-derived mesenchymal stem cells; SF-MSCs, synovial fluid-derived mesenchymal stem cells; MHC, major histocompatibility complex.

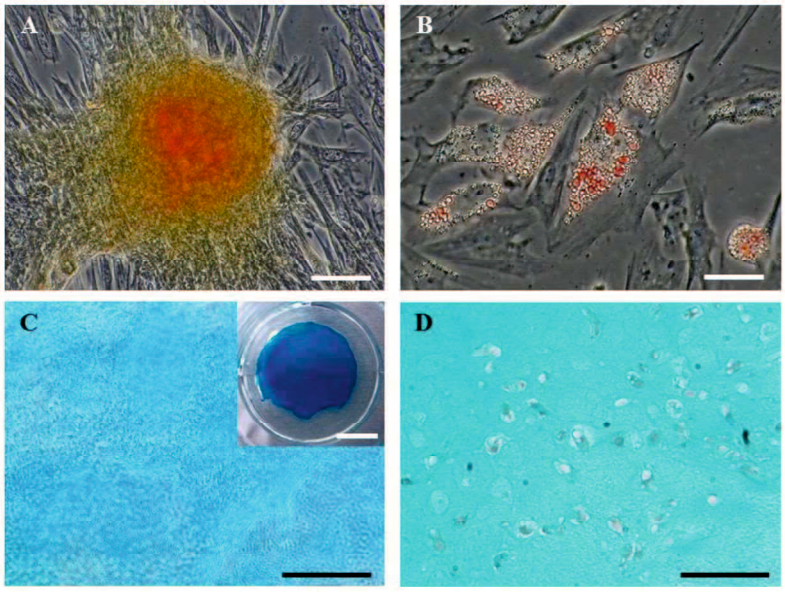

Figure 3.7 Representative images showing staining with alizarin red for osteogenic differentiation (A), oil red O for adipogenic differentiation (B) and Alcian blue for chondrogenic differentiation (C and D) of SF-MSCs. Following 2 weeks of osteogenic induction, the SF-MSCs aggregated and contracted to form a colony and showed a characteristic of the stroma (calcium apatite crystals as stained with alizarin red). Scale bar = 100 µm (A). Adipogenic induction of SF-MSCs resulted in adipocyte-like flattened cells with small lipid vesicles that stained with oil red O. Scale bar = 50 µm (B). The chondrogenic dish culture of SF-MSCs induced a change in cell shape into a stone-wall structure. Scale bar = 500 µm. A gelatinous monolayer sheet was present that intensely stained with Alcian blue, scale bar indicates 1 cm in an inset picture (C). Histological observation of the cell pellets showed a hyaline cartilage-like structure that was positively stained with Alcian blue. Scale bar = 100 µm (D).

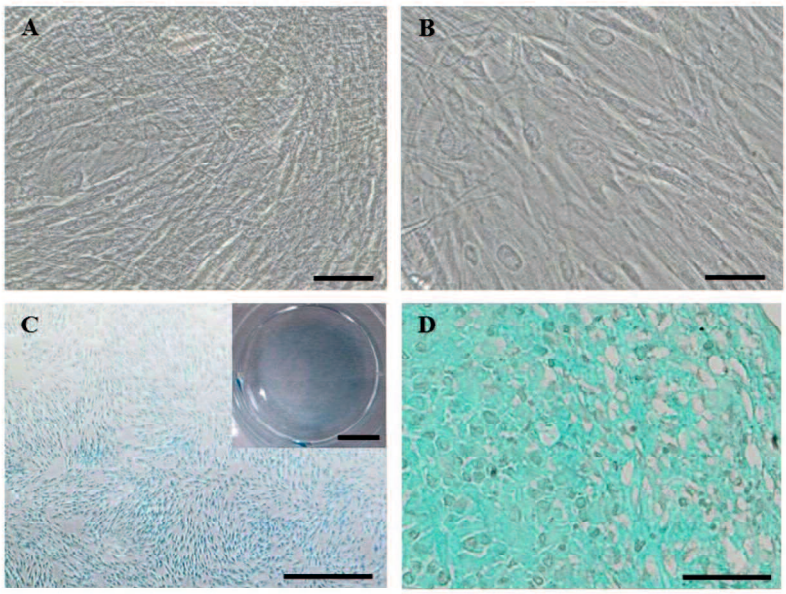

Figure 3.8 Representative images showing SF-MSCs staining with alizarin red oil red O (B) and Alcian blue (C and D). They were negative controls in dishes with CCM for the corresponding weeks to osteogenic, adipogenic and chondrogenic differentiation (A-C). The negative control of cell pellet (D) was cultured in chondrogenic induction medium not containing TGF-β3. Positive staining was not seen in A and B at all, and also gelatinous monolayer sheet was not formed (C). Chondrocyte and hyaline matrix were not seen in the pellet (D). SF, synovial fluid; MSCs, mesenchymal stem cells; SF-MSCs, synovial fluid-derived mesenchymal stem cells; CCM, complete culture medium.

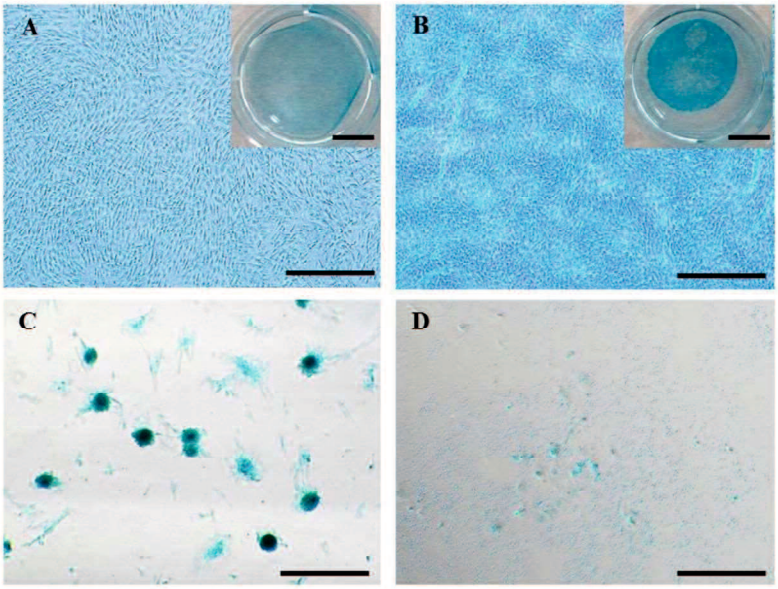

Figure 3.9 Representative images showing staining chondrogenic dish culture of SF-MSCs, AT-MSCs, and BM-MSCs with Alcian blue. Staining of the gelatinous sheets in SFs-MSCs was intensely blue throughout in SF-MSCs at P10 (A) from the diseased joints, as well as SF-MSCs from the normal joints (B). Blue sheets were not formed by chondrogenic induction of AT-MSCs and BM-MSCs (C and D). SF, synovial fluid; AT, adipose tissue; BM, bone marrow; MSCs, mesenchymal stem cells; SF-MSCs, synovial fluid-derived mesenchymal stem cells; AT-MSCs, adipose tissue-derived mesenchymal stem cells; BM-MSCs, bone marrow-derived mesenchymal stem cells. Scale bar = 500 μm

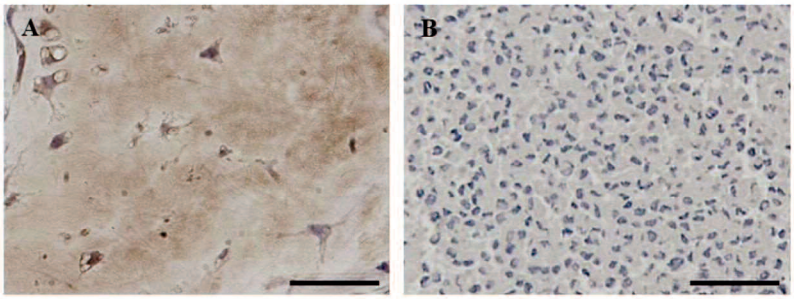

Figure 3.10 Representative images showing immunohistochemistry using a specific antibody against equine COMP for the chondrogenic differentiation of synovial fluid (SF)-derived mesenchymal stem cells (MSCs) (A) and the negative control cultured in chondrogenic induction medium without transforming growth factor (TGF)-β3 (B). Scale bar = 100 μm.

Chapter 4

A preliminary study on

characteristics of equine dedifferentiated fat cells

4.1 Introduction

To prepare the number of multi-potency cells required for clinical use during a short period, various cell sources, different culture media and protocols have been studied on mesenchymal stem cells (MSCs) of horses. Adipose tissue (AT) contains more numerous MSCs per unit weight of tissue, comparing to the other tissues such as bone marrow, umbilical cord, and so on (Burk et al., 2013). However, a regeneration therapy using AT-derived mesenchymal stem cells (AT-MSCs) could be less acceptable in racehorse practice, because of the lower body fat rate in Thoroughbreds (Kearns et al., 2002).

In Previous studies, it has been shown that mature adipocytes isolated from fat tissue could be dedifferentiated into fibroblast like cells with ceiling-culture method (Sugihara et al., 1986). The adipocyte-derived fibroblast-like cells also show proliferative activity (Sugihara et al., 1987; Sugihara et al., 1989). The recent studies reported mature adipocyte-derived dedifferentiated fat (DFAT) cells which are multi-potent and obtained abundantly in ceiling-culture of mouse, human, rat, porcine, rabbit, bovine and feline cells (Kikuta et al., 2013; Kono et al., 2014; Matumoto et al., 2008; Ono et al., 2011; Wei et al., 2013; Yagi et al., 2004). Because mature adipocytes are most abundant cells in adipose tissue (Matumoto et al., 2008), they could be more numerous than MSCs in AT. Therefore, if equine adipocytes could be converted into DFAT cells, it would be helpful to increase the number of multi-potency cells derived from AT and to shorten the time to prepare the number of the stem cells required for the therapy. The aims of this study were to establish equine DFAT cells derived from mature adipocytes and to investigate the characteristics and multi-potency of the cells.

4.2 Materials & Methods

4.2.1 Animals & Samples

Nine horses (one male and eight females, 2-10 years old) in slaughterhouse were used to obtain AT samples. All procedures were approved by the Animal Care and Use Committee of Kagoshima University (Approval No. A11037).

4.2.2 Collection of AT from animals

Five gram of AT was obtained from the gluteal region of nine horses.

4.2.3 Adipocyte isolation

Five gram of AT was treated with a 5 × volume of PBS containing 0.1% collagenase (Collagenase Type I; Worthington Biochemical, Lake Wood, NJ) at 37 °C for 90 min, filtered through a 70 μm nylon filter (Cell Strainer; BD, Franklin Lakes, NJ) and centrifuged at 160 × *g* for 5 min at room temperature (RT). One ml of supernatant (containing the mature adipocyte) was collected for DFAT culture. This procedure was performed for AT from nine horses.

4.2.4 Adipocyte dedifferentiation

The supernatant was placed in 12.5-cm^2 culture flask filled completely with complete culture medium (CCM) consisting of Dulbecco's Modified Eagle's Medium (DMEM, Thermo Fisher Scientific, Waltham, MA), 10% fetal bovine serum (FBS, Thermo Fisher Scientific, Waltham, MA) and 1% antibiotic-antimycotic preparation (500 U Penicillin G, 500 μg streptomycin and 1.25 μg amphotericin B as final

concentrations; Antibiotic-Antimycotic; Thermo Fisher Scientific, Waltham, MA). As the flask was inverted, and the floating cells on the medium were touched on the ceiling plane of the flask (Ceiling culture: CC). Following 7 days of CC at 37°C in 5% CO_2, the medium was changed and the flask return to usual culture from CC on the 7th day at Passage 0 (P0D7). Following other 7 days, the cells adhering to the bottom plane of the flask were washed with PBS and harvested with 0.05% trypsin and 0.2 mM ethylene diamine tetraacetic acid (EDTA) (Trypsin-EDTA; Thermo Fisher Scientific, Waltham, MA) as DFAT cells and centrifuged (P0D14).

4.2.5 Isolation of mesenchymal stem cells from AT

Subcutaneous AT was obtained from the gluteal region of two horses (a male aged 10 years old and a female aged 3 years old), using liposection under the epidural anaesthesia with 2% lidocaine (Xylocaine injection 2%; AstraZeneca, London, U.K.) following pre-medication with 40 μg/kg medetomidine HCl (Domitor, Zenoaq, Fukushima, Japan) and 10 μg/kg butorphanol tartate (Vetorphale, Meiji Seika, Tokyo, Japan). After the subcutaneous injection of 100-200 ml liposuction solution consisted of 500 ml physiological saline (Otsuka Normal Saline, Otsuka, Tokyo, Japan), 20 ml 1% lidocaine and 20 ml 0.001% adrenaline (200mg lidocaine and 200μg adrenaline; Xylocaine injection 1% with Epinephrine, AstraZeneca, London, U.K.) through a 5 mm skin incision, the swollen AT was aspirated with a probe (Collection Cannula, 14G, 30cm long, Cytori, San Diego, CA) connected to a 50 ml syringe. This procedure was repeated 3 times. Fifteen gm of AT was digested with a 5 × volume of PBS containing 0.1% collagenase (Collagenase type I, Worthington Biochemical, Lake Wood, NJ) at 37 °C for 90 min, filtered through a 70 μm nylon filter (Cell Strainer, BD, Franklin

Lakes, NJ) and centrifuged at 160 g for 5 min at room temperature. The cell pellet was resuspended in CCM and incubated at 37 °C in 5% CO_2 for 9 days, then cells adhering to the bottom of the flask were washed with PBS and harvested as AT-MSCs. The medium was changed on the day 6 (D6; P0). This procedure was performed for AT from two horses.

4.2.6 Cell expansion

The non-adhering sediment was re-suspended in CCM, and incubated at 37 °C in 5% CO_2 for 6 days (P1D0). The medium was changed every 3 days for 6 days after P1. The cells were harvested and centrifuged (P1D6). After decanting the supernatant, the pellet was rinsed with CCM and the cells were replated at 1×10^6 cells in 150 cm^2 dishes and cultured for 6 days (P2D0). This serial process of passaging was repeated to obtain > 1×10^7 cells for the following analysis in vitro. The total number of the cells at every passage from P0 was determined with a cell counter (TC10, BioRad, Hercules, CA). Proliferation rates were calculated as the cell doubling number and cell doubling time using the following formulas:

Cell doubling number = ln(final number of cells/initial number of cells)/ln(2)

Cell doubling time = Cell culture time/cell doubling number

Expression of genetic markers, immunological cell-surface markers and multi-potency of the cells were analysed at P5.

4.2.7 Analysis for premature marker genes with RT-PCR

Total RNA from the cultured cells was prepared with an RNA Isolation kit (mirVana miRNA Isolation Kit, Thermo Fisher Scientific, Waltham, MA), and then was

converted to cDNA with an RT-PCR kit (ReverTra Dash, TOYOBO, Osaka, Japan) according to the manufacturer's instructions. As multipotency markers, sex determining region Y-box 2 (SOX-2) were evaluated the expression of mRNA by RT-PCR (Table 4.1). The PCR products were separated by electrophoresis on a 1.5% agarose gel (Agarose WP; Wako Pure Chemical Industries, Osaka, Japan) and labelled with SYBR green (Takara Bio, Otu, Japan) .

4.2.6 Analysis for immunological cell-surface markers with flow cytometry

Cells (1×10^4) were resuspended in 500 μl staining buffer (SB; PBS containing 1% FBS) and incubated for 30 min at RT with 20 μg/ml antibodies, which have been known the specificity or cross-reaction to equine CD11a/CD18, CD34, CD44, CD45, CD90, CD105 and major histocompatibility complex (MHC) classes I and II (Table 4.2). Antibodies against CD11a/CD18, CD44 and MHC classes I and II were coupled with secondary antibodies conjugated to fluorescein isothiocyanate (FITC). Non-specific FITC mouse immunoglobulin G1κ was used as a negative control. Cell fluorescence was evaluated as a shift in the mean fluorescence intensity (MFI) by flow cytometry instrument (FACS Aria II, BD). The data were analysed using flow cytometry software (FACS Diva software, BD).

4.2.7 Analysis for Tri-linage differentiation

4.2.7.1 Osteogenic differentiation assay

To investigate osteogenic differentiation, cells were plated in 6-well plates (6 Well Plate-N, NEST Biotech) in CCM at an initial density of 2.5×10^3 cells/cm^2. After 24 h

incubation, CCM was replaced with osteogenic induction medium (Differentiation Basal Medium-Osteogenic, LONZA, Basel, Switzerland) supplemented with 100μM ascorbic acid, 10mM β-glycerophosphate and 1μM dexamethasone. After 2 weeks in induction medium, production of calcium crystal in the osteogenic extracellular matrix was evaluated by staining with Alizarin Red.

4.2.7.2 Chondrogenic differentiation assay

For chondrogenic differentiation, cells were plated in 6-well plates (6 Well Plate-N, NEST Biotech) in CCM at an initial density of 2.5×10^3 cells/cm^2 as same as osteogenic induction. Chondrogenic differentiation was induced in 6-well plates in 2 ml induction medium (Differentiation Basal Medium-Chondrogenic, LONZA) supplemented with 4.5g/l $_D$-glucose, 350μM $_L$-proline, 100nM dexamethasone and 0.02g/l transforming growth factor beta 3 (TGF-β3), which was replaced three times per week, similar to osteogenic induction. After 2 weeks, production of mucopolysaccharide in the chondrogenic extracellular matrix was determined by staining with Alcian blue.

4.2.7.3 Adipogenic differentiation assay

Adipogenic induction was begun when cells reached a density of 1.5×10^4 cells/cm^2 on 6-well plates (6 Well Plate-N, NEST Biotech) in basal medium. Following pre-incubation for 24 h, CCM was replaced with adipogenic induction medium (Differentiation Basal Medium-Adipogenic, LONZA), composed of DMEM supplemented with 4.5g/l $_D$-glucose, 100μM indomethacin, 10μg/ml insulin, 0.5mM 3-isobutyl-1-methylxanthine, 1μM dexamethasone and 5% rabbit serum. Five days later, adipocyte-specific intracellular lipids were stained with oil red O.

4.2.8 Statistical analysis

All quantitative group data are shown as the mean ± standard deviation (SD). Data were analysed using Student's t-test (Excel, Microsoft). Differences of $P < 0.05$ were considered to be statistically significant.

4.3 Results

4.3.1 Adipocyte isolation and dedifferentiation

After collagenase treatment and centrifugation of AT, most of the floating cells in the upper layer were mono-vacuolar spherical adipocytes. Approximately 50% of the cells adhered to the ceiling of the flask and exhibited extended cytoplasm by day 5 (P0D5; Figure 4.1A). Some of the cells had many divided droplets in their cytoplasm (P0D6; Figure 4.1B). The cells generated fibroblast-like DFAT cells, colonised by day 7 (P0D7; Figure 4.1C), and thereafter became DFAT cells exhibiting spindle-shaped morphology without droplets by day 14 at P0 (P0D14; Figure 4.1D).

4.3.2 Proliferation of DFAT cells

The proliferation rates of DFAT cells and AT-MSCs were summarised in Table 4.3. DFAT cells proliferated over 1×10^7 cells at P3 or P4 (Figure 4.2A), and the average numbers of them were $1.54 \times 10^5 \pm 9.27 \times 10^4$, $1.3 \times 10^6 \pm 6.76 \times 10^5$, $3.44 \times 10^6 \pm 1.75 \times 10^6$, $1.02 \times 10^7 \pm 5.98 \times 10^6$, and $1.68 \times 10^7 \pm 3.61 \times 10^6$ at P0, P1, P2, P3, and P4, respectively (Figure 4.2B). Thus, the total cell doubling numbers of DFAT cells were 3.08 ± 0.57, 4.52 ± 0.78, 6.02 ± 0.99, and 7.28 ± 0.69 at P1, P2, P3, and P4, respectively (Figure 4.2C), and the cell doubling times (days) were 2.01 ± 0.33, 4.8 ± 1.73, 4.32 ± 1.14, and 3.33 ± 0.46 at P1, P2, P3, and P4, respectively (Figure 4.2D).

AT-MSCs proliferated over 1×10^7 cells at P3 (Figure 4.3A), and the average numbers of the cells were $2.24 \times 10^5 \pm 6.4 \times 10^4$, $1.11 \times 10^6 \pm 3.34 \times 10^5$, $4.89 \times 10^6 \pm 9.05 \times 10^5$, and $1.96 \times 10^7 \pm 2.35 \times 10^6$ at P0, P1, P2, and P3, respectively (Figure 4.3A). Thus, the total cell doubling numbers of AT-MCSs were 2.3 ± 0.02, 4.48 ± 0.15, and 6.5 ± 0.25 at P1, P2, and P3, respectively (Figure 4.3B) and the cell doubling times (days)

of them were 2.61 ± 0.03, 2.76 ± 0.23, and 2.98 ± 0.14 at P1, P2, and P3, respectively (Figure 4.3C).

4.3.3 Expression of premature marker genes and immunological cell-surface markers of DFAT cells

DFAT cells were positive for the expression of SOX-2 as multi-potency marker genes (Figure 4.4). As shown in Figure 5, the MFI strongly shift using antibodies against CD44 (91.8%), CD90 (99.0%), and MHC class I (89.3%). The positive shifts were moderate with antibodies against CD11a/18 (81.2%), CD105 (84.6%), and MHC class II (83.5%) were moderate, whereas no positive reactions were detected with antibodies against CD34 (0.5%) and CD45 (0.6%). The antibodies against CD34 and CD45 were positive in the equine mononuclear blood cells (The data was not shown), as previously presented (Barberini et al., 2014; Mohanty et al., 2014).

In accordance with our previous results of AT-MSCs (in Chapter 3), the MFI strongly shifted using antibodies against CD44, CD90, CD105 and MHC class I. Similarly, positive shifts were moderate with antibodies against CD11a/18 and MHC class II, whereas no positive reactions were detected with antibodies against CD34 and CD45.

4.3.4 Tri-linage differentiation

Following the osteogenic induction, a cluster of DFAT cells produced a specific matrix including calcium apatite crystals, which were positively stained with alizarin red (Figure 4.6A, negative control is shown in Figure 4.6B), correspondingly in AT-MSCs (Figure 4.7A). After the chondrogenic induction, DFAT cells aggregated and

then contracted to form colonies that stained intensely with Alcian blue (Figure 4.6C, negative control is shown in Figure 4.6D), correspondingly in AT-MSCs (Figure 4.7B). Adipogenic induction of DFAT cells resulted in adipocyte-like flattened cells with small lipid vesicles that stained positively with oil red O (Figure 4.6E, negative control is shown in Figure 4.6F), correspondingly in AT-MSCs (Figure 4.7C).

4.4 Discussion

We started the culture of equine DFAT cells from 1ml supernatant which was totally collected 5 ml after treated approximately 5 gram AT with collagenase. On the other hand, we digested 15ml AT which was treated approximately 15 gram AT with collagenase, separated the cell pellet as the sediment after centrifugation, and cultured AT-MSCs. Therefore, initial AT volume of DFAT cells was fifteen times lower than that of DFAT cells. However, the average numbers of DFAT cells made a little difference from those of AT-MSCs at P0, P1, and P2 as presented above (Table 4.3). The results indicated that average numbers of DFAT cells in the initial culture would be approximately fifteen times as high as those of AT-MSCs. Therefore, we suggested that equine AT could include approximately fifteen times of DFAT cell sources comparing to AT-MSCs. Thus, equine adipocytes which have been suggested the source of DFAT cells could be more included than MSCs in AT, as previously reported in other animals (Matumoto et al., 2008).

A previous study indicated that equine adipocytes were harvested 1.8×10^6 cells per gm on average (Carrington et al., 2003). As another papers reported, approximately 40-50 % of adipocytes adhered to the ceiling of the flask during ceiling culture (Kono et al., 2014; Matsumoto et al., 2008). Mathematically speculating about those reports, we could make approximately 8×10^6 adipocytes dedifferentiate into DFAT cells. However, we actually obtained about 1.5×10^5 cells, which is less than expected. On the other hand, another report mentioned that DFAT cells from 1g of AT could be prepared only 5×10^4 cells, which was approximately 40 times lower than AT-MSCs (2×10^6) at the beginning of primary culture (Kono et al., 2014). Total doubling numbers of equine DFAT cells were little less than those of AT-MSCs at P1, P2, and P3, respectively.

Doubling time of equine DFAT cells was at the range of 48 to 120 h, which was longer than those in the other species such as human and feline (Kono et al., 2014; Matsumoto et al., 2008). The results of flow cytometry analysis showed the same immunophenotypes (positive to CD44 and CD90; negative to CD34 and CD45) in both equine DFAT cells and AT-MSCs. Equine DFAT cells showed similar multi-lineage differentiation potentials to AT-MSCs as reported in the other animals (Kono et al., 2014; Matsumoto et al., 2008). These findings suggest that not only AT-MSCs, but also DFAT cells are a candidate cell source for cell-based therapies in horses.

Table 4.1 Reverse transcriptase PCR primer sequences, annealing temperatures and amplification product sizes for multipotent genes.

Marker	Gene	Sequence (Forward/Reverse)	Annealing temperature (°C)	Fragment (base pairs)
Multipotency	SOX-2	5'-TGGTTACCTCTTCCTCCCACT-3' 5'-GGGCAGTGTGCCGTTAAT-3'	58.0	179
Housekeeping	GAPDH	5'-ACCACAGTCCATGCCATCAC-3' 5'-TCCACCACCCTGTTGCTGTA-3'	60.0	450

SOX-2, sex determining region Y-box 2; GAPDH, glyceraldehyde-3-phosphate dehydrogenase

Table 4.2 Antibodies for analysing the specific molecular markers on the cell surface.

Antibody	Company	Clone	Epitope	Dilution
CD11a/CD18	Gifted	CZ3.2, 117, 2E11, B10	Not confirmed	1:10
CD34	BD Bioscience	581/CD34	O-glycosylated transmembrane glycoprotein	1:5
CD44	AbD Serotec	CVS18	Not confirmed	1:10
CD45	BD Bioscience	2D1	T200 family	1:2.5
CD90	BD Bioscience	5E10	Not confirmed	1:10
CD105	AbD Serotec	SN6	Glycoprotein homodimer	1:10
MHC class I	Gifted	CZ3, 117,1B12, C11	Not confirmed	1:10
MHC class II	Gifted	CZ11, 130, 8E8, D9	Not confirmed	1:10
Secondary (FITC)	Rockland	-	Mouse IgG (H and L)	1:500
Isotype control	BD Bioscience	MOPC-21	Not confirmed	1:10

MHC, major histocompatibility complex; FITC, fluorescein isothiocyanate.

The antibodies against CD11a/18 and MHC classes I and II were gifted from Dr Douglas Antczak, Cornell University, Ithaca, New York 14853, USA.

Table 4.3 Summary of proliferation rate in DFAT cells and AT-MSCs

Passage	Proliferation rate	DFAT cells	AT-MSCs	P value
P0	Average number	$1.54\times10^5\pm9.27\times10^4$	$2.24\times10^5\pm6.4\times10^4$	—
P1	Average number	$1.3\times10^6\pm6.76\times10^5$	$1.11\times10^6\pm3.34\times10^5$	—
	Total doubling number	3.08±0.57	2.3±0.02	0.005 (< 0.05)
	Doubling time	2.01±0.33	2.61±0.03	0.0007 (<0.05)
P2	Average numbers	$3.44\times10^6\pm1.75\times10^6$	$4.89\times10^6\pm9.05\times10^5$	—
	Total doubling number	4.52±0.78	4.48±0.15	0.905
	Doubling time	4.8±1.73	2.76±0.23	0.012 (< 0.05)
P3	Average numbers	$1.02\times10^7\pm5.98\times10^6$	$1.96\times10^7\pm2.35\times10^6$	—
	Total doubling number	6.02±0.99	6.5±0.25	0.313
	Doubling time	4.32±1.14	2.98±0.14	0.012 (< 0.05)
P4	Average numbers	$1.68\times10^7\pm3.61\times10^6$	—	
	Total doubling number	7.28±0.69		
	Doubling time	3.33±0.46		

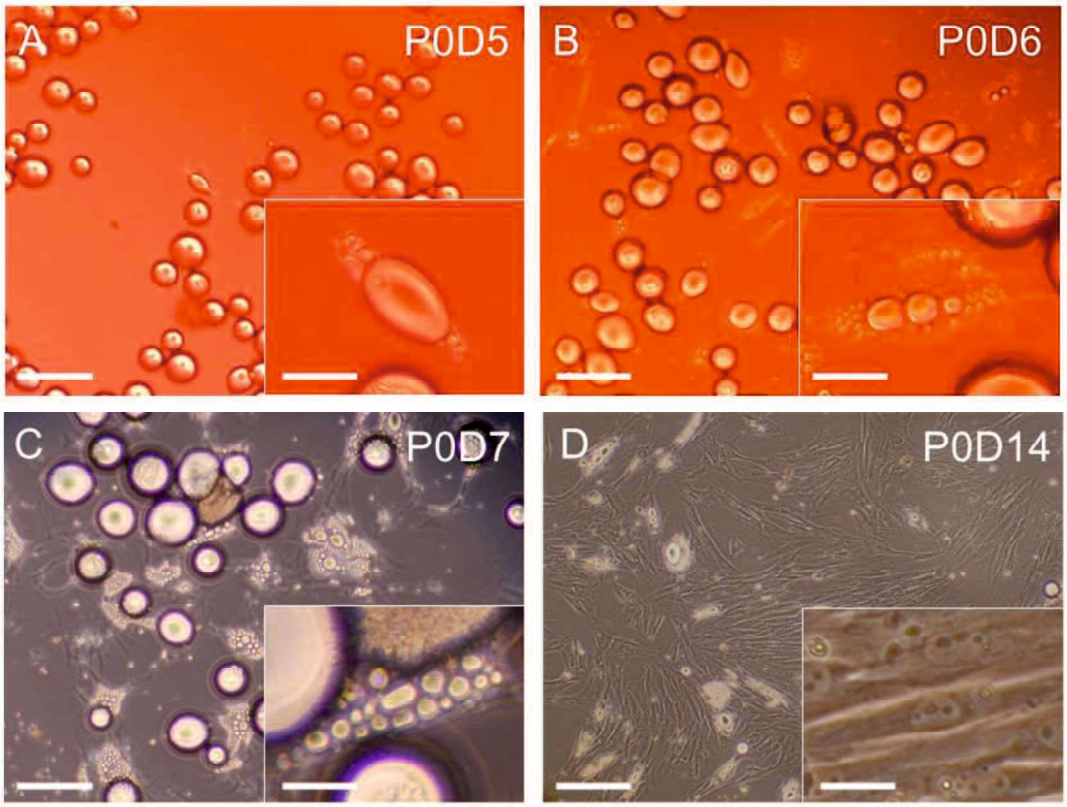

Figure 4.1 Representative images showing a series of dedifferentiation of equine mature fat cells prepared from gluteal subcutaneous adipose tissue. The majority of cells floating in the upper layer were mono-vacuolar spherical adipocytes at the beginning of ceiling culture, but approximately 50% of isolated cells adhered to the ceiling of the flask and exhibited extended cytoplasm by day 5 (P0D5; A). Some cells had many divided droplets in their cytoplasm (P0D6; B). The cells divided and generated fibroblast-like DFAT cells, and thereafter colonised by day 7 (P0D7; C). DFAT cells exhibited spindle-shaped morphology without droplet by day 14 at P0 (P0D14; D). Scale bar = 100 μm, Scale bar (in insert images) = 10 μm

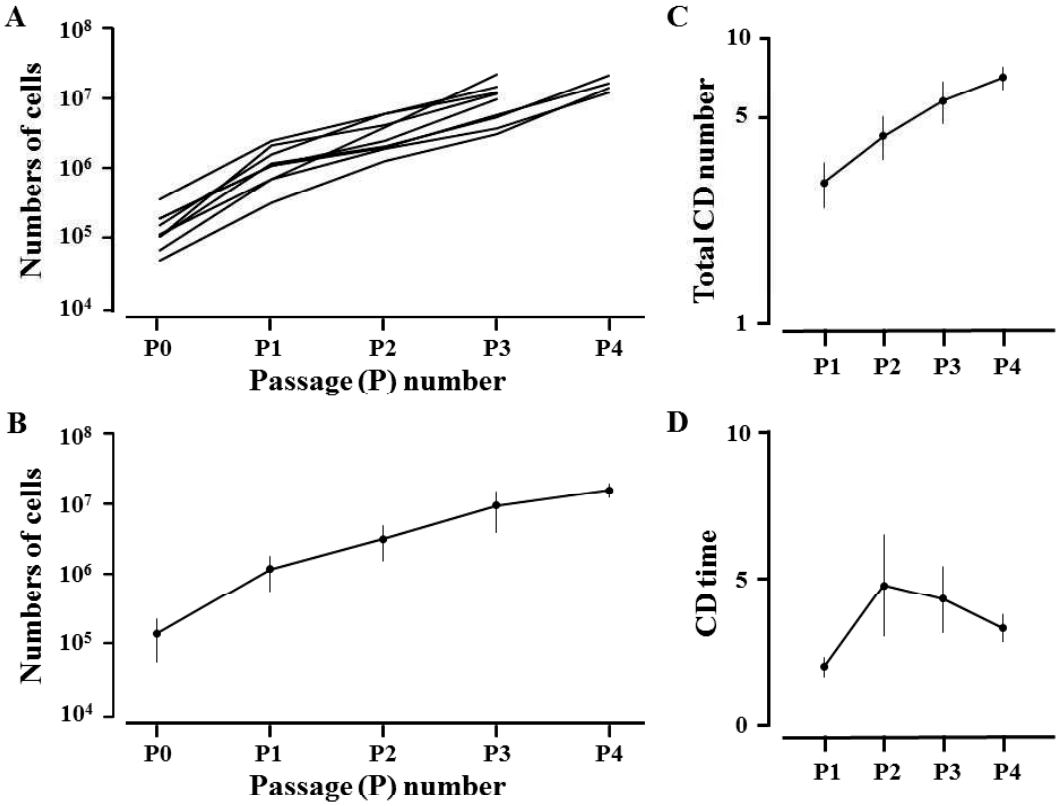

Figure 4.2 Growth curves (A), Average growth curve (B), total cell doubling numbers (C) and cell doubling (CD) times (D) from passages 0 to 4 (P0-P4) of dedifferentiated fat (DFAT) cells collected from nine horses. Five samples produced > 1×10^7 cells at P3 and four samples required more 6 weeks to reach > 1×10^7 cells (at P4). CD number = ln(Nf/Ni)/ln(2). CD time = cell culture time/CD number. Nf, final number of cells; Ni, initial number of cells.

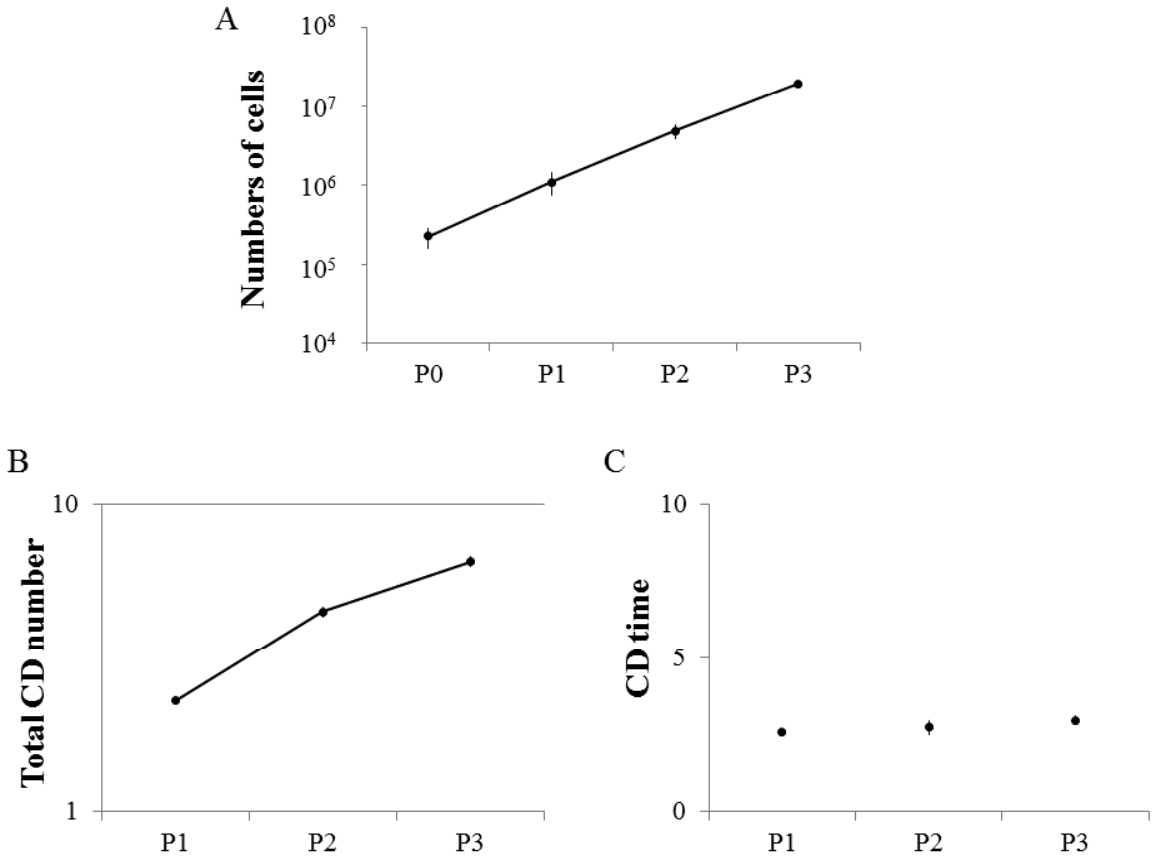

Figure 4.3 Average growth curve (A), total cell doubling numbers (B) and cell doubling (CD) times (C) from passages 0 to 3 (P0-P3) of AT-MSCs collected from two horses. Both samples produced > 1×10^7 cells at P3. CD number = ln(Nf/Ni)/ln(2). CD time = cell culture time/CD number. Nf, final number of cells; Ni, initial number of cells.

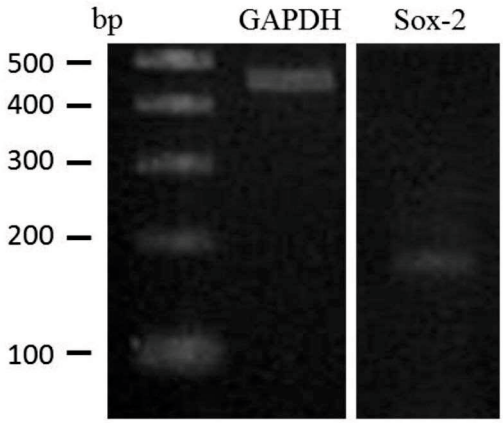

Figure 4.4 Results of reverse transcriptase-PCR using Sox-2 as multipotency marker gene. Sox2, sex determining region Y-box 2; G3PDH, glyceraldehyde-3-phosphate dehydrogenase.

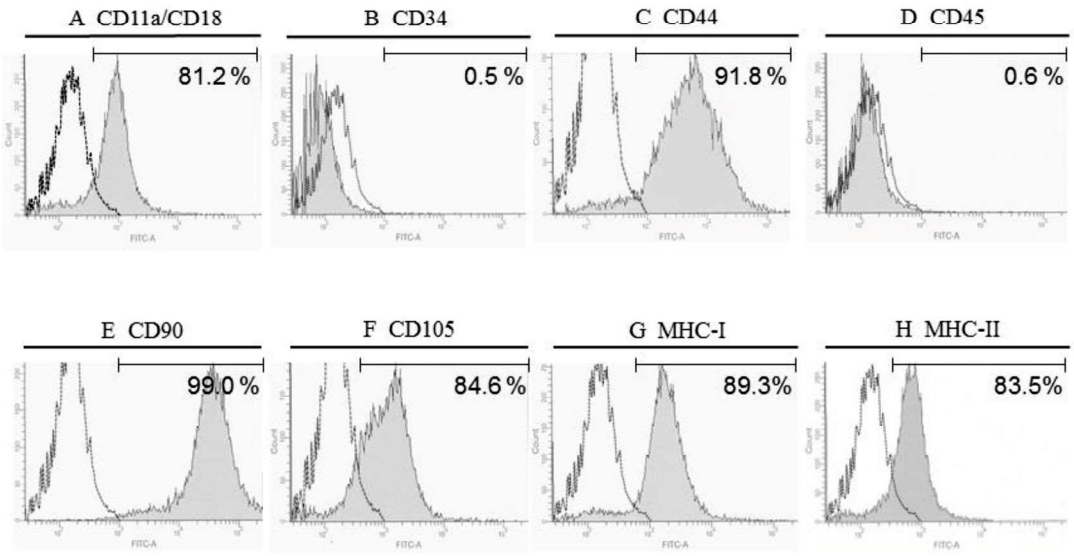

Figure 4.5 Results of flow cytometry using immunological markers on synovial fluid (SF)-derived mesenchymal stem cells (MSCs) from normal and diseased joints. A strong shift in mean fluorescence intensity (MFI) was detected with antibodies against CD44 (C), CD90 (E) and major histocompatibility complex (MHC) class I (G); a positive signal with antibodies against CD11a/18 (A), CD105 (F) and MHC class II (H) partially overlapped with the negative control; no positive signal was detected with antibodies against CD34 (B) and CD45 (D). The dotted line represents the negative control. The horizontal line in individual histograms indicates the population of the positive cells.

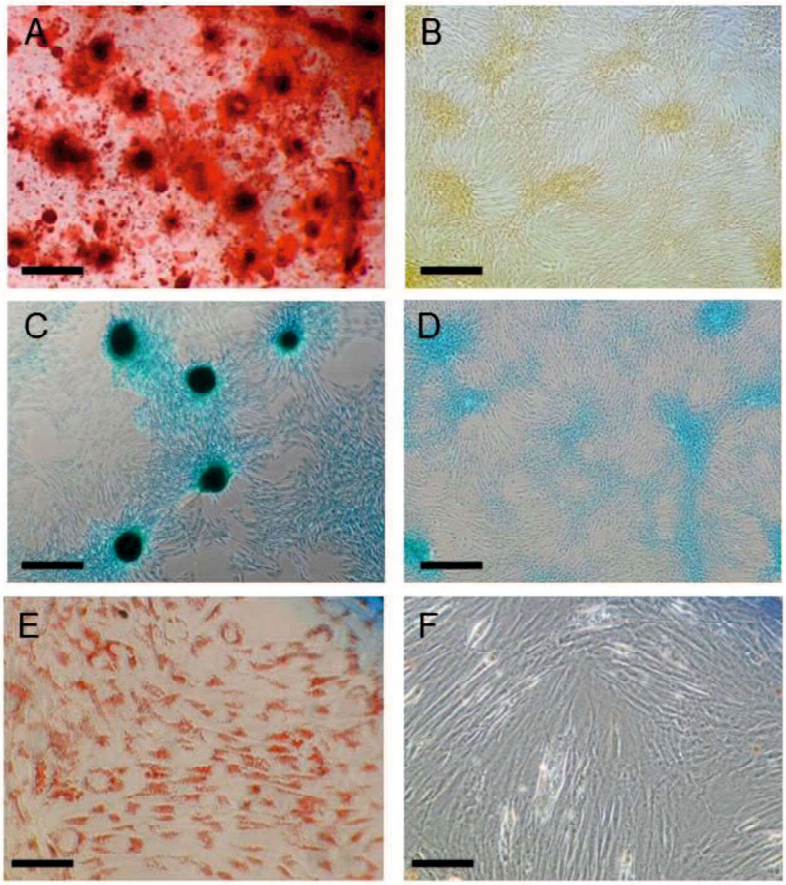

Figure 4.6 Representative images showing staining with alizarin red (A, B), alcian blue (C, D), and oil red O (E, F) of dedifferentiated fat (DFAT) cells. Following 2 weeks of osteogenic induction, the DFAT cells aggregated and contracted to form colonies and produced a specific matrix including calcium apatite crystals, which were positively stained with alizarin red. Scale bar = 500 μm (A). The plate culture of DFAT cells in chondrogenic induction medium induced a formation of colonies and a production of extracellular matrix stained with alcian blue. Scale bar = 500 μm (C). Adipogenic induction of DFAT cells resulted in adipocyte-like flattened cells with small lipid vesicles that stained red with oil red O. Scale bar = 250 μm (E). The negative controls of were cultured with complete culture medium (CCM) during the corresponding periods of time taken to induce osteogenic, adipogenic and chondrogenic differentiation (B, D, F).

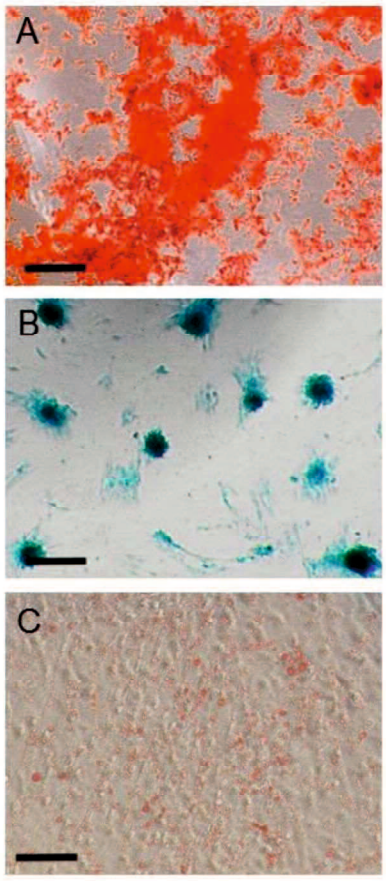

Figure 4.7 Representative images showing staining with alizarin red (A), alcian blue (B), and oil red O (C) of adipose tissue-derived mesenchymal stem cells (AT-MSCs). Following 2 weeks of osteogenic induction, AT-MSCs aggregated and contracted to form colonies and produced a specific matrix including calcium apatite crystals, which were positively stained with alizarin red. Scale bar = 500 μm (A). The plate culture of AT-MSCs in chondrogenic induction medium induced a formation of colonies and a production of extracellular matrix stained with alcian blue. Scale bar = 500 μm (B). Adipogenic induction of AT-MSCs resulted in adipocyte-like flattened cells with small lipid vesicles that stained red with oil red O. Scale bar = 250 μm (C).

General Discussion

OA is degenerative disease caused by abuse, and cartilage is degeneratively changed at first. Once a degenerative change, collagen fibers running parallel to the surface in superficial zone is split. As the changes progressing, intermediate zone is degenerated and radial zone is cracked and broken. As the mechanical loading on the degenerated site repeated, calcified zone and subchondral bone are fractured and gouged. And then, cortical bone is rubbed and deformed to sclerosis.

Osteochondral defects in our studies presented here were created as complete defects of articular cartilages and subchondral bones. Although inner surface of subchondral bone has endosteum consisting of progenitor cells which can regenerate bone tissue, new bones were not formed in the defects of subchondral bones at the control sites in theses studies. As one of the reasons for that, the defects of subchondral bones were too wide in these studies so that new bones were formed in the defects. Instead of the formation of new bones, fibrous connective tissues and fatty marrow were filled in the defects of subchondral bones. Fat tissue is known to be obstructive to bone formation so that fatty marrow is considered to suppress the formation of new bone in the defects.

On the other hand, a smooth and continuous surface was restored by thickened fibrocartilage at the implanted sites 6 months after surgery, and endochondral ossification progressed upward and inward from the boundary between the implanted construct and bone. These results suggest fibrocartilage formation and endochondral ossification during the process of MSC-based regeneration were present at the implanted site, unlike the process of endochondral ossification which occurs at primary

and secondary ossification center during fetal period or in the growth plate during growth period. Furthermore, subchondral bone was symmetrically reconstructed in the defect and was covered by a mixed matrix of hyaline cartilage and fibrocartilage in which clusters and columnar clusters of cells were observed at the implanted site 12 months after surgery. These findings may suggest transformation of fibrocartilage into hyaline cartilage during the process of MSC-based osteochondal regeneration. However, more time may be required to regenerate pure, high-quality hyaline cartilage as well as to complete subchondral regeneration in the implanted defect. Similarly, partially thickened fibrocartilage at the center of the defect also suggests that a longer time may be needed to complete subchondral regeneration.

The planaria is known to be able to regenerate a complete individual from a head, trunk or tail fragment following (or due to) the activation of somatic pluripotent stem cells. About a century ago, the extraordinary regenerative ability of planarians was explained by positing two opposing morphogenetic gradients of formative ‘‘head stuff’’ and ‘‘tail stuff’’ along the anterior–posterior axis. And recently, some studies suggest that extracellular signal-related kinase (ERK) and Wnt/β-catenin signalling pathways are important for the establishment of a solid framework for planarian regeneration (Tasaki et al. 2011; Umesono st al. 2013). ERK signaling forms a spatial gradient in the anterior region during regeneration and posteriorly biased β-catenin activity negatively regulate ERK signalling along the anterior–posterior axis in distinct manners. ERK signalling has a pivotal role in triggering globally dynamic differentiation of stem cells in a head-to-tail sequence through a default program that promotes head tissue specification in the absence of posteriorizing signals. β-catenin signalling is responsible for the lack of head-regenerative ability of tail fragments and posterior β-catenin signalling negatively modulates the ERK signalling involved in anteriorization. And

also, Wnt signal transduction plays a crucial role in stem cell proliferation and regeneration (Robertis et al. 2010). When canonical Wnt signaling is low, heads develop, and when it is high, tails are formed. In planarians, Wnt transcription is activated by wounding in a β-catenin independent way. Hedgehog is also one of the signals involved in posteriorization, because it induces regeneration of tails (instead of heads) through the activation of Wnt transcription. Depletion of Smad4 blocks regeneration entirely, it is suggesting that the bone morphogenetic protein signaling pathway and the Wnt pathway are required for regeneration and body patterning. In the regeneration of cartilage, ERK signalling may have important roles in cartilage differentiation of stem cells on a center-to-epiphisis sequence of bone through a program that promotes articular cartilage specification. Wnt/β-catenin signal transduction as well as ERK signal may play a crucial role in stem cell regeneration for cartilage. And also, Wnt/β-catenin signal has been reported to be involved in the aging of cartilage (Hiyama et al. 2010). Fibrocartilage has been known to be ossificated as age advances, so Wnt/β-catenin signal may be involve in the endochondral ossifciation of fibrocartilage observed 6 months after AT-MSCs implantation. Hedgehog has been also already known to be one of the crucial signals involved in the suppression on the hypertrophy of cartilage formation (Kierszenbaum et al. 2002).

Articular cartilage is composed of four layers such as superficial zone, intermediate zone, radial zone, and calcified zone, and not covered with perichondrium so that articular surface is very smooth. Superficial zone is a superficial layer consisting of tightly woven collagen fibers which curve in arche shape toward the surface and run alongside each other near the surface. However, recent study reveals that most superficial zone (MSZ) are preset above superficial zone and the MSZ is subdivided into three layers (Fujioka et al. 2013). The first layer includes amorphous substance, the

second layer consists of a uniform structure, and the third layer comprises collagen fibrils such as collagen subtypes I, II, and III. Collagen type I is observed in the third layer and the upper zone of the superficial zone. Collagen type II is in the third layer and in the entire supercficial zone. Collagen type III is more widely distributed than collagen type I. This fiber structures of MSZ are very similar to that of fibrocartilage.

Lateral mesoderm includes MSCs differentiated into many kinds of cells such as chondrocytes, osteocytes, myocytes, fibroblasts, adipocytes, and stromal cells. In particular, cartilage, bone, muscle, tendon, ligament, and dermal fibroblast generate in mesenchymal connective tissues. Synovial membrane layer is also one of mesenchymal connective tissues and composed of endosynovial layer and subsynovial layer consisting of macrophage-like synovial cell (type A) and fibroblast-like synovial cell (type B). The first role of fibloblast-like cells is the secretion of hyaluronan which is component of synovial fluid, and also second role of the cells is the repair or regeneration for cartilage defects as SM-MSCs. I speculate that equine SF-MSCs may be SM-MSCs released from the synovium. Unfortunately, we have no useful data indicating the specific markers of MSCs to demonstrate that equine SF-MSCs is derived from synovium. However, both of SF-MSCs and SM-MSCs could be suitable for generating cartilage matrix during chondrogenic differentiation compared to AT-MSCs or BM-MSCs.

Differentiated cells can be reprogrammed to an embryonic-like state by transfer of nuclear contents into oocytes or by fusion with embryonic stem cells (ESCs). Induction of pluripotent stem cells from embryonic or adult fibroblasts by introducing four factors of Oct3/4, Sox2, c-Myc, and Klf4, under ES cell culture conditions. These cells were designated as induced pluripotent stem cells (iPSCs), exhibit the morphology and growth properties of ESCs and express ESC marker genes (Takahashi et al. 2006).

Neural crest cells (NCCs) are an embryonic migratory cell population via ectoderm from ESCs. NCCs have the potential ability to differentiate into a wide variety of cell types. This suggests the promising role of NCCs as a source for cell-based therapy. Several methods have been used to induce NCCs from pluripotent stem cells (PSCs), such as ESCs and iPSCs. Chemically defined medium (CDM) was used as the basal medium in the induction and maintenance steps. By optimizing the culture conditions, the combination of the GSK3b inhibitor and TGFb inhibitor with a minimum growth factor (insulin) very efficiently induced NCCs (70–80%) from PSCs. Differentiation properties were confirmed for peripheral neurons, glia, melanocytes, and corneal endothelial cells. In addition, cells with differentiation characteristics similar to MSCs were induced from NCCs using CDM specific for human MSCs (Fukata et al. 2014).

From these studies, it has been gradually revealed that osteochondral regeneration by implantation of scaffold free three-dimensional structure using MSCs could regenerate bone and cartilage similar to original osteocartilage. To applicate this method to animal and/or human medicine, we must solve following three challenges.

1) To make up a stable quality of construct that would be also easy to manipulate in the implantation surgery

2) To form a various shape of constructs by piling up cell aggregates

3) To reduce the time “from diagnosis to therapy” and “from cell therapy to osteochondral regeneration”

In near future, we perform next studies to solve the above challenges for following three purpose.

1) To give the uniformity in adhesion patterns of mutual aggregates

2) To prepare the same shape of the implant as the shape of osteochondral defect.

3) To use any other stem cells with superior ability to differentiate into the bone or the cartilage.

Therefore, we are going to study about osteochondral regeneration with using a specific machine such as bio-3D-printer which can laminate aggregates automatically and specific stem cells such as SF-MSCs, NCCs, and iPSCs in order to achieve the above purposes.

Acknowledgement

I would like to give heartful thanks to Prof. Dr. Kazuhiro MISUMI (Kagoshima University) who has been extraordinarily tolerant and offered continuing support and constant encouragement. Without his guidance, this thesis would not have materialized.

I would like to express the deepest appreciation to Associate Prof. Dr. Makoto FUJIKI (Kagoshima University) and Prof. Dr. Yoshinao HOSAKA (Tottori University) whose opinions and information have helped me very much throughout the production of this thsis.

I would like to show my greatest appreciation to Prof. Dr. Koichi NAKAYAMA who has gave me successful suggestions and offered constant encouragement. Without his suggestions and encouragement, this thesis would not have been possible.

I would like to express my gratitude to the assistant professors in Kagoshima University Veterinary Teaching Hospital, the postdoctoral researchers in Dr. NAKAYAMA's laboratory, and the reserchers in Cyfuse Biomedical K.K. who have offered their valuable technical support to perform the experiments of this research.

I would also like to express my gratitude to my family, my parents, asnd my relatives for their moral support and warm encouragements.

Finally, I gratefully appreciate the financial support of Japan Society for the Promotion of Sience Research Fellowship that made it possible to complete my thesis.

Reference

(alphabetical order)

1. Arnhold SJ, Goletz I, Klein H, Stumpf G, Beluche LA, Rohde C, Addicks K, Litzke LF: Isolation and characterization of bone marrow-derived equine mesenchymal stem cells. Am J Vet Res 2007, 68:1095-1105.
2. Arrigoni E, De-Girolamo L, Di-Giancamillo A, Stanco D, Dellavia C, Carnelli D, Campagnol M, Domeneghini C, Brini AT: Adipose-derived stem cells and rabbit bone regeneration: histomorphometric, immunohistochemical and mechanical characterization. J Orthop Sci 2013, 18:331-339.
3. Asumda FZ, Chase PB: Age-related changes in rat bone-marrow mesenchymal stem cell plasticity. BMC Cell Biol 2011, 12:44.
4. Barberini DJ, Freitas NP, Magnoni MS, Maia L, Listoni AJ, Heckler MC, Sudano MJ, Golim MA, DA Cruz LAF, Amorim RM: Equine mesenchymal stem cells from bone marrow, adipose tissue and umbilical cord: immunophenotypic characterization and differentiation potential. Stem Cell Res Ther 2014, 5: 25.
5. Bentley G, Biant LC, Carrington RW, Akmal M, Goldberg A, Williams AM, Skinner JA, Pringle J: A prospective, randomised comparison of autologous chondrocyte implantation versus mosaicplasty for osteochondral defects in the knee. J Bone Joint Surg Br 2003, 85:223-230.
6. Bodó G, Hangody L, Szabó Z, Peham C, Schinzel M, Girtler D, Sótonyi P: Arthroscopic autologous osteochondral mosaicplasty for the treatment of subchondral cystic lesion in the medial femoral condyle in a horse. Acta Vet Hung 2000, 48:343-354.

7. Bodo G, Hangody L, Modis L, Hurtig M: Autologous osteochondral grafting (mosaic arthroplasty) for treatment of subchondral cystic lesions in the equine stifle and fetlock joints. Vet Surg 2004, 33:588-596.
8. Bragulla H, Burdras KD, Forstenpointner G, König HE, Liebich HG, Maierl J, Mülling C, Probst A, Reese S, Ruberte J: In veterinary anatomy of domestic mammals: Textbook and colour atlas third edition. Edited by König HE, Liebich HG. Stuttgart: Schattauer; 2007.
9. Braun J, Hack A, Weis-Klemm M, Conrad S, Treml S, Kohler K, Walliser U, Skutella T, Aicher WK: Evaluation of the osteogenic and chondrogenic differentiation capacities of equine adipose tissue-derived mesenchymal stem cells. Am J Vet Res 2010, 71:1228-1236.
10. Burk J, Ribitsch I, Gittel C, Juelke H, Kasper C, Staszyk C, Brehm W: Growth and differentiation characteristics of equine mesenchymal stromal cells derived from different sources. Vet J 2013,195:98-106.
11. Carrade DD, Owens SD, Galuppo LD, Vidal MA, Ferraro GL, Librach F, Buerchler S, Friedman MS, Walker NJ, Borjesson DL: Clinicopathologic findings following intra-articular injection of autologous and allogeneic placentally derived equine mesenchymal stem cells in horses. Cytotherapy 2011, 13:419-430.
12. Carrington EF, Desautels M, Naylor JM: beta-Adrenergic stimulated lipolysis in pony adipocytes is exclusively via a beta2-subtype and is not affected by lactation. Comp Biochem Physiol A Mol Integr Physiol 2003, 136:311-320.
13. Casado JG, Gomez-Mauricio G, Alvarez V, Mijares J, Tarazona R, Bernad A, Sanchez-Margallo FM: Comparative phenotypic and molecular characterization of porcine mesenchymal stem cells from different sources for translational studies in a large animal model. Vet Immunol Immunopathol 2012, 147:104-112.

14. Chen J, Lu Z, Cheng D, Peng S, Wang H: Isolation and characterization of porcine amniotic fluid-derived multipotent stem cells. PLoS One 2011, 6:e19964.
15. Chen WC, Yao CL, Wei YH, Chu IM: Evaluating osteochondral defect repair potential of autologous rabbit bone marrow cells on type II collagen scaffold. Cytotechnology 2011, 63:13-23.
16. Clancy J, Crom R, Gibbins I, Gunasegaran JP, Gustafson AW, Heath JW, Kumer D, Lowe JS, Murphy CR, Sanchez HC, Sanger JW, Spitalnik PF, Steavens A, Telser A, Wadwha S, Young B, Young J: In wheater's Functional histology: A text and colour atlas fifth edition. Editted by Young B, Lowe JS, Steavens A, Heath JW. Kindlington: Elsevier; 2006.
17. Dashtdar H, Rothan HA, Tay T, Ahmad RE, Ali R, Tay LX, Chong PP, Kamarul T: A preliminary study comparing the use of allogenic chondrogenic pre-differentiated and undifferentiated mesenchymal stem cells for the repair of full thickness articular cartilage defects in rabbits. J Orthop Res 2011, 29:1336-1342.
18. De Robertis EM: Wnt signaling in axial patterning and regeneration: lessons from planaria. Sci Signal 2010, 3:21.
19. Dhar M, Neilsen N, Beatty K, Eaker S, Adair H, Geiser D: Equine peripheral blood-derived mesenchymal stem cells: Isolation, identification, trilineage differentiation and effect of hyperbaric oxygen treatment. Equine Vet J 2012, 44:600-605.
20. Diaz-Romero J, Gaillard JP, Grogan SP, Nesic D, Trub T, Mainil-Varlet P: Immunophenotypic analysis of human articular chondrocytes: changes in surface markers associated with cell expansion in monolayer culture. J Cell Physiol 2005, 202:731-742.

21. Ding C, Cicuttini F, Scott F, Cooley H, Boon C, Jones G: Natural history of knee cartilage defects and factors affecting change. Arch Intern Med 2006, 166:651-658.
22. Fernandes JC, Martel-Pelletier J, Pelletier JP: The role of cytokines in osteoarthritis pathophysiology. Biorheology 2002, 39:237-246.
23. Friedenstein AJ: Precursor cells of mechanocytes. International Review of Cytology 1976, 47:327-359.
24. Fujioka R, Aoyama T, Takakuwa T: The layered structure of the articular surface. Osteoarthritis Cartilage 2013, 21:1092-1098.
25. Fujisato T, Sajiki T, Liu Q, Ikada Y: Effect of basic fibroblast growth factor on cartilage regeneration in chondrocyte-seeded collagen sponge scaffold. Biomaterials 1996, 17:155-162.
26. Fukuta M, Nakai Y, Kirino K, Nakagawa M, Sekiguchi K, Nagata S, Matsumoto Y, Yamamoto T, Umeda K, Heike T, Okumura N, Koizumi N, Sato T, Nakahata T, Saito M, Otsuka T, Kinoshita S, Ueno M, Ikeya M, Toguchida J: Derivation of mesenchymal stromal cells from pluripotent stem cells through a neural crest lineage using small molecule compounds with defined media. PLoS One 2014, 9:e112291.
27. Funayama A, Niki Y, Matsumoto H, Maeno S, Yatabe T, Morioka H, Yanagimoto S, Taguchi T, Tanaka J, Toyama Y: Repair of full-thickness articular cartilage defects using injectable type II collagen gel embedded with cultured chondrocytes in a rabbit model. J Orthop Sci 2008, 13:225-232.
28. Gelber AC, Hochberg MC, Mead LA, Wang NY, Wigley FM, Klag MJ: Joint injury in young adults and risk for subsequent knee and hip osteoarthritis. Ann Intern Med 2000, 133:321-328.

29. Gao Q, Zhao L, Song Z, Yang G: Expression pattern of embryonic stem cell markers in DFAT cells and ADSCs. Mol Biol Rep 2012, 39:5791-5804.
30. Guo KT, SchAfer R, Paul A, Gerber A, Ziemer G, Wendel HP: A new technique for the isolation and surface immobilization of mesenchymal stem cells from whole bone marrow using high-specific DNA aptamers. Stem Cells 2006, 10:2220-2231.
31. Gurevitch O, Slavin S, Resnick I, Khitrin S, Feldman A: Mesenchymal progenitor cells in red and yellow bone marrow. Folia Biol 2009, 55:27-34.
32. Hiyama A, Sakai D, Risbud MV, Tanaka M, Arai F, Abe K, Mochida J: Enhancement of intervertebral disc cell senescence by WNT/β-catenin signaling-induced matrix metalloproteinase expression. Arthritis Rheum 2010, 62:3036-3047.
33. Huntley JS, Bush PG, McBirnie JM, Simpson AH, Hall AC: Chondrocyte death associated with human femoral osteochondral harvest as performed for mosaicplasty. J Bone Joint Surg Am 2005, 87:351-360.
34. Hunziker EB, Rosenberg LC, 1996. Repair of partial-thickness defects in articular cartilage: cell recruitment from the synovial membrane. Journal of Bone and Joint Surgery - American Volume 78, 721-733.
35. Im GI, Kim DY, Shin JH, Hyun CW, Cho WH: Repair of cartilage defect in the rabbit with cultured mesenchymal stem cells from bone marrow. J Bone Joint Surg Br 2001, 83:289-294.
36. Ishihara K, Nakayama K, Akieda S, Matsuda S, Iwamoto Y: Simultaneous regeneration of full-thickness cartilage and subchondral bone defects in vivo using a three-dimensional scaffold-free autologous construct derived from high-density bone marrow-derived mesenchymal stem cells. J Orthop Surg Res 2014, 9:98.

37. Jansen BJ, Gilissen C, Roelofs H, Schaap-Ozielak A, Veltman JA, Raymakers RA, Jansen JH, Kögler G, Figdor CG, Torensma R, Adema GJ: Functional differences between mesenchymal stem cell population are reflected by their transcriptome. Stem Cells Dev 2010, 19:481-490.
38. Jones EA, English A, Henshaw K, Kinsey SE, Markham AF, Emery P, McGonagle D: Enumeration and phenotypic characterization of synovial fluid multipotential mesenchymal progenitor cells in inflammatory and degenerative arthritis. Arthritis Rheum 2004, 50:817-827.
39. Kang SK, Putnam LA, Ylostalo J, Popescu R, Dufour J, Belousov A, Bunnell BA: Neurogenesis of Rhesus adipose stromal cells. J Cell Sci 2004, 117:4289-4299.
40. Kawaguchi H, Miyoshi N, Miura N, Fujiki M, Horiuchi M, Izumi Y, Miyajima H, Nagata R, Misumi K, Takeuchi T, Tanimoto A, Yoshida H: Microminipig, a non-rodent experimental animal optimized for life science research: novel atherosclerosis model induced by high fat and cholesterol diet. J Pharmacol Sci 2011, 115:115-121.
41. Kearns CF, McKeever KH, Malinowski K, Struck MB, Abe T: Chronic administration of therapeutic levels of clenbuterol acts as a repartitioning agent. J Appl Physiol 2001, 91:2064-2070.
42. Kearns CF, McKeever KH, Kumagai K, Abe T: Fat-free mass is related to one-mile race performance in elite standardbred horses. Vet J 2002, 163:260-266.
43. Kierszenbaum AL: In histology and cell biology: An introduction to pathology. Edited by Kierszenbaum AL: Maryland Heights: Elsevier; 2002.

44. Kikuta S, Tanaka N, Kazama T, Kazama M, Kano K, Ryu J, Tokuhashi Y, Matsumoto T: Osteogenic effects of dedifferentiated fat cell transplantation in rabbit models of bone defect and ovariectomy-induced osteoporosis. Tissue Eng Part A 2013, 19:1792-1802.
45. Kitamura PH, Yanase H, Kitamura H, Iwanaga T: Unigue localization of protein gene product 9.5 in type B synoviocytes in the joints of the horse. J Histochem Cytochem 1999, 47:343-351.
46. Koga H, Shimaya M, Muneta T, Nimura A, Morito T, Hayashi M, Suzuki S, Ju YJ, Mochizuki T, Sekiya I: Local adherent technique for transplanting mesenchymal stem cells as a potential treatment of cartilage defect. Arthritis Res Ther 2008, 10:R84.
47. Kono S, Kazama T, Kano K, Harada K, Uechi M, Matsumoto T: Phenotypic and functional properties of feline dedifferentiated fat cells and adipose-derived stem cells. Vet J 2014, 199:88-96.
48. Lane JG, Massie JB, Ball ST: Follow-up of osteochondral plug transfers in a goat model: a 6-month study. Am J Sports Med 2004, 32:1440-1450.
49. Lee DH, Joo SD, Han SB, Im J, Lee SH, Sonn CH, Lee KM: Isolation and expansion of synovial CD34- CD44+ CD90+ mesenchymal stem cells: comparison of an enzymatic method and a direct explant technique. Connect Tissue Res 2011, 52:226-234.
50. Lee HJ, Jung J, Cho KJ, Lee CK, Hwang SG, Kim GJ: Comparison of in vitro hepatogenic differentiation potential between various placenta-derived stem cells and other adult stem cells as an alternative source of functional hepatocytes. Differentiation 2012, 84:223-231.

51. Lee JI, Sato M, Kim HW, Mochida J: Transplantation of scaffold-free spheroids composed of synovium-derived cells and chondrocytes for the treatment of cartilage defects of the knee. Eur Cell Mater 2011, 22:275-290.
52. Lee WC, Sepulveda JL, Rubin JP, Marra KG: Cardiomyogenic differentiation potential of human adipose precursor cells. Int J Cardiol 2009, 133:399-401.
53. Lu Z, Doulabi BZ, Huang C, Bank RA, Helder MN: Collagen type II enhances chondrogenesis in adipose tissue-derived stem cells by affecting cell shape. Tissue Eng Part A 2010, 16:81-90.
54. Matsumoto T, Kano K, Kondo D, Fukuda N, Iribe Y, Tanaka N, Matsubara Y, Sakuma T, Satomi A, Otaki M, Ryu J, Mugishima H: Mature adipocyte-derived dedifferentiated fat cells exhibit multilineage potential. J Cell Physiol 2008, 215:210-222.
55. Mankin HJ: The response of articular cartilage to mechanical injury. J Bone Joint Surg Am 1982, 64:460-466.
56. McIntosh K, Zvonic S, Garrett S, Mitchell JB, Floyd ZE, Hammill L, Kloster A, Di Halvorsen Y, Ting JP, Storms RW, Goh B, Kilroy G, Wu X, Gimble JM: The immunogenicity of human adipose-derived cells: temporal changes in vitro. Stem Cells 2006, 24:1246-1253.
57. Mendelson A, Frank E, Allred C, Jones E, Chen M, Zhao W, Mao JJ: Chondrogenesis by chemotactic homing of synovium, bone marrow, and adipose stem cells in vitro. FASEB J 2011, 25:3496-3504.
58. Mitchell JB, McIntosh K, Zvonic S, Garrett S, Floyd ZE, Kloster A, Di Halvorsen, Y, Storms RW, Goh B, Kilroy G, Wu X, Gimble JM: Immunophenotype of human adipose-derived cells: temporal changes in stromal-associated and stem cell-associated markers. Stem Cells 2006, 24:376-385.

59. Mohanty N, Gulati BR, Kumar R, Gera S, Kumar P, Somasundaram RK, Kumar S: Immunophenotypic characterization and tenogenic differentiation of mesenchymal stromal cells isolated from equine umbilical cord blood. In Vitro Cell Devl Biol Anim 2014, 50:538-548.
60. Morito T, Muneta T, Hara K, Ju YJ, Mochizuki T, Makino H, Umezawa A, Sekiya I: Synovial fluid-derived mesenchymal stem cells increase after intra-articular ligament injury in humans. Rheumatology 2008, 47:1137-1143.
61. Muraki S, Akune T, Oka H, Mabuchi A, En-Yo Y, Yoshida M, Saika A, Nakamura K, Kawaguchi H, Yoshimura N: Association of occupational activity with radiographic knee osteoarthritis and lumbar spondylosis in elderly patients of population-based cohorts: A large-scale population-based study. Arthritis Rheum 2009, 61:779-786.
62. Muraki S, Oka H, Akune T, Mabuchi A, En-Yo Y, Yoshida M, Saika A, Suzuki T, Yoshida H, Ishibashi H, Yamamoto S, Nakamura K, Kawaguchi H, Yoshimura N: Prevalence of radiographic knee osteoarthritis and its association with knee pain in the elderly of Japanese population-based cohorts: The ROAD study. Osteoarthritis Cartilage 2009, 17:1137-1143.
63. Mohanty N, Gulati BR, Kumar R, Gera S, Kumar P, Somasundaram RK, Kumar S: Immunophenotypic characterization and tenogenic differentiation of mesenchymal stromal cells isolated from equine umbilical cord blood. In Vitro Cell Dev Biol Anim 2014, 50:538-548.

64. Nakamura T, Sekiya I, Muneta T, Hatsushika D, Horie M, Tsuji K, Kawarasaki T, Watanabe A, Hishikawa S, Fujimoto Y, Tanaka H, Kobayashi E: Arthroscopic, histological and MRI analyses of cartilage repair after a minimally invasive method of transplantation of allogeneic synovial mesenchymal stromal cells into cartilage defects in pigs. Cytotherapy 2012, 14:327-338.
65. Nakayama K: In vitro biofabrication of tissues and organs. In biofabrication: Micro- and nano-fabrication, printing, patterning and assemblies. Edited by Forgacs G, Sun W. Oxford: William Andrew; 2013:1-21.
66. Nam H, Karunanithi P, Loo WC, Naveen S, Chen H, Hussin P, Chan L, Kamarul T: The effects of staged intra-articular injection of cultured autologous mesenchymal stromal cells on the repair of damaged cartilage: a pilot study in caprine model. Arthritis Res Ther 2013, 15:R129.
67. Nimura A, Muneta T, Koga H, Mochizuki T, Suzuki K, Makino H, Umezawa A, Sekiya I: Increased proliferation of human synovial mesenchymal stem cells with autologous human serum: Comparisons with bone marrow mesenchymal stem cells and with fetal bovine serum. Arthritis Rheum 2008, 58:501-510.
68. Ono H, Oki Y, Bono H, Kano K: Gene expression profiling in multipotent DFAT cells derived from mature adipocytes. Biochem Biophys Res Commun 2011, 407:562-567.
69. Palpant NJ, Metzger JM: Aesthetic cardiology; adipose-derived stem cells for myocardial repair. Curr Stem Cell Res Ther 2010, 5:145-152.
70. Park CW, Rhee YS, Park SH, Danh SD, Ahn SH, Chi SC, Park ES: In vitro / in vivo evaluation of NCDS-micro-fabricated biodegradable implant. Arch Pharm Res 2010, 33:427-432.

71. Pittenger MF, Mackay AM, Beck SC, Jaiswal RK, Douglas R, Mosca JD, Moorman MA, Simonetti DW, Craig S, Marshak DR: Multilineage potential of adult human mesenchymal stem cells. Science 1999, 284:143-147.
72. Poloni A, Maurizi G, Leoni P, Serrani F, Mancini S, Frontini A, Zingaretti MC, Siquini W, Sarzani R, Cinti S: Human dedifferentiated adipocytes show similar properties to bone marrow-derived mesenchymal stem cells. Stem Cells 2012, 30:965-974.
73. Ranela B, Ordovás L, Lyahyai J, Bernal ML, Fernandes F, Remacha AR, Romero A, Vázquez FL, Osta R, Cons C, Varona L, Zaragoza P, Martín-Burriel I, Rodellar C: Comparative study of equine bone marrow and adipose tissue-derived mesenchymal stromal cells. Equine Vet J 2012, 44:33-42.
74. Rehnitz C, Kupfer J, Streich NA, Burkholder I, Schmitt B, Lauer L, Kauczor HU, Weber MA: Comparison of biochemical cartilage imaging techniques at 3 T MRI. Osteoarthritis Cartilage 2014, 22:1732-1742.
75. Riekstina U, Cakstina I, Parfejevs V, Hoogduijn M, Jankovskis G, Muiznieks I, Muceniece R, Ancans J: Embryonic stem cell marker expression pattern in human mesenchymal stem cells derived from bone marrow, adipose tissue, heart and dermis. Stem Cell Rev 2009, 5:378-386.
76. Robinson D, Efrat M, Mendes DG, Halperin N, Nevo Z: Implants composed of carbon fiber mesh and bone-marrow-derived, chondrocyte-enriched cultures for joint surface reconstruction. Bull Hosp Jt Dis 1993, 53:75-82.
77. Sakaguchi Y, Sekiya I, Yagishita K, Muneta T: Comparison of human stem cells derived from various mesenchymal tissues: superiority of synovium as a cell source. Arthritis Rheum 2005, 52:2521-2529.

78. Sekiya I, Ojima M, Suzuki S, Yamaga M, Horie M, Koga H, Tsuji K, Miyaguchi K, Ogishima S, Tanaka H, Muneta T: Human mesenchymal stem cells in synovial fluid increase in the knee with degenerated cartilage and osteoarthritis. J Orthop Res 2012, 30:943-949.
79. Shimaya M, Muneta T, Ichinose S, Tsuji K, Sekiya I: Magnesium enhances adherence and cartilage formation of synovial mesenchymal stem cells through integrins. Osteoarthritis Cartilage 2010, 18:1300-1309.
80. Smith RK, Dyson SJ, Schramme MC, Head MJ, Payne RJ, Platt D, Walmsley J: Osteoarthritis of the talocalcaneal joint in 18 horses. Equine Vet J 2005, 37:166-171.
81. Stock P, Staege MS, Müller LP, Sgodda M, Völker A, Volkmer I, Lützkendorf J, Christ B: Hepatocytes derived from adult stem cells. Transplantation Proc 2008, 40:620-623.
82. Stolzing A, Jones E, McGonagle D, Scutt A: Age-related changes in human bone marrow-derived mesenchymal stem cells: consequences for cell therapies. Mech Ageing Dev 2008, 129:163-173.
83. Sugihara H, Funatsumaru S, Yonemitsu N, Miyabara S, Toda S, Hikichi Y: A simple culture method of fat cells from mature fat tissue fragments. J Lipid Res 1989, 30:1987-1995.
84. Sugihara H, Yonemitsu N, Miyabara S, Toda S: Proliferation of unilocular fat cells in the primary culture. J Lipid Res 1987, 28:1038-1045.
85. Sugihara H, Yonemitsu N, Miyabara S, Yun K: Primary cultures of unilocular fat cells: characteristics of growth in vitro and changes in differentiation properties. Differentiation 1986, 31:42-49.

86. Suzuki S, Muneta T, Tsuji K, Ichinose S, Makino H, Umezawa A, Sekiya I: Properties and usefulness of aggregates of synovial mesenchymal stem cells as a source for cartilage regeneration. Arthritis Res Ther 2012, 14:R136.

87. Szerb I, Hangody L, Duska Z, Kaposi NP: Mosaicplasty: long-term follow-up. Bull Hosp Jt Dis 2005, 63:54-62.

88. Tatebe M, Nakamura R, Kagami H, Okada K, Ueda M: Differentiation of transplanted mesenchymal stem cells in a large osteochondral defect in rabbit. Cytotherapy 2005, 7:520-530.

89. Takahashi K, Yamanaka S: Induction of pluripotent stem cells from mouse embryonic and adult fibroblast cultures by defined factors. Cell 2006, 126:663-676.

90. Takeishi K, Horiuchi M, Kawaguchi H, Deguchi Y, Izumi H, Arimura E, Kuchiiwa S, Tanimoto A, Takeuchi T: Acupuncture improves sleep conditions of minipigs representing diurnal animals through an anatomically similar point to the acupoint (GV20) effective for humans. Evid Based Complement Alternat Med 2012, 2012:472982.

91. Taléns-Visconti R, Bonora A, Jover R, Mirabet V, Carbonell F, Castell JV, Gómez-Lechón MJ: Hepatogenic differentiation of human mesenchymal stem cells from adipose tissue in comparison with bone marrow mesenchymal stem cells. World J Gastroenterol 2006, 12:5834-5845.

92. Tang L, Yin Y, Zhou H, Song G, Fan A, Tang B, Shi W, Li Z: Proliferative capacity and pluripotent characteristics of porcine adult stem cells derived from adipose tissue and bone marrow. Cell Reprogram 2012, 14:342-352.

93. Tasaki J, Shibata N, Nishimura O, Itomi K, Tabata Y, Son F, Suzuki N, Araki R, Abe M, Agata K, Umesono Y: ERK signaling controls blastema cell differentiation during planarian regeneration. Development 2011, 138:2417-2427.

94. Toghraie F, Razmkhah M, Gholipour MA, Faghih Z, Chenari N, Torabi-Nezhad S, Nazhvani-Dehghani S, Ghaderi A: Scaffold-free adipose-derived stem cells (ASCs) improve experimentally induced osteoarthritis in rabbits. Arch Iran Med 2012, 15:495-499.

95. Toupadakis CA, Wong A, Genetos DC, Cheung WK, Borjesson DL, Ferraro GL, Galuppo LD, Leach JK, Owens SD, Yellowley CE: Comparison of the osteogenic potential of equine mesenchymal stem cells from bone marrow, adipose tissue, umbilical cord blood, and umbilical cord tissue. Am J Vet Res 2010, 71:1237-1245.

96. Umesono Y, Tasaki J, Nishimura Y, Hrouda M, Kawaguchi E, Yazawa S, Nishimura O, Hosoda K, Inoue T, Agata K: The molecular logic for planarian regeneration along the anterior-posterior axis. Nature 2013, 500:73-76.

97. Unterman SA, Gibson M, Lee JH, Crist J, Chansakul T, Yang EC, Elisseeff JH: Hyaluronic acid-binding scaffold for articular cartilage repair. Tissue Eng Part A 2012, 18:2497-2506.

98. Vidal MA, Robinson SO, Lopez MJ, Paulsen DB, Borkhsenious O, Johnson JR, Moore RM, Gimble JM: Comparison of chondrogenic potential in equine mesenchymal stromal cells derived from adipose tissue and bone marrow. Vet Surg 2008, 37:713-724.

99. Vidal MA, Lopez MJ: Adipogenic differentiation of adult equine mesenchymal stromal cells. Methods Mol Biol 2011, 702:61-75.

100. Vidal MA, Kilroy GE, Lopez MJ, Johnson JR, Moore RM, Gimble JM: Characterization of equine adipose tissue-derived stromal cells: adipogenic and osteogenic capacity and comparison with bone marrow-derived mesenchymal stromal cells. Vet Surg 2007, 36:613-622.

101. Violini S, Ramelli P, Pisani LF, Gorni C, Mariani P: Horse bone marrow mesenchymal stem cells express embryo stem cell markers and show the ability for tenogenic differentiation by in vitro exposure to BMP-12. BMC Cell Biol 2009, 10:29:1471-2121.

102. Wei S, Du M, Jiang Z, Duarte MS, Fernyhough-Culver M, Albrecht E, Will K, Zan L, Hausman GJ, Elabd EM, Bergen WG, Basu U, Dodson MV: Bovine dedifferentiated adipose tissue (DFAT) cells: DFAT cell isolation. Adipocyte 2013, 2:148-159.

103. Windmolders S, De-Boeck A, Koninckx R, Daniëls A, De-Wever O, Bracke M, Hendrikx M, Hensen K, Rummens JL: Mesenchymal stem cell secreted platelet derived growth factor exerts a pro-migratory effect on resident Cardiac Atrial appendage Stem Cells. J Mol Cell Cardiol 2014, 66:177-188.

104. Xie X, Wang Y, Zhao C, Guo S, Lui S, Jia W, Tuan RS, Zhang C: Comparative evaluation of MSCs from bone marrow and adipose tissue seeded in PRP-derived scaffold for cartilage regeneration. Biomaterials 2012, 33:7008-7018.

105. Yagi K, Kondo D, Okazaki Y, Kano K: A novel preadipocyte cell line established from mouse adult mature adipocytes. Biochem Biophys Res Commun 2004, 321:967-974.

106. Yin S, Cen L, Wang C, Zhao G, Sun J, Liu W, Cao Y, Cui L: Chondrogenic transdifferentiation of human dermal fibroblasts stimulated with cartilage-derived morphogenetic protein 1. Tissue Eng Part A 2010, 16:1633-1643.

107. Yoon IS, Chung CW, Sung JH, Cho HJ, Kim JS, Shim WS, Shim CK, Chung SJ, Kim DD: Proliferation and chondrogenic differentiation of human adipose-derived mesenchymal stem cells in porous hyaluronic acid scaffold. J Biosci Bioeng 2011, 112:402-408.

108. Yoshioka T, Mishima H, Kaul Z, Ohyabu Y, Sakai S, Ochiai N, Kaul SC, Wadhwa R, Uemura T: Fate of bone marrow mesenchymal stem cells following the allogeneic transplantation of cartilaginous aggregates into osteochondral defects of rabbits. J Tissue Eng Regen Med 2011, 5:437-443.

109. Young DA, DeQuach JA, Christman KL: Human cardiomyogenesis and the need for systems biology analysis. Wiley Interdiscip Rev Syst Biol Med 2011, 3:666-680.

110. Zhou G, Liu W, Cui L, Wang X, Liu T, Cao Y: Repair of porcine articular osteochondral defects in non-weightbearing areas with autologous bone marrow stromal cells. Tissue Eng 2006, 12:3209-3221.

111. Zola H, Swart B, Nicholson I, Voss E: Leukocyte and Stromal Cell Molecules: The CD Markers. Hoboken: John Wiley & Sons Inc; 2007.

112. Zuk PA, Zhu M, Ashjian P, De-Ugarte DA, Huang JI, Mizuno H, Alfonso ZC, Fraser JK, Benhaim P, Hedrick MH: Human adipose tissue is a source of multipotent stem cells. Mol Bio Cell 2002, 13:4279-4295.

113. Zuk PA, Zhu M, Mizuno H, Huang J, Futrell JW, Katz AJ, Benhaim P, Lorenz HP, Hedrick MH: Multilineage cells from human adipose tissue: implications for cell-based therapies. Tissue Eng 2001, 7:211-228.